Diss. ETH No. 18224

Poly(L-lysine)-*g*-dextran (PLL-*g*-dex): brush-forming, biomimetic carbohydrate chains that inhibit fouling and promote lubricity

A dissertation submitted to the
ETH ZURICH

for the degree of
DOCTOR OF SCIENCES

presented by

CHIARA PERRINO
Diploma in Biomedical Engineering (Politecnico di Milano) 2005
born on July 30, 1981
citizen of Italy

accepted on the recommendation of

Prof. Dr. N.D. Spencer, examiner
Prof. Dr. S. Lee, co-examiner
Prof. Dr. S. Perry, co-examiner

Zurich, February 2009

A Giuseppe.

Abstract

The subject of this thesis was the development of carbohydrate-based graft copolymers with both antifouling and aqueous lubricating properties. Sugars are known to be major components of common natural lubricants (e.g. mucin, glycoproteins) and also to be mainly responsible for the ability of the endothelial glycocalyx—a dense and highly hydrated membrane-bound layer rich in proteoglycans, glycosaminoglycans and other glycosylated molecules—to prevent non-specific protein adsorption.

Besides the many industrial applications of aqueous lubricant additives (food processing, textile or pharmaceutical manufacturing) and antifouling coatings (ships' hulls, water-purification systems, heat-transfer components), the combination of good lubricating and antifouling properties is highly desirable for those biomedical applications involving moving parts in contact with tissue, e.g. coatings for stents, catheters, and endoscopes.

The brush-like graft polymer, poly(L-lysine)-*graft*-poly(ethylene glycol) (PLL-*g*-PEG), a copolymer consisting of PEG chains grafted onto a polycationic PLL backbone, has been previously demonstrated to spontaneously adsorb onto negatively charged surfaces, such as many metal oxides, and to be highly effective at both preventing non-specific protein adsorption onto and lubricating oxide surfaces in an aqueous environment. Poly(L-lysine)-*graft*-dextran (PLL-*g*-dex) copolymers, which display a very similar structure, have now been developed by grafting dextran (dex) chains onto the same PLL backbone.

A matrix of PLL-*g*-dex copolymers with varying grafting ratio, *g*[y] (number of lysine monomers per dextran side chain), between ca. *g*[2] and *g*[9] and dextran molecular weights (5, 10 and 20 kDa) was synthesized. Poly(L-lysine) hydrobromide (PLL-HBr) with molecular weight of 20 kDa was used as backbone for the copolymers. Some PLL-*g*-dex copolymers with dextran with molecular weight of 5.9 kDa on a PLL backbone with molecular weight of 6 or 13 kDa were also kindly provided by Prof. Maruyama (Institute for Materials Chemistry and Engineering, Kyushu University, Japan) and their antifouling capabilities were also examined in this thesis. A series of PLL(20)-*g*-PEG(5) (20 kDa for the molecular weight of PLL backbone and 5 kDa for the molecular weight of PEG side chains) with varying grafting ratios, roughly *g*[3] to *g*[11], was purchased and used for comparison purposes.

Optical waveguide lightmode spectroscopy (OWLS) has been employed to examine the adsorption behavior of the polymers onto silica-titania surfaces and to investigate the protein-resistance properties of PLL-*g*-dex copolymers. The measurements revealed that PLL-*g*-dex

copolymers readily adsorb from aqueous solution onto negatively charged oxide surfaces, similarly to PLL-*g*-PEG, and significantly reduce the non-specific protein adsorption to levels comparable to those observed from PLL-*g*-PEG coatings.

Macrotribological characterization of PLL-*g*-dex copolymers under pure sliding (pin-on-disk tribometer) or mixed sliding/rolling conditions (Mini Traction Machine, MTM) showed that PLL-*g*-dex is very effective for the lubrication of oxide-based tribosystems and a direct comparison between the lubricating capabilities of PLL-*g*-dex and their PLL-*g*-PEG counterparts revealed somewhat better lubricating performance of PLL-*g*-dex copolymers with certain molecular structures (in particular, low side-chain density along the backbone) under particular measurement conditions (in particular, high frequency of tribocontact).

The study of the effects of aging (exposure to ambient daylight and bacterial contamination) on the lubricating properties of PLL-*g*-dex copolymers revealed no influence of storage and aging of polymer solutions in daylight, but bacterially induced degradation, which impairs the lubricating performance, was observed, suggesting the need for biocide use (such as sodium azide) or sterile conditions for applications of PLL-*g*-dex as a lubricant additive.

Finally, a study of the hydration capabilities of PLL-*g*-PEG and PLL-*g*-dex copolymers by means of OWLS and quartz crystal microbalance with dissipation monitoring (QCM-D) has demonstrated the higher hydration power of PLL-*g*-PEG copolymers compared to the PLL-*g*-dex counterparts and provided a possible explanation for the differences in antifouling and aqueous lubrication properties between PLL-*g*-dex and PLL-*g*-PEG copolymers.

Riassunto

L'oggetto di questa tesi è stato lo sviluppo di copolimeri a base di zuccheri con proprietà lubrificanti e di riduzione dell'assorbimento non specifico di proteine. Gli zuccheri sono i principali componenti dei comuni lubrificanti naturali (e.g. mucina ed altre glicoproteine) e sono anche considerati principali responsabili delle proprietà di resistenza all'assorbimento proteico non specifico del glicocalice, un denso e idratato rivestimento della membrana cellulare composto prevalentemente da proteoglicani, glicosaminoglicani e altre molecole a base di zuccheri.

Oltre alle numerose applicazioni in campo industriale di additivi lubrificanti acquosi (per la lavorazione di generi alimentari, nell'industria tessile e farmaceutica) e di rivestimenti con proprietà *antifouling* (per gli scafi delle navi, sistemi di purificazione dell'acqua, sistemi per lo scambio di calore), la combinazione di buone proprietà lubrificanti e di resistenza all'assorbimento non specifico di proteine è auspicabile per applicazioni in campo biomedico che prevedono il contatto dei tessuti biologici con componenti artificiali in movimento, per esempio rivestimenti per stent, cateteri o endoscopi.

PLL-*g*-PEG, poli(L-lisina)-*g*-polietilenglicole, è un copolimero con struttura a pettine (*brush-like)* costituito da molecole di polilisina (PLL) (*backbone*) sulle quali vengono innestate, mediante un legame covalente, catene di polietilenglicole (PEG). Studi precedenti hanno dimostrato che PLL-*g*-PEG si assorbe spontaneamente su superfici cariche negativamente, come molti ossidi di metallo, e che è molto efficace sia nella prevenzione dell'assorbimento non-specifico di proteine su ossidi di metalli che nella lubrificazione in ambiente acquoso degli stessi. PLL-*g*-dex, poli(L-lisina)-*g*-destrano, il copolimero sviluppato in questo lavoro di tesi, ha struttura molto simile al PLL-*g*-PEG, ed è ottenuto sostituendo catene di destrano (dex) alle catene di PEG, ma mantenendo la polilisina come *backbone*.

In questa tesi sono stati sintetizzati copolimeri PLL-*g*-dex variando il rapporto di innesto (*grafting ratio)*, *g*[y] (numero di monomeri di lisina per catena di destrano), tra ca. *g*[2] e *g*[9] e peso molecolare del destrano (5, 10 e 20 kDa). Come *backbone* è stata utilizzata una polilisina idrobromuro con peso molecolare di 20 kDa. Sono state anche studiate le proprietà *antifouling* di alcuni copolimeri con destrano con peso molecolare di 5.9 kDa su PLL con peso molecolare di 6 o 13 kDa, gentilmente forniti dal Prof. Maruyama (Institute for Materials Chemistry and Engineering, Kyushu University, Japan). Copolimeri commerciali di PLL(20)-*g*-PEG(5) (20 kDa come peso molecolare della polilisina e 5 kDa per le catene laterali di

PEG) con *grafting ratio* variante tra ca. *g*[3] e *g*[11] sono stati utilizzati per paragonarne le proprietà con quelle di PLL-*g*-dex.

Optical waveguide lightmode spectroscopy (OWLS) è la tecnica di caratterizzazione utilizzata per lo studio dell'assorbimento dei copolimeri su superfici di silicio-titanio e per l'analisi delle proprietà *antifouling*. I risultati degli esperimenti hanno dimostrato che PLL-*g*-dex assorbe spontaneamente da soluzione acquosa su ossidi di metallo carichi negativamente, in modo simile al PLL-*g*-PEG, e che riduce sensibilmente l'assorbimento non-specifico di proteine a valori confrontabili con quelli relativi a rivestimenti di PLL-*g*-PEG.

La caratterizzazione delle proprietà lubrificanti macroscopiche di PLL-*g*-dex in condizioni di puro scivolamento (condotta con un tribometro pin-on-disk) o di scivolamento misto a rotolamento (condotta con una Mini Traction Machine, MTM) ha dimostrato l'efficacia di PLL-*g*-dex nella lubrificazione di accoppiamenti a base di ossidi e le proprietà lubrificanti di PLL-*g*-dex con una certa struttura molecolare (in particolare alta grafting ratio) e in certe condizioni sperimentali (in particolare alta frequenza di contatti) sono risultate, da un confronto diretto, leggermente superiori a quelle di PLL-*g*-PEG.

I risultati dello studio degli effetti di invecchiamento (esposizione alla normale luce ambientale e contaminazione batterica) sulle proprietà lubrificanti di PLL-*g*-dex indicano che non c'è alcuna influenza dell'esposizione prolungata di soluzioni di polimero alla luce. E' stato osservato tuttavia un peggioramento delle proprietà lubrificanti dovuto a contaminazione batterica. Condizioni sterili o l'uso di un biocida (come per esempio sodio azide) sono di conseguenza richiesti per l'impiego di PLL-*g*-dex come additivo lubrificante.

L'analisi condotta tramite OWLS e quartz crystal microbalance with dissipation monitoring (QCM-D) dell'"idratazione" (definita in questo contesto come quantità di acqua trattenuta dalla struttura polimerica) dei copolimeri PLL-*g*-dex e PLL-*g*-PEG immobilizzati sulla superficie ha infine rivelato le maggiori potenzialità di idratazione del PLL-*g*-PEG, fornendo una possibile spiegazione delle differenze nelle proprietà lubrificanti e *antifouling*.

1 INTRODUCTION

1.1 Aqueous Lubrication

The lubrication of engineering materials is traditionally based on the usage of mineral oils as base lubricants. However, oil-based lubricants usually contain toxic and poorly degradable substances, which are source of pollution and health hazards. Strong environmental concerns and growing regulations over contamination and pollution started increasing the need for renewable, biodegradable, and environmentally friendly lubricants [1, 2].

Water could represent a good alternative to oil-based lubricants for its distinctive advantages (environmental compatibility, biocompatibility, availability, cost effectiveness, ease of disposal, excellent heat-transfer properties), and water-lubricated systems are therefore interesting to a number of industries. The usage of oil-based lubricants in the food, textile or pharmaceutical industries is, for instance, highly discouraged as a consequence of contamination issues.

Despite the various potential advantages of water-based lubricants, they are currently used only in few areas, such as in the mining industry, partially for safety issues, and for some applications in the biomedical field (lubrication of catheters, stents, endoscopes), where water is virtually the only acceptable base lubricant.

Obstacles to the usage of water as a lubricant are represented by its lower boiling temperature compared to oils, corrosion of ferrous materials, and its very low pressure-coefficient of viscosity, which limits the load-carrying capacity of water-lubricated systems [3]: unlike oil-based lubricants, an increase in pressure does not correspond to an exponential

increase of viscosity and the formation of a lubricating film is therefore not as readily achieved with water itself.

1.2 Protein-Resistant Surfaces

Control of the non-specific adsorption of biomolecules (biofouling) onto biomaterials has been the subject of much research in the biomedical field.

A precise control of the chemical and biological processes occurring at the biomaterial-biological environment interface is of crucial importance to avoid unfavorable host responses, such as thrombus formation and chronic inflammation that are initiated by non-specific protein adsorption followed by platelet adhesion, activation and aggregation on biomaterial surface [4-6], and can be life threatening and certainly impair the performance of the implanted devices, impacting their long-term viability.

The undesirable adsorption of microorganisms and the formation of biofilms are also detrimental in several nonbiomedical areas, especially where aqueous systems are present: the consequences of biofouling for water purification systems, water cooling pipes, heat exchangers, static marine structures, ships' hulls are considerable, both economically and ecologically [7-10]. In the shipping industry, biofouling is actually a costly, worldwide problem: even within few hours of immersion, a slimy biofilm of bacteria and microscopic algae adheres to the ship's hull and it is rapidly overgrown by other organisms, including barnacles, seaweeds, sponges, resulting in loss of speed, increased fuel consumption, faster ship's deterioration and therefore in a general economic and environmental penalty [11].

Many efforts have been focused on the development of antifouling surfaces in all areas where biofouling represents a major problem.

Surface modification by physical or chemical immobilization of polymers or other organic layers is the most common method to reduce or prevent non-specific adsorption of proteins in the biomedical field. While a number of polymers have been explored for this purpose, including polyacrylates, oligosaccharides, phosphorylcholines (mimics of phospholipids), coatings from poly(ethylene glycol) (PEG) have attracted particularly strong attention and provided very promising results in terms of protein resistance [4, 12, 13]. PEG fully conforms, in fact, to certain characteristics that polymers have been reported to require if non-specific protein adsorption is to be reduced, such as hydrophilicity, neutrality, presence of hydrogen-bond acceptors and absence of hydrogen-bond donors, and flexibility [14].

Furthermore its low toxicity and immunogenicity make it suitable for applications in the biomedical field.

Antifouling coatings represent a common method of controlling and preventing biofouling, also for industrial applications. One of the most widespread of these is tin-based coatings, specifically triorganotin- or organostannic-, or simply, tributyl tin-coatings (TBT-coatings). TBT is however toxic and, when used for instance as coating for ships' hulls, it is toxic to biofouling organisms, as desired, but also interferes with major biological processes of "non-target" organisms, and that is why United States Navy discontinued use of such paints at the beginning of the decade [15].

Copper-based coatings have replaced TBT-coatings for some applications, but many claim that they are responsible for similar negative effects as TBT. There is therefore much interest in developing non-toxic, environmentally friendly coatings. Some polymers, such as silicones or fluoropolymers, are already employed and thought to have a natural resistance to biofouling by creating a low surface tension and having a low glass-transition temperature. Natural antifouling methods are also under investigation, they would be of course non-toxic and cost effective compared to many specialized coatings that have been used so far [15].

1.3 Lubrication and Protein Resistance in Nature

Lubrication and protein resistance mechanisms in living systems both involve sugars.

Lubrication mechanisms in nature are exclusively based on water and the weak point of water as lubricant, its very low viscosity at high pressures, is overcome partly by complex biomolecules, usually glycoproteins, in which large numbers of sugar chains are anchored to a protein backbone, forming bottlebrush structures [16, 17]. Mucins are large glycoproteins, and are major components of the mucosal layers that cover epithelial cell surfaces and function as both a protective and lubricious coating: their lubrication potential is mostly associated with their structure, their adsorption behavior and conformation at solid/liquid interface, and the carbohydrate portion of the molecule that confers considerable water-holding capacity and facilitates the formation of a hydration shell [18]. Proteoglycan aggregate, a sugar-based bottlebrush, is also supposed to be involved in natural lubrication mechanisms, playing a key structural role in cartilage [19, 20].

As already mentioned above, carbohydrates can immobilize large amounts of water, this resulting in a heavily hydrated, hydrogel-like structure: hydrophilicity, together with chain flexibility, provides a steric entropic contribution towards repulsion of non-specific protein

adsorption. An example in nature of a structure with antiadhesive properties mainly attributed to the sugar component is the endothelial glycocalyx, a dense and highly hydrated network of membrane-bound proteoglycans and glycoproteins, covering endothelial cell surfaces and known to be able to prevent undesirable molecular and cellular adhesion [5, 21-23].

1.4 Polymer Brushes

Polymer brushes can be defined as polymer chains attached by one end to a surface or interface by some means with a sufficiently high tethering density (lateral spacing between grafted chains smaller than the undisturbed dimension of the polymer coils) that the polymer chains are forced to stretch away from the surface or interface [24, 25].

This stretched configuration is quite different from the typical behavior of flexible polymer chains in solution, where the molecules assume a random-walk configuration.

Polymer brushes represent a central model for many polymer systems such as adsorbed diblock copolymers, graft copolymers at fluid-fluid interfaces, end-grafted polymers on a solid surface and polymer micelles. Solvent can be either present ("swollen brush") and absent (solvent-free brush, "dense brush") in polymer brushes: in the presence of a good solvent, the polymer chains try to avoid contact with each other to maximize contact with solvent molecules, whereas in the case of solvent-free brushes there is no solvent filling voids between polymer segments and the balance between strong attraction and hard core repulsion essentially fixes the concentration of segments at a value close to the bulk density. In both cases the polymer chains exhibit deformed configuration and are forced away from the interface [25, 26].

Some important parameters characterizing a polymer brush are the segment-density profile of the surface-attached chains, the brush thickness as a function of the grafting density, the molecular weight of the polymer chains and the solvent quality [27, 28].

The interface to which polymer chains are tethered in the polymer brushes can be a solid surface or an interface between two liquids, a liquid and air, or between melts or solutions of homopolymers [25].

Focusing on polymer brushes at solid surfaces, depending on the grafting density two cases can be distinguished:

- if the distance between two anchoring points (L) is larger than the size of the unperturbed surface-attached chains ($L >> 2R_g$, with R_g = radius of gyration of the unperturbed chains in solution), the polymer chains do not "feel" each other and

assume either a "mushroom" (Fig. 1.1(B)) or "pancake" (Fig. 1.1(A)) conformation, depending on the strength of interaction of the chains with the surface, weak or even repulsive in the first case, attractive in the latter case;

- if the grafting density is high enough that the polymer molecules overlap ($L < 2R_g$), there are strong interchain repulsive interactions that cause the chains to stretch out in a direction normal to the grafting surface, forming a swollen "brush", when in the presence of a good solvent (Fig. 1.1(C)). [29]

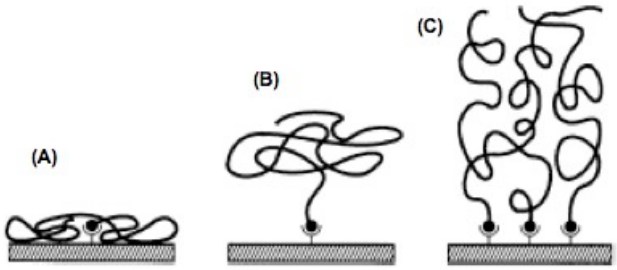

Fig. 1.1 "Pancake" (A), mushroom (B) and brush (C) conformation of end-grafted polymer chains.

Physisorption and covalent attachment are two common strategies to synthesize polymer brushes: in the first case polymer chains are reversibly tethered on the surface, irreversibly in the latter case.

Physisorption on a solid surface is usually achieved by the self-assembly of block copolymers or graft copolymers and occurs in the presence of selective solvents or selective surfaces, leading to selective brush solvation or adsorption behavior. Taking the case of block copolymers as an example, one block strongly interacts with the surface and acts as an "anchor" for the polymer chains, the other block having only weak interactions with the substrate, but interacting strongly with the solvent, floating in the solvent like a "buoy" [27].

Covalent attachment can be accomplished by either "grafting to" or "grafting from" approaches. In the "grafting to" method, preformed end-functionalized polymer chains are grafted to the surface from solution. This method is very simple and straightforward but has some limitations: firstly, it is very difficult to produce dense brushes due to the self-exclusion of chains as the surface polymer concentration increases. Secondly, a fast and high-yield surface reaction with a high number of chains covalently binding onto the surface requires rather reactive anchor groups, which will not tolerate the coexistence of a large number of functional groups in the same molecule [25, 27, 30].

To overcome the drawbacks of the "grafting to" method and prepare thick polymer brushes (more than 2000 nm) with high grafting density (distance between anchor points less than 3 nm) [27], the "grafting from" approach can be used: initiators are, in this case, either generated by plasma or glow discharge treatment or self-assembled on the substrate. The polymer chains are hence grown from these surface-immobilized initiators *in situ* [25, 31]. Drawbacks of this approach are, however, the high polydispersity of the grafted polymer chains, caused by the difficulty to control propagation and termination of the polymerization reaction, the necessity of many, not straightforward, reaction steps for the synthesis of the initiators and also the demand of a high-energy source for both the synthesis of the initiators and the polymerization step.

1.5 Poly(L-lysine)-*g*-poly(ethylene glycol) (PLL-*g*-PEG) and Poly(L-lysine)-*g*-dextran (PLL-*g*-dex)

Polymer brushes have attracted significant attention for many applications involving surface modification and are increasingly being employed to develop new adhesive materials [32, 33], protein-resistant surfaces [34-36], lubricants [37], and surfactants [24].

For protein-resistant surfaces, due to the well-established antifouling properties of poly(ethylene glycol) (PEG), several methods have been employed to immobilize PEG onto surfaces; they can be classified as physisorption, hydrophobic attraction, electrostatic interaction, or covalent bonding according to the surface-bonding characteristics, or classified as "grafting from" or "grafting to" approach depending on that the polymers are pre-formed to be attached onto surface or generated from the surface. Although "grafting from" approach readily allows for the preparation of dense brushes, its tribological application often reveals a serious drawback: once the brush-like films are scrapped away from the surface due to tribostress, re-formation of film *during* the tribological contacts is nearly impossible. "Grafting-to" approach, on the other hand, can overcome such problem as long as the polymers are present in excess in base lubricant and surface-adsorption kinetics is sufficiently fast [38]. However, it is generally difficult to produce high surface densities using the "grafting to" method, especially with polymer chains with single anchoring groups via physisorption or electrostatic interactions, due to steric hindrance or stability issues. Grafting polymer chains onto a backbone, i.e. graft copolymerization, is an alternative approach to the formation of a dense polymer brush; when adsorbed onto a surface via the backbone, the side chains, which are radially distributed along the backbone in bulk solution, are forced to

stretch away from the surface spontaneously, forming a higher grafting chain density than achievable with a conventional "grafting to" approach.

Poly(L-lysine)-g-poly(ethylene glycol) (PLL-g-PEG)

Poly(L-lysine)-*graft*-poly(ethylene glycol) (PLL-*g*-PEG) (a scheme of PLL-*g*-PEG is shown in Fig. 1.2) represents an example of the above-mentioned approach: it is a graft copolymer consisting of PEG chains grafted onto a PLL polycationic backbone, originally developed for improving the biocompatibility of microcapsules [39] and then proven to be highly effective at preventing non-specific adsorption of proteins onto oxide surfaces in an aqueous environment [40-46].

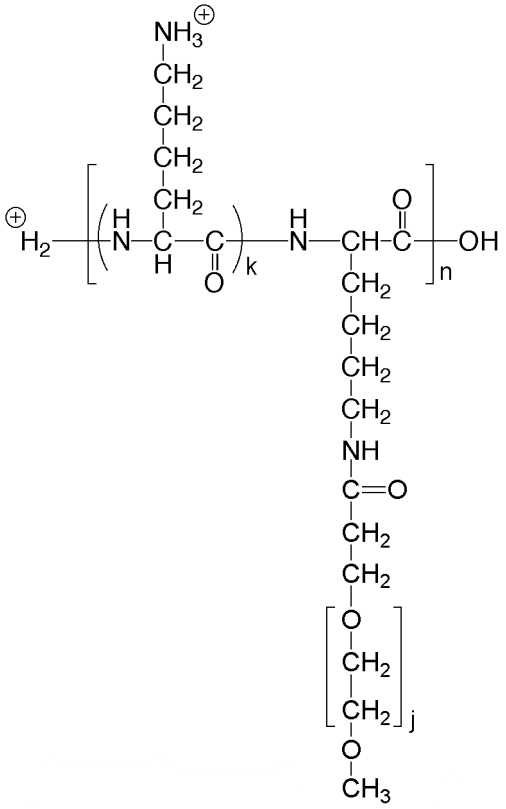

Fig. 1.2 Structural formula of the PLL-*g*-PEG copolymer. *k* should be taken as an average value. *k*+1 represents the grafting ratio of the polymer. The grafting ratio is defined as the number of lysine monomers per PEG chain.

PLL-*g*-PEG has also been shown to be a particularly attractive system for lubrication purposes: some properties of PEG, such as hydrophilicity, flexibility, solubility in water make it suitable, in fact, for the design of aqueous lubricants, and the brush-structure of PLL-*g*-PEG mimics in particular one of natural structures involved in lubrication mechanisms [38, 47-50].

Carrying out the synthesis of PLL-*g*-PEG ourselves allows the variation of architectural features, such as the molecular weight of both PLL and PEG and the grafting ratio of the PEG side chains along the backbone.

PLL-*g*-PEG copolymers spontaneously adsorb from aqueous solutions onto negatively charged surfaces via electrostatic interactions; the positive charges present on the protonated primary amine groups of the PLL backbone in a neutral aqueous environment lead to its rapid and stable immobilization onto negatively charged surfaces.

Despite its impressive performance as both an antifouling polymer and a lubricant additive in an aqueous environment, PLL-*g*-PEG shows some disadvantages, such as oxidation to peroxides in air [51] and the inverse solubility-temperature relationship in water: while completely soluble in water at low temperatures, PEG loses its solubility at elevated temperatures [52-55].

Poly(L-lysine)-g-dextran (PLL-g-dex)

Poly(L-lysine)-*g*-dextran (PLL-*g*-dex) (Fig. 1.3) is a graft copolymer having a very similar structure to PLL-*g*-PEG, with dextran being grafted onto the same PLL backbone instead of PEG chains. It can be easily synthesized by a reductive amination reaction between the amine groups of PLL and the reducing end of dextran which, being neutral like PEG, has no electrostatic interactions with the polycationic backbone.

Dextran is a natural polysaccharide consisting of an $\alpha(1\rightarrow6)$-linked glucan with side chains attached to the 3-positions of the backbone glucose units; it is hydrophilic, non-charged and water soluble and its essentially non-branched polymer chains are highly flexible.

PLL-*g*-dex has been developed as a stabilizer of DNA triple helices and a carrier of functional genes to target cells or tissues [56-60]. In the present work, it has proven to adsorb onto negatively charged surfaces in a similar fashion to PLL-*g*-PEG and to be highly effective as antifouling coating [61] and as a lubricant additive for oxide-based tribosystems in an aqueous environment [62].

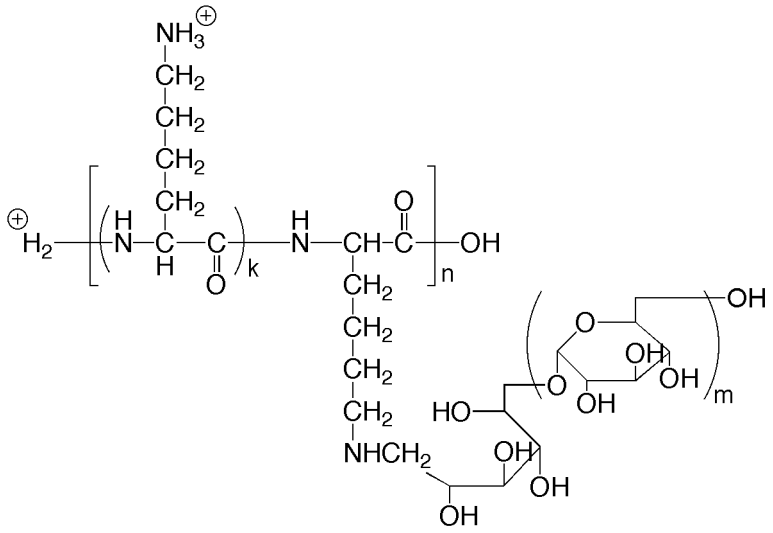

Fig. 1.3 Structural formula of the PLL-*g*-dex copolymer. *k* should be taken as an average value. *k*+1 represents the grafting ratio of the polymer. The grafting ratio is defined as the number of lysine monomers per dextran chain.

1.6 Scope of the Thesis

The main objective of the present study is to synthesize and investigate the lubricating and antifouling properties of the brush-like copolymer PLL-*g*-dex. Comparison of PLL-*g*-dex performance to that of PLL-*g*-PEG copolymers, previously shown to be an attractive system for both prevention of non-specific protein adsorption [42-44] and lubrication of oxide surfaces in an aqueous environment, is also included [47, 49, 50].

This study was motivated by several considerations:

- combination of a brush-like structure and a carbohydrate component for the development of lubricating and antifouling polymers, i.e. brush-forming sugar chains, represents a highly biomimetic approach. As mentioned in Section 1.3, sugars and brush-like structures are in fact major ingredients for natural lubrication and prevention of adsorption of undesired molecules and cells;
- PLL-*g*-dex represents the first well-defined carbohydrate-based copolymer that has been the subject of tribological research: while several "natural" carbohydrate-based copolymers have been employed for tribological studies (e.g. lubricin [63-65], mucins [18, 66, 67]), a common drawback of these studies is the lack of detailed information on the molecular structure of those copolymers;

- dextran shows some advantages over PEG: concerning the structure it possesses multiple reactive sites for surface immobilization of bioactive molecules for biomedical applications and, from a "commercial" point of view, it is much cheaper (ca. two orders of magnitude) than the end-functionalized PEG used for the synthesis of PLL-*g*-PEG; furthermore dextran behavior at elevated temperatures is likely to be better than that of PEG-based systems;
- PLL-*g*-dex might be suitable for many industrial applications requiring environmentally friendly solutions (water-based lubricants in the food or textile industry, antifouling coatings in the shipping industry) and also, and in particular, in the biomedical field where the combination of water compatibility, good lubricating and protein-resistance properties is highly desirable for some applications involving moving parts, e.g. coating for stents, catheters and endoscopes.

2 CHARACTERIZATION TECHNIQUES

2.1 Bulk Characterization Techniques

2.1.1 Nuclear Magnetic Resonance (NMR)

Nuclear magnetic resonance spectroscopy is a characterization technique for determining the structure of organic compounds.

The nuclear magnetic resonance phenomenon is based on the fact that nuclei of atoms have magnetic properties that can be used to yield chemical information. Quantum mechanical subatomic particles (protons, neutrons and electrons) have spin (non-zero magnetic moment). In some atoms (e.g. ^{12}C, ^{16}O, ^{32}S) these spins are paired such that the nucleus of the atom has no overall spin. Any atomic nucleus (e.g. ^{1}H, ^{13}C, ^{31}P, ^{15}N, ^{19}F etc) with either odd mass, odd atomic number, or both odd mass and odd atomic number has a spin.

NMR occurs when the nuclei of certain atoms are placed in a static magnetic field and exposed to a second oscillating field.

A nucleus with spin I has 2I + 1 possible orientations (spin states or energy levels). A nucleus with spin I = 1/2 therefore has 2 possible orientations. As shown in Fig. 2.1, in the absence of an external magnetic field, these orientations are of equal energy, whereas when an external magnetic field of strength $\mathbf{B_0}$ is applied, the energy levels split; the energetically preferred state has its magnetic moment aligned parallel to the applied field (magnetic quantum number, m = +1/2) and it is slightly more populated than the high-energy level with magnetic moment aligned antiparallel with the applied field (m = -1/2).

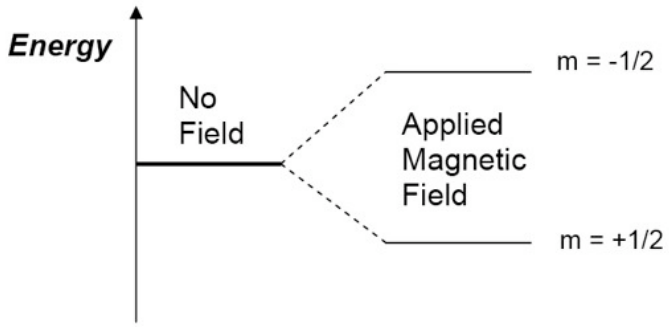

Fig. 2.1 Schematic representation of energy levels for a nucleus with spin I = 1/2 [68].

The spin angular momentum of the nucleus will undergo a cone-shaped rotation motion, called precession, around the applied magnetic field (Fig. 2.2). The rate (frequency) of precession for each isotope is dependent on the strength of the external field and is unique for each isotope.

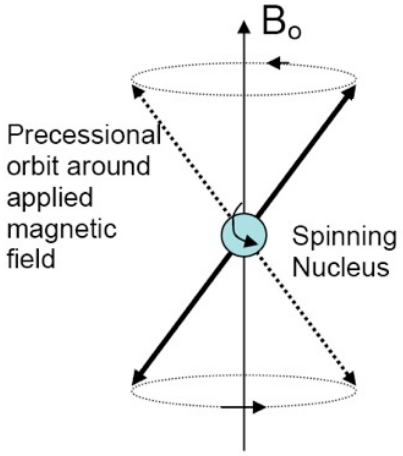

Fig. 2.2 Schematic representation of a nucleus precessing about the applied magnetic field ($\mathbf{B_0}$) [68].

In an NMR experiment, transitions are induced between the different energy levels by irradiating the nuclei with an oscillating field $\mathbf{B_1}$ of the correct quantum energy (e.g. electromagnetic waves of the appropriate frequency).

Transitions from the lower to the upper energy level correspond to an adsorption of energy, and those in the reverse direction to an emission of energy. Both transitions are possible; each transition is associated with a reversal of the spin orientation. Due to the population excess in the low-energy level, the absorption of energy from the irradiating field is the dominant process.

Spin transitions occur when the nuclei come into resonance with the oscillating magnetic field, in other words, when the frequency of the oscillating field is identical to the frequency of the nucleus.

The signal in NMR spectroscopy results in the difference between the adsorbed and emitted energy associated with spin transitions and its intensity is proportional to the population difference between two energy levels.

Each atom in a molecule resonates at a slightly different frequency depending on the proximity of other atoms and on the local environment (solvent, temperature…). This gives an idea of how the atoms are joined together in the molecule, as well as how many different atoms are in the molecule.

The chemical shifts, δ, displayed in NMR spectra represent the difference between the resonance frequency of the nucleus and a standard reference (tetramethylsilane, TMS, was chosen for ^{1}H-NMR). The chemical shifts are measured in parts per million (ppm). The ppm scale is another form of standardization that allows one to compare directly the ^{1}H spectra obtained on NMR instruments with different magnetic fields (different sensitivities) [68, 69].

The PLL-*g*-dex copolymers synthesized in the present thesis were characterized by ^{1}H-NMR spectroscopy, using D_2O as solvent, on a 300 MHz Bruker spectrometer. The ratio between the intensities of selected peaks in the NMR spectrum of PLL-*g*-dex molecules provides information on the molecular composition of the copolymers and enables the determination of the grafting ratio.

2.1.2 Elemental Analysis

Elemental analysis data were used in combination with NMR spectra for the determination of the grafting ratio of PLL-*g*-dex copolymers. Elemental analyses were performed on all synthesized copolymers using different techniques depending on the type of element and its abundance.

For the determination of C, H, and N ratios, either a FLASH EA 1112 (THERMOFINNIGAN) apparatus operated by the Eager 300 software or a LECO CHN-900 machine were used in this thesis. O amounts were determined using a LECO RO-478 setup.

Both analyzers for the determination of C, H, and N ratios are based on the dynamic flash combustion (at 900-1000 °C) of the sample under an oxygen/helium atmosphere. Detection of the generated gases (CO_2, H_2O, NO_2) is carried out by chromatographic separation followed by quantification using a thermal conductivity or infrared detector. Quantification of the

elements requires calibration for each element by using high-purity "micro-analytical standard" compounds such as acetanilide and benzoic acid.

O is determined by dynamic flash combustion of the samples using a catalyst. The generated elemental gases (CO, CO_2) are analyzed with an infrared detector using a vector gas mixture (10% H_2, 90% N_2).

2.2 Surface-Analytical Techniques

2.2.1 Optical Waveguide Lightmode Spectroscopy (OWLS)

Optical Waveguide Lightmode Spectroscopy (OWLS) is a powerful optical biosensing technique for the *in situ,* label-free analysis of adsorption processes from liquids [70]. Its sensing principle is based on the evanescent electromagnetic field of guided light, which extends about 200 nm above the waveguide [71]. The sensitivity is typically 1-2 ng/cm^2.

The grating-assisted in-coupling of a He-Ne laser into the waveguide layer allows for a direct online monitoring of molecular adsorption. The in-coupling is a resonance phenomenon that occurs at a very precise angle of incidence (α), which depends on the refractive index of the optical waveguide chip and the medium covering it. When the in-coupling condition is fulfilled, the light propagates by total internal reflection to the ends of the waveguide, where it is detected by a photodiode detector (Fig. 2.3). By varying the angle of the incident light beam the transverse electric (TE) and transverse magnetic (TM) polarization modes of the light can be excited. The intensity of the in-coupled light is recorded as a function of angle in the mode spectrum. On the basis of the mode spectrum, in-coupling angles of the guided modes (α_{TE} and α_{TM}) can be determined, and from α_{TE} and α_{TM} effective refractive indices (N_{TE} and N_{TM}) are calculated. Thickness (d_A), refractive index (n_a), and mass (M) of the adsorbed layer can be calculated on the basis of N_{TE} and N_{TM}, assuming that the adlayer is homogeneous [70, 72].

In the present thesis, OWLS was employed to characterize the adsorption properties of the polymers and to evaluate their ability to prevent non-specific adsorption of proteins.

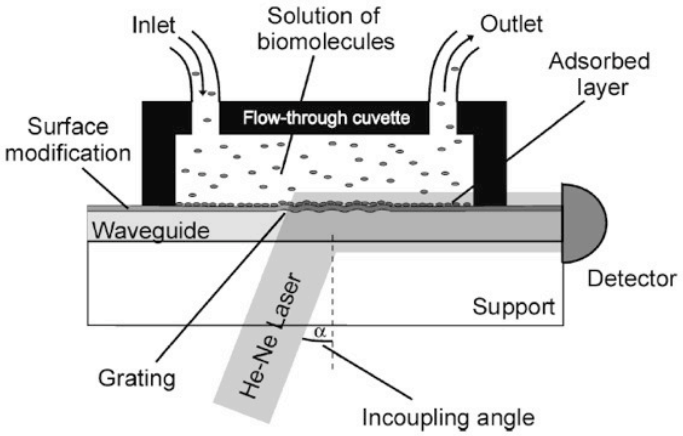

Fig. 2.3 Scheme of an OWLS flow-through cuvette mounted on the top of the waveguide. The whole system rotates clockwise and counterclockwise in order to scan the in-coupling angle α, and the in-coupled light is detected with a photodiode at each end of the waveguide.

Experiments were performed using an OWLS 110 instrument (MicroVacuum, Budapest, Hungary). The inner temperature is controlled by a heater/cooler unit that allows for vibration-free heating and cooling of the sample holder in the temperature range from 20 °C to 80 °C. Standard waveguide chips ($Si_{0.75}Ti_{0.25}O_2$ on glass, 1.2 × 0.8 cm^2) were also purchased by MicroVacuum.

2.2.2 Quartz Crystal Microbalance with Dissipation Monitoring (QCM-D)

QCM-D flow measurements were performed in order to study the hydration of the PLL-*g*-dex and the counterpart PLL-*g*-PEG copolymers, by comparing QCM-D and OWLS data of adsorbed mass.

QCM is a well-established technique that senses variations in the natural resonance of a quartz crystal upon mass adsorption.

The heart of the instrument is the piezoelectric AT-cut thin (~ 200-400 μm) quartz crystal sandwiched between two metal electrodes (usually gold) (Fig. 2.4). When the electrodes are connected to an oscillator and an AC voltage is applied across the crystal, the crystal starts to oscillate.

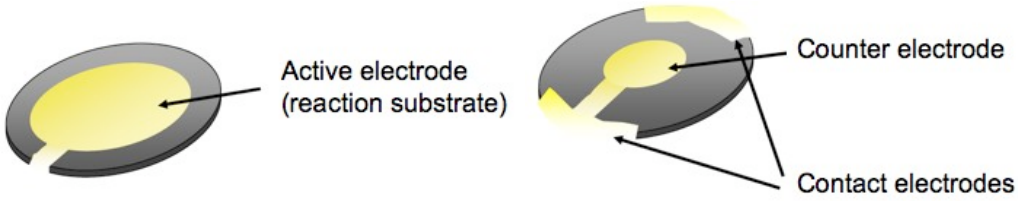

Fig. 2.4 Schematic representation of a QCM quartz crystal.

At certain frequencies of the applied alternating electric field, the amplitude of the oscillation will be strongly enhanced, i.e. the crystal will be in resonance. This occurs at the resonance frequency of the crystal and at its odd overtones. The resonance frequency of the crystal depends on the total oscillating mass. When a thin film is adsorbed onto the sensor, the frequency decreases. In vacuum and gaseous environments, and if the adsorbed mass is small compared to the weight of the crystal, the film is rigid and evenly distributed over the sensing area of the crystal, the decrease in frequency is related to the adsorbed mass, through the Sauerbrey equation:

$$\Delta m = -\frac{C \cdot \Delta f}{n} \qquad \text{Eq. 2.1}$$

where Δm is the change in the total mass of the crystal induced upon adsorption, Δf is the change in frequency, n is the overtone number and C is a constant characteristic of the crystal (C = 17.7 ng/Hz for a 5 MHz quartz crystal).

There are situations where the Eq. 2.1 does not hold, underestimating the mass at the surface: in particular the combined effect of hydration water (water trapped between adsorbed species) and the non-rigid character of many polymers/biomolecules causes viscoelastic dissipation and thus a dampening of the crystal's oscillation.

Quartz Crystal Microbalance with Dissipation monitoring (QCM-D) allows for simultaneous measurement of both frequency and dissipation of the crystal. Dissipation occurs when the driving voltage to the crystal is shut off and the energy from the oscillating crystal dissipates from the system. Dissipation measurements enable qualitative analysis of the structural properties of adsorbed molecular layers. Quantitative analysis of the thickness (h_{film}), shear elastic modulus (E_{shear}), and viscosity (η_{shear}) of the adlayer can be achieved by combining frequency and dissipation measurements from multiple overtones and applying simulations using a Voigt-based viscoelastic model, assuming the film has a uniform thickness and density [73-76].

For the present work, measurements were performed with a commercial quartz crystal microbalance with dissipation monitoring (Q-Sense E4, Gothenburg, Sweden). The instrument includes 4 sensors that were used in a parallel configuration.

In contrast to optical techniques, such as OWLS, QCM-D is sensitive, as mentioned above, to viscoelastic properties and density of any mass coupled to the mechanical oscillation of the quartz crystal. For the polymers employed in this work, PLL-*g*-dex and PLL-*g*-PEG, the adsorbed mass consists of the polymer along with solvent molecules that may be either hydrodynamically associated or strongly attracted (e.g. via hydrogen bonds) to the polymers. The total mass sensed by QCM-D is therefore the mass of the polymer plus that of the adsorbed solvent molecules, m_{wet}, in contrast to the "dry mass", m_{dry}, that can be measured by optical methods, for instance, by OWLS.

2.3 Tribological Characterization Techniques

2.3.1 Pin-on-Disk Tribometry

The pin-on-disk tribometer is a simple instrument for the study of the friction and wear behavior of almost every solid material, with or without lubricant. It allows for the measurement of coefficient of friction of sliding contacts between pin and disk and the calculation of wear coefficients of both pin and disk from the volume of material lost during the test.

A pin-on-disk tribometer (CSM Instruments, Switzerland) (Fig. 2.5) was employed in this work to investigate the lubricating properties of PLL-*g*-dex and PLL-*g*-PEG polymer solutions in a pure sliding-contact regime. As schematically shown in Fig. 2.5(A), the instrument consists of a pin loaded onto the disk, which represents the test sample, to form a contact. The disk is allowed to rotate to generate sliding contact. The pin holder is mounted on a stiff elastic arm, designed as a frictionless force transducer. The coefficient of friction, μ (= friction force/load) is determined during the test by measuring the deflection of the arm.

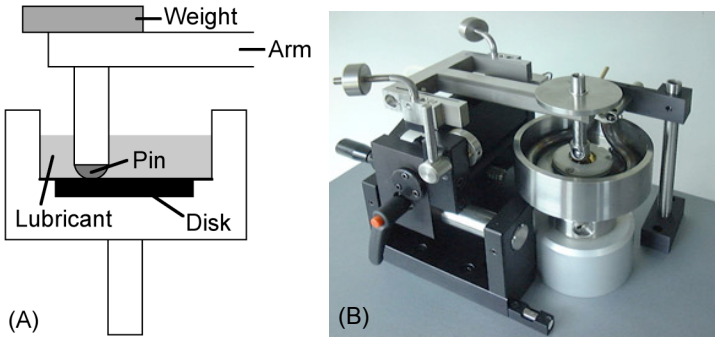

Fig. 2.5 Schematic representation of a pin-on-disk tribometer (A) and the photograph of the CSM pin-on-disk machine used for this thesis (B).

Many parameters can be controlled; load can be changed by applying different dead weights, speed is controlled by varying rpm (rotations per minute) of the rotating motor on which the disk is held. The pin is normally a sphere, but different shapes (semi-sphere, flat-ends) can be used and pin size can be also varied. Environmental conditions, such as humidity, temperature, lubricant, vacuum, can be controlled, allowing simulation of real contacts of interest.

2.3.2 Mini Traction Machine (MTM)

A Mini Traction Machine (MTM) (PCS Instruments, London, U.K.) (Fig. 2.6) was employed to characterize the lubricating properties of PLL-*g*-dex and PLL-*g*-PEG solutions in a mixed sliding/rolling contact regime over a speed range of 0-2500 mm s^{-1}.

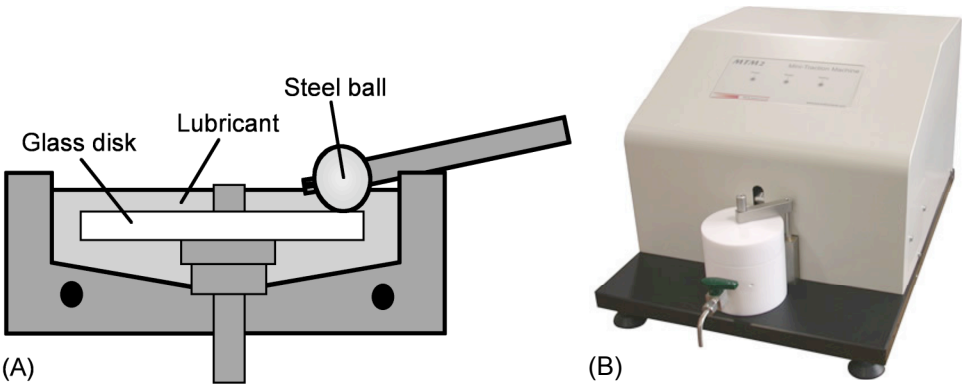

Fig. 2.6 Schematic representation of a Mini Traction Machine (A) and PCS Instruments MTM employed in this work (B).

In the configuration used in this thesis, a steel ball (AISI 52100, 9.5 mm in radius, PCS Instruments, London, U.K.) is loaded against the face of a flat silicate glass disk (46 mm in

diameter, PCS Instruments, London, U.K.), as schematically shown in Fig. 2.6(A). Ball and disk are driven independently to create a mixed sliding/rolling contact. The frictional force between the ball and the disk is measured by a force transducer and additional sensors measure the applied load and the lubricant temperature.

The software allows for the setting of a test profile (temperature, loads, speeds, slide/roll ratio) in an easy way, and during the test data are recorded according to the selected profile, no intervention by the user being required.

The slide/roll ratio (SRR) is defined as the percentage ratio of the difference to the mean of the ball speed (u_{ball}) and disk speed (u_{disk}); i.e., SRR = $[|u_{ball} - u_{disc}|/(u_{ball} + u_{disc})/2] \times 100\%$. Thus, SRR = 0% (i.e. $u_{ball} = u_{disk}$) represents a pure rolling contact and higher SRR values represent a higher portion of the sliding character. With the software provided by the manufacturer (PCS Instruments, MTM version 1.0, London, U.K.), values in the range SRR 1% to 200% are accessible. SRR = 200% represents a pure sliding contact, either the ball or the disk being stationary. For the present work, an SRR value of 10% was chosen, which enables friction measurements under conditions close to pure rolling.

2.3.3 Atomic Force Microscopy (AFM)

Atomic force microscopy (AFM) is a scanning-probe technique, originally developed for atomic scale imaging in the 1980s, and nowadays used for several purposes, ranging from surface topographic imaging, chemical mapping, and nanotribological studies.

In this approach, a sharp tip attached at the end of a flexible cantilever is scanned over the sample surface by the control of a piezoelectric tube scanner, which consists of separate electrodes to scan precisely the sample in the XY plane and to move the sample in the vertical direction (Z). The cantilever deflection due to the normal and lateral (frictional) forces that act on it is measured using a laser-beam-deflection technique. A laser beam from a diode laser is directed onto the back of the cantilever, at its free end. The beam is reflected from the cantilever onto a position-sensitive, four-quadrant photodiode detector (Fig. 2.7). The presence of four quadrants allows for discrimination of the normal deflection signal (differential signal from the top and bottom photodiodes) from the lateral deflection signal (differential signal from the left and right photodiodes). Topographical (normal force) and frictional (lateral force) images can be therefore measured simultaneously.

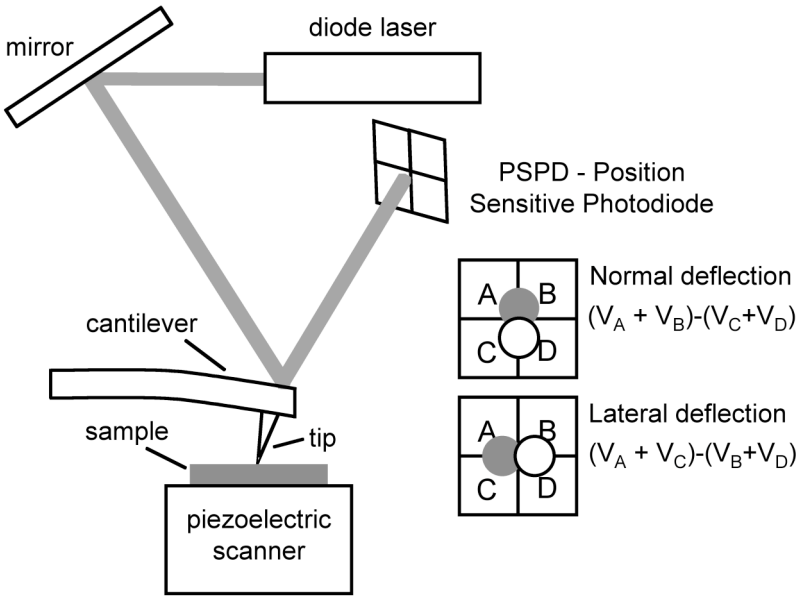

Fig. 2.7 Schematic of the working principle of AFM: the laser beam is reflected from the cantilever that scans the sample surface. The deflection of the laser beam is detected with a four-quadrant photodetector, which allows for the independent determination of normal and lateral deflection signal (V_X).

A conventional beam-deflection-based atomic force microscope was employed in this thesis to characterize the frictional properties of the PLL-*g*-dex copolymers adsorbed on SiO_2 surfaces on a nanometer scale in an aqueous environment.

A commercial SPM scan head (Nanoscope IIIa, MultiMode, Veeco Instruments Inc., Santa Barbara, CA) equipped with a liquid cell/tip holder (Veeco Instruments Inc.) was used, and the fine movement of the sample, placed on top of the piezo scan tube, was controlled by SPM 1000 electronics and SPM 32 software (RHK Technology, Inc., Troy, MI), using an SPM Interface Module (RHK Technology) to interface the scan head and the controller.

3 POLYMER SYNTHESIS

3.1 Synthesis of PLL-*g*-dex

Poly(L-lysine)-*graft*-dextran (PLL-*g*-dex) copolymers were synthesized by a reductive amination reaction of poly(L-lysine) hydrobromide, PLL-HBr, (20 kDa, polydispersity 1.1, Sigma-Aldrich, Buchs, Switzerland) with dextran (dextran T5, 5 kDa, T10, 10 kDa and T20, 20 kDa, polydispersity 1.4-1.8, Pharmacosmos A/S, Denmark). Borate buffer (50 mM, pH 8.5) was used as solvent for the reaction.

The reaction proceeded in two steps: first, the formation of a Schiff base between the terminal dextran aldehyde group and primary amine groups of PLL, and second, the reduction of the unstable Schiff base to secondary amines. PLL was dissolved in borate buffer solution at 40 °C, dextran was subsequently added to the solution (a 2-3× molar excess of dextran was required for the synthesis to obtain a given degree of grafting of dextran chains onto PLL backbone), and the mixture was incubated with stirring overnight for the formation of the Schiff base. Sodium cyanoborohydride ($NaBH_3CN$, Fluka Chemika, Switzerland) was then added to the mixture (10× molar excess to dextran was used) and it was kept under stirring for two more days. The resulting copolymers were isolated by ultracentrifugation (Vivaspin 15R centrifugation tubes, 30000 MWCO, Sartorius AG, Switzerland) to remove the unreacted starting materials. The products were freeze-dried and stored at -20 °C before use.

The yield of the synthesis was calculated by the ratio of the targeted polymer mass to the mass of polymer obtained after lyophilization.

The notation PLL(x)-*g*[y]-dex(z) for the copolymers was used to represent the molar mass of PLL in kDa (x) (including the counterions, Br-, as precursor), the molar mass of dextran in

kDa (z), and the grafting ratio $g[y]$ (defined as the number of lysine monomers/dextran side chain).

3.2 Determination of the Grafting Ratio

All the investigated PLL-*g*-dex molecules were characterized by elemental analysis (EA) and ^{1}H-NMR spectroscopy, in order to obtain information on the molecular structure, particularly on the grafting ratio.

The grafting ratio, defined as the number of lysine monomers per dextran side chain, could be roughly determined by means of EA, from the C/N ratio.

NMR spectroscopy was also used to gain information on the grafting ratio, using the ratio between the intensities of the characteristic peaks of lysine and dextran: Fig. 3.1 shows a representative NMR spectrum for one of the synthesized copolymers, PLL(20)-*g*[5.3]-dex(5). Based on the spectra of PLL and dex (data not shown) the peaks in the spectrum were assigned as displayed in Fig. 3.1.

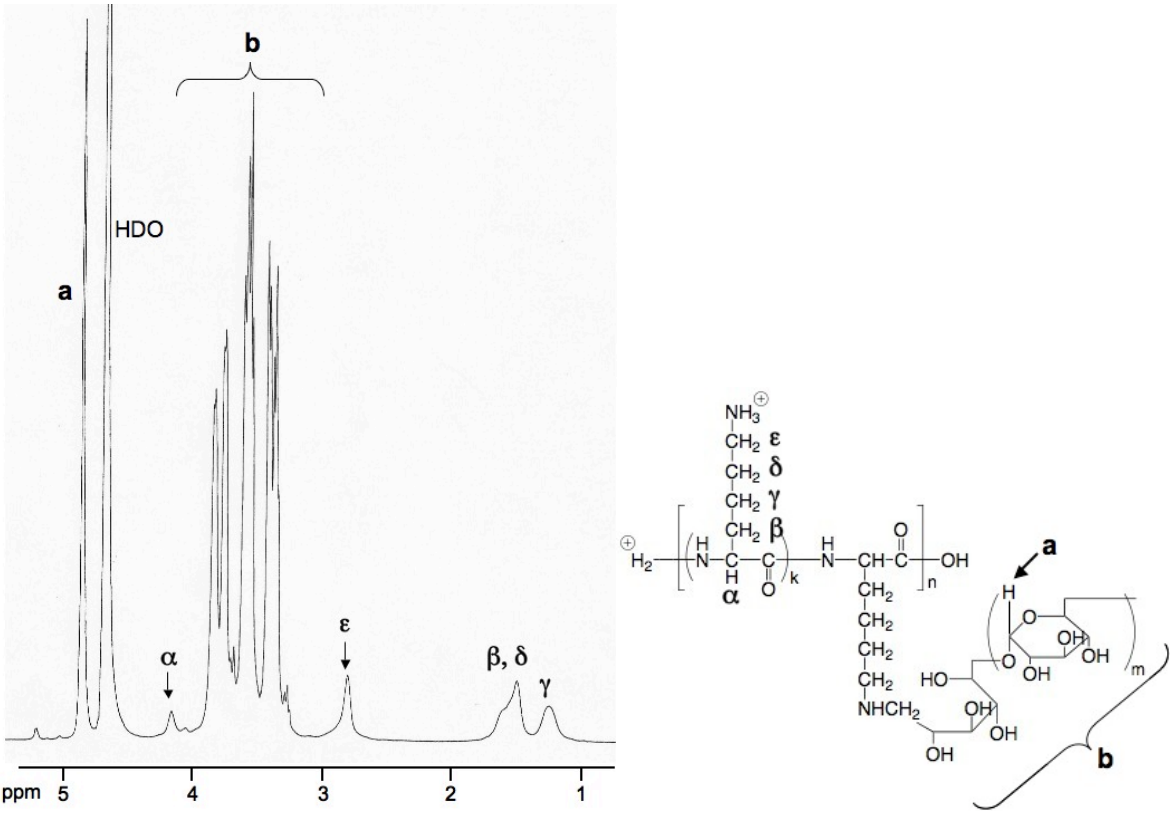

Fig. 3.1 ^{1}H-NMR spectrum for PLL(20)-*g*[5.3]-dex(5) (on the left) and assignment of the peaks according to the PLL-*g*-dex chemical formula (on the right).

3.3 List of All Copolymers

A matrix of PLL-*g*-dex copolymers with different molecular weights and grafting ratios of dextran side chains was synthesized. The nominal molecular weight of PLL was kept constant at 20 kDa (molecular weight of PLL-HBr), corresponding to 115-126 lysine monomers for the actual molecular weights reported in Table 3.1. Dextrans with molecular weights 5, 10 and 20 kDa, dex(5), dex(10) and dex(20), were grafted to the PLL backbone, with grafting ratios varying between roughly *g*[2] and *g*[9]. Dex(5), dex(10) and dex(20) correspond to 31.8, 61.7 and 126.5 sugar rings per chain. Table 3.1 reports the grafting ratios derived from EA, the yields of the synthesis and the molecular weights of the PLL-*g*-dex copolymers calculated with Eq. 3.1:

$$MW_{PLL-g-dex} = \frac{MW_{PLL-HBr}}{MW_{Lys-HBr}} \cdot \left(\frac{MW_{dex}}{g} + MW_{Lys} \right) \qquad \text{Eq. 3.1}$$

where $MW_{Lys\text{-}HBr}$ = 209 Da and MW_{Lys} = 128 Da.

For comparison purpose, PLL(20)-*g*-PEG(5) copolymers provided by SuSoS AG (Dübendorf, Switzerland) have also been investigated, with PEG(5) side chains (nominal molecular weight, 5 kDa) on a PLL(20) backbone and covering a similar range of grafting ratios to that of the PLL-*g*-dex copolymers employed. Same notation as the one used for PLL-*g*-dex copolymers is used for PLL-*g*-PEG.

Table 3.1 Matrix of all copolymers (synthesized PLL-*g*-dex copolymers and PLL-*g*-PEG copolymers used for comparison purpose) employed in this work, with the names of the copolymers, the exact molecular weights of PLL and dex/PEG reagents, the grafting ratio from EA data, the yield of the synthesis and the molecular weights of the copolymers.

Polymer	PLL-HBr [kDa]	PLL MW [kDa]	dex/PEG MW [Da]	*g*	Yield [%]	MW [kDa]
PLL(20)-*g*[3.4]-dex(5)	26.3	16.1	5157	3.4	30	207
PLL(20)-*g*[5.3]-dex(5)	26.3	16.1	5157	5.3	46	139
PLL(20)-*g*[6.6]-dex(5)	26.3	16.1	5157	6.6	60	114
PLL(20)-*g*[7.3]-dex(5)	26.3	16.1	5157	7.3	56	105
PLL(20)-*g*[8.7]-dex(5)	26.3	16.1	5157	8.7	60	91
PLL(20)-*g*[3.7]-dex(10)	26.3	16.1	10000	3.7	46	356
PLL(20)-*g*[4.8]-dex(10)	26.3	16.1	10000	4.8	40	278
PLL(20)-*g*[6.5]-dex(10)	26.3	16.1	10000	6.5	59	210
PLL(20)-*g*[8.6]-dex(10)	26.3	16.1	10000	8.6	58	162
PLL(20)-*g*[1.7]-dex(20)	26.3	16.1	20500	1.7	36	1580
PLL(20)-*g*[3.6]-dex(20)	24	14.7	20500	3.6	70	669
PLL(20)-*g*[5.1]-dex(20)	26.3	16.1	20500	5.1	53	520
PLL(20)-*g*[8.8]-dex(20)	26.3	16.1	20500	8.8	69	311
PLL(20)-*g*[3.0]-PEG(5)	25.5	15.6	4834	3	-	212
PLL(20)-*g*[3.6]-PEG(5)	25.5	15.6	4834	3.6	-	180
PLL(20)-*g*[4.4]-PEG(5)	25.5	15.6	4834	4.4	-	150
PLL(20)-*g*[6.6]-PEG(5)	25.5	15.6	4834	6.6	-	105
PLL(20)-*g*[11.2]-PEG(5)	24	14.7	4834	11.2	-	64

4 MACROSCOPIC LUBRICATING PROPERTIES OF PLL-*G*-DEX: INFLUENCE OF THE POLYMER ARCHITECTURE AND COMPARISON TO PLL-*G*-PEG

This chapter is focussed on the characterization of adsorption and aqueous lubricating properties of PLL-*g*-dex copolymers on oxide surfaces under standard, macroscopic tribological conditions at ambient temperature, including sliding and mixed sliding/rolling contacts. In particular, various PLL-*g*-dex copolymers with varying architectural features, including the molecular weight and the grafting ratio of the dextran side chains along the backbone, were synthesized and employed to characterize the relative lubricating capabilities compared with counterpart PLL-*g*-PEG copolymers.

4.1 Experimental

4.1.1 Materials

PLL-*g*-dex copolymers with various architectures (dextran chain length and grafting ratio, i.e. number of lysine monomers/dextran side chain) were synthesized by a reductive amination reaction of PLL-HBr (20 kDa, polydispersity 1.1, Sigma-Aldrich, Switzerland) with dextran (dextran T5, 5 kDa and T10, 10 kDa, polydispersity 1.4-1.8, Pharmacosmos A/S, Denmark). The polymer synthesis and the notation for the copolymers are described in more detail in Section 3.1.

Varying the ratio of Lys/dex allowed for the control of the degree of grafting of dextran chains onto the PLL backbone.

For comparison purposes, PLL(20)-*g*-PEG(5) copolymers provided by SuSoS AG (Dübendorf, Switzerland) have also been investigated, with PEG(5) side chains (molecular weight, 5 kDa) on a PLL(20) backbone and covering a similar range of grafting ratios to that of the PLL-*g*-dex copolymers employed [42].

4.1.2 Optical Waveguide Lightmode Spectroscopy

Optical waveguide lightmode spectroscopy (OWLS) was used to characterize the adsorption properties of the polymers. The operational principle of OWLS is described in detail in Section 2.2.1. Experiments were performed using an OWLS 110 instrument (Microvacuum, Budapest, Hungary).

The refractive index increment (dn/dc) of dextran was measured by means of a refractometer and a value of 0.131 was used for all measurements to calculate the mass of polymer adsorbed. For PLL-*g*-PEG copolymers a value of 0.139 was always used [43]. Since the dn/dc values of dextran or PEG and PLL are very similar, no dn/dc correction was made for the different structures investigated.

Prior to the experiments, optical waveguides chips (standard: $Si_{0.75}Ti_{0.25}O_2$ on glass, 1.2 × 0.8 cm^2, Microvacuum, Budapest, Hungary) were ultrasonicated in 0.1 M HCl for 10 min, rinsed with Millipore water, ultrasonicated in 2-propanol for 10 min, rinsed again with Millipore water, and then dried under a dry nitrogen stream. The substrates were subsequently cleaned by UV/ozone cleaner (Boeckel industries Inc., model 135500) for 30 min.

The cleaned waveguides were assembled into the OWLS flow cell and equilibrated by exposing to HEPES buffer solution (10 mM 4-(2-hydroxyethyl)piperazine-1-ethanesulfonic acid (Sigma, St. Louis, MO, USA), adjusted to pH 7.4 with 6.0 M NaOH solution) overnight in order to obtain a stable baseline. The waveguides were then exposed to a polymer solution (0.25 mg ml^{-1} in HEPES buffer) for at least 30 min, resulting in the formation of a polymer adlayer, and rinsed three times with buffer solution for another 30 min.

4.1.3 Pin-on-Disk Tribometry

A pin-on-disk tribometer (CSM Instruments, Switzerland) was employed to investigate the lubricating properties of the polymer solutions under pure sliding conditions.

Steel balls (6 mm in diameter, DIN 5401-20 G20, Hydrel AG, Romanshorn, Switzerland) against flat glass squares (2.5 × 2.5 cm^2, 1 mm thick), cut from microscope slides (Medite Medizintechnik AG, Switzerland, approximate chemical composition according to the

manufacturer: 72.2 % SiO_2, 14.3 % Na_2O, traces of K_2O, CaO, MgO, Al_2O_3, Fe_2O_3, SO_3) were used as a tribopair. The lubricating properties of the polymers were evaluated by acquiring the coefficient of friction, μ (= friction force/load), as a function of speed under a fixed load (2 N, dead weights) at room temperature. The maximum Hertzian contact pressure in this configuration is estimated to be 0.5 GPa. The sliding speed was controlled to vary from 1 to 19 mm s^{-1} using the instrument's software (InstrumX version 2.5A, CSM Instruments, Switzerland). The weight concentration of the polymer solutions was chosen in order to attain similar molar concentrations for all copolymers (0.25 mg ml^{-1} for PLL-*g*-dex(5) and PLL-*g*-PEG(5) copolymers and 0.5 mg ml^{-1} for PLL-*g*-dex(10)) with a similar range of grafting ratios as used in the OWLS experiments. The number of rotations was fixed at 200. For each measurement with a given copolymer, the same pair of pin and disk was used. However, the contact point of the ball and the radius of the sliding track on the disk were changed for each speed, to provide fresh tribocontact points. Balls and disks were cleaned immediately before each measurement as follows; they were ultrasonicated in ethanol for 10 min, dried under a nitrogen stream and then oxygen-plasma cleaned for 2 min. All instrumental parts expected to be in contact with the polymer solution were cleaned by rinsing first with ethanol and then with water.

4.1.4 Mini Traction Machine (MTM)

A mini traction machine (MTM, PCS Instruments, London, UK) was employed to characterize the lubricating behavior of the copolymer solutions in a mixed sliding/rolling contact regime. Details on the working principle of the instrument and on the configuration used in this thesis (tribopair, speed range, slide/roll ratio) are presented in Section 2.3.2.

Speed-dependence tests on polymer solutions (0.25 or 0.5 mg ml^{-1} depending on molecular weight) were carried out at a constant load of 10 N (Hertzian contact pressure, 0.42 GPa) and at a controlled temperature (25 °C). The disk track radius was fixed at 21 mm and for each measurement a new ball and a new disk were used. Balls and disks were cleaned according to the same procedure used for pin-on-disk tribometry experiments, except that air-plasma was used instead of oxygen-plasma. The instrumental parts expected to be in contact with the polymer solution were cleaned with a commercial cleaner (Hydrochloric acid 300 mmol/L and detergent 1 %, Roche Diagnostics GmbH, Mannheim, Germany).

4.2 Results and Discussion

4.2.1 Synthesis and Structural Features of PLL-g-dex copolymers

PLL-*g*-dextran copolymers with different molecular weights and grafting ratios of dextran side chains were successfully synthesized and characterized by ^{1}H-NMR. The nominal molecular weights of the selected dextrans were 5 kDa and 10 kDa (denoted as dex(5) and dex(10)). The grafting ratio was varied between roughly *g*[3] and *g*[9] and evaluated by means of NMR and EA. As a reference, a series of PLL(20)-*g*-PEG(5) (20 kDa for the molecular weight of PLL backbone and 5 kDa for the molecular weight of PEG side chains) with varying grafting ratios, roughly *g*[3] to *g*[11], were purchased from SuSoS AG (Dübendorf, Switzerland). In Table 4.1, the structural features of the synthesized copolymers are presented in detail.

It should be noted that the two dextran polymers with different molecular weights in this work, dex(5) and dex(10), were selected to maintain the structural features that may critically influence adsorption and lubricating properties comparable with those of PLL(20)-*g*-PEG(5). Firstly, dex(5) is nearly identical with PEG(5) in molecular weight, and thus can be employed to generate PLL-*g*-dex copolymers with similar molecular weights to those of PLL-*g*-PEG at the same grafting ratio. As will be addressed below, the molecular weights of the copolymers need to be comparable when the diffusion properties of copolymers through the liquid medium play an important role in the lubricating behavior.

PEG(5) is composed of 109.9 monomer units (ethylene glycol (EG)), whose fully extended chain length is estimated to be 39.3 nm (based on the molecular length of EG, 0.358 nm [77]), whereas dex(5) is composed of 31.8 monomer units (sugar rings), whose fully extended chain length is estimated to be only 22.3 nm (based on the molecular length of dextran: 0.7 nm [78]). While the lubricating film thickness generated by the adsorption of comb-like copolymer will be determined by many parameters, the fully extended length of side chains will set the upper bound of the film thickness. For this reason, dex(10) (fully extended length, 43.2 nm) was employed to generate PLL-*g*-dex copolymers that can potentially generate comparable film thicknesses with those of PLL-*g*-PEG(5) copolymers. The molecular weights of PLL-*g*-dex(10) are, of course, significantly higher than those of PLL-*g*-dex(5) or PLL-*g*-PEG(5) at the same grafting ratio (see Table 4.1).

Table 4.1 Matrix of all copolymers (synthesized PLL-*g*-dex copolymers and PLL-*g*-PEG copolymers used for comparison purpose) employed in this study, with the names of the copolymers, the number of grafted side chains and of free lysines per PLL, the percentage of side-chain grafting and the molecular weights of the copolymers.

Polymer	No. of grafted side chains per PLL	No. of free lysines per PLL	Percentage of side-chain grafting (%)	MW [kDa]
PLL(20)-*g*[3.4]-dex(5)	37.0	88.8	29.4	207
PLL(20)-*g*[5.3]-dex(5)	23.7	102.1	18.9	139
PLL(20)-*g*[6.6]-dex(5)	19.1	106.8	15.2	114
PLL(20)-*g*[7.3]-dex(5)	17.2	108.6	13.7	105
PLL(20)-*g*[8.7]-dex(5)	14.5	111.4	11.5	91
PLL(20)-*g*[3.7]-dex(10)	34.0	91.8	27.0	356
PLL(20)-*g*[4.8]-dex(10)	26.2	99.6	20.8	278
PLL(20)-*g*[6.5]-dex(10)	19.4	106.5	15.4	210
PLL(20)-*g*[8.6]-dex(10)	14.6	111.2	11.6	162
PLL(20)-*g*[3.0]-PEG(5)	40.7	81.3	33.3	212
PLL(20)-*g*[4.4]-PEG(5)	27.7	94.3	22.7	150
PLL(20)-*g*[6.6]-PEG(5)	18.5	103.5	15.2	105
PLL(20)-*g*[11.2]-PEG(5)	10.3	104.6	8.9	64

4.2.2 Adsorption Behavior of PLL-g-dex: OWLS

A representative adsorption profile for PLL-*g*-dex copolymer onto the oxide surface as characterized by OWLS is presented in Fig. 4.1 (for the case of PLL(20)-*g*[3.4]-dex(5)).

Upon exposure of a waveguide surface to the polymer solution (after ca. 60 min exposure to HEPES buffer to achieve the baseline), the adsorption of PLL-*g*-dex proceeded very rapidly so that more than the 90% of the final mass of adsorbed polymer was reached within the first 5 min. Since the raw data signals (change in the refractive index) at this stage reflect the contributions from both the surface-bound polymers and the bulk polymer solution, the final adsorbed mass was determined after the flow cell was rinsed with buffer solution (after ca. 50 min exposure to the polymer solution) to exclude the contribution from the bulk solution and loosely bound polymers. The negligible reduction in the adsorbed mass after the rinse indicates that no noticeable polymer desorption occurred during rinsing and assures the formation of a stable polymer adlayer. The same procedure was repeated for all the PLL-*g*-dex and PLL-*g*-PEG copolymers, as well as dex(5). The resulting adsorbed masses per unit area are presented as a function of grafting ratio for the series of PLL-*g*-dex(5), PLL-*g*-dex(10), and PLL-*g*-PEG(5) copolymers, as shown in Fig. 4.2.

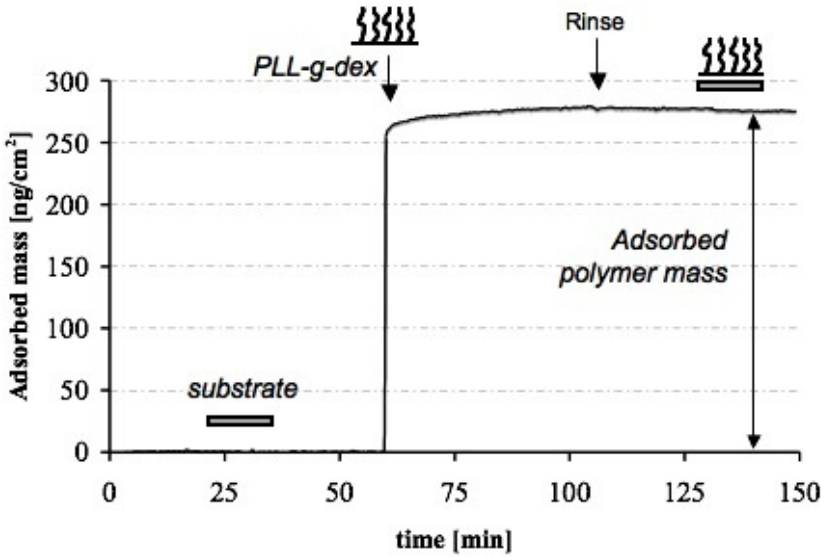

Fig. 4.1 In situ OWLS measurement of the polymer adsorption from solution onto uncoated waveguide chips.

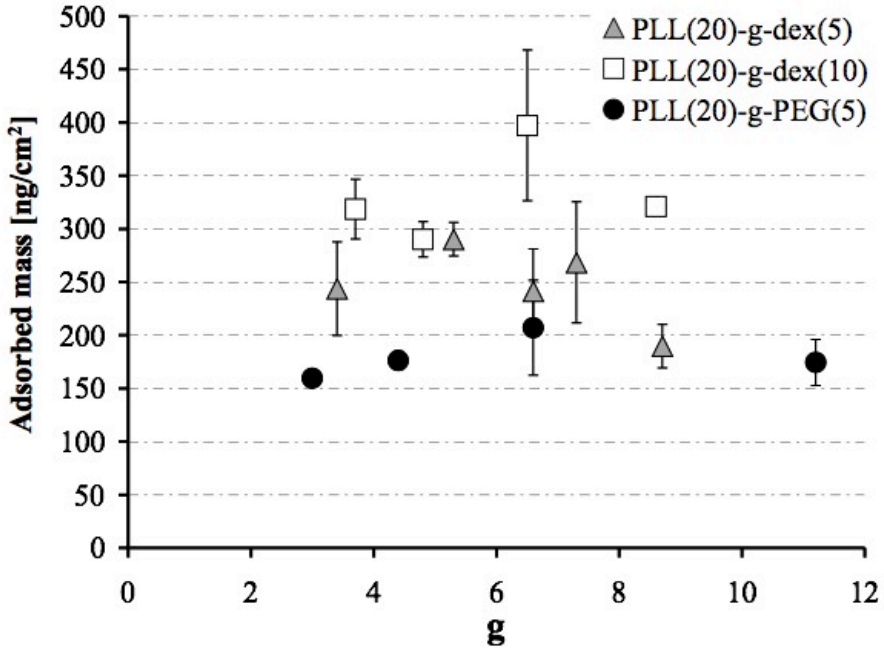

Fig. 4.2 OWLS results for the adsorption of PLL-*g*-dex copolymers and the counterpart PLL-*g*-PEG copolymers employed in this work. For some data points, error bars are smaller than the symbols.

All the copolymers employed in this study showed a significant amount of adsorption onto the OWLS waveguide surfaces, ranging from ca. 200 to 290 ng cm^{-2} for PLL-*g*-dex(5), ca. 290 to 400 ng cm^{-2} for PLL-*g*-dex(10), and ca. 160 to 210 ng cm^{-2} for PLL-*g*-PEG(5) on

average (see Table 4.2 and Fig. 4.2). Meanwhile, dextran (dex(5)) alone revealed negligible adsorption onto the surfaces (5.6 ± 3.7 ng cm^{-2}). This observation supports the hypothesis that both the adsorption mechanism and the conformation of the PLL-*g*-dex copolymer on negatively charged surfaces are very similar to those of PLL-*g*-PEG copolymer [42, 43, 47]; the adsorption of the copolymer proceeds through an electrostatic interaction between the PLL backbone and the surface in an aqueous environment, and thus the PLL backbone generally lies flat on the substrate surface, whereas the dextran side chains stretch into bulk aqueous solution due to their hydrophilic characteristics, forming brush layers.

Table 4.2 Summary of the adsorption data determined by OWLS for the synthesized PLL-*g*-dex copolymers. (m_{pol} = adsorbed polymer mass, n_{lys} = surface density of lysine monomers, $n_{dex\ or\ PEG}$ = surface density of dextran or PEG, $n_{monomer\ units}$ = surface density of the monomer units of dextran or PEG, L = spacing between grafted dextran/PEG chains, $L/2R_g$ = degree of overlap of dextran/PEG chains).

Surface-bound copolymer	m_{pol} [ng/cm^2]	n_{lys} [1/nm^2]	$n_{dex\ or\ PEG}$ [1/nm^2]	$n_{monomer\ units}$ [1/nm^2]	L [nm]	L/2Rg
PLL(20)-*g*[3.4]-dex(5)	244 ± 44	0.89 ± 0.20	0.26 ± 0.05	8.36 ± 1.51	2.12 ± 0.21	0.45 ± 0.04
PLL(20)-*g*[5.3]-dex(5)	290 ± 16	1.59 ± 0.09	0.30 ± 0.02	9.53 ± 0.52	1.96 ± 0.05	0.42 ± 0.01
PLL(20)-*g*[6.6]-dex(5)	241 ± 40	1.60 ± 0.26	0.24 ± 0.04	7.71 ± 1.27	2.19 ± 0.18	0.47 ± 0.04
PLL(20)-*g*[7.3]-dex(5)	269 ± 57	1.94 ± 0.41	0.27 ± 0.06	8.45 ± 1.80	2.10 ± 0.22	0.45 ± 0.05
PLL(20)-*g*[8.7]-dex(5)	190 ± 21	1.59 ± 0.17	0.18 ± 0.02	5.80 ± 0.62	2.52 ± 0.14	0.54 ± 0.03
PLL(20)-*g*[3.7]-dex(10)	319 ± 28	0.68 ± 0.06	0.18 ± 0.02	11.31 ± 0.99	2.51 ± 0.11	0.36 ± 0.02
PLL(20)-*g*[4.8]-dex(10)	290 ± 17	0.79 ± 0.05	0.16 ± 0.01	10.16 ± 0.58	2.65 ± 0.08	0.38 ± 0.01
PLL(20)-*g*[6.5]-dex(10)	397 ± 71	1.44 ± 0.26	0.22 ± 0.04	13.63 ± 2.43	2.31 ± 0.21	0.33 ± 0.03
PLL(20)-*g*[8.6]-dex(10)	321 ± 2	1.50 ± 0.01	0.17 ± 0.00	10.75 ± 0.07	2.57 ± 0.01	0.37 ± 0.00
PLL(20)-*g*(3)-PEG(5)	160 ± 3	0.54 ± 0.00	0.19 ± 0.00	20.44 ± 0.07	2.49 ± 0.00	0.44 ± 0.00
PLL(20)-*g*[4.4]-PEG(5)	176 ± 9	0.84 ± 0.04	0.20 ± 0.01	21.62 ± 1.07	2.42 ± 0.06	0.43 ± 0.01
PLL(20)-*g*[6.6]-PEG(5)	207 ± 45	1.41 ± 0.30	0.22 ± 0.05	24.12 ± 5.17	2.32 ± 0.23	0.41 ± 0.04
PLL(20)-*g*[11.2]-PEG(5)	174 ± 22	1.82 ± 0.22	0.17 ± 0.02	18.37 ± 2.25	2.64 ± 0.16	0.47 ± 0.03

As shown in Fig. 4.2, the PLL-*g*-dex(10) copolymers employed in this work lead to either comparable or slightly higher adsorbed masses compared to PLL(20)-*g*-dex(5) copolymers, whereas both of them show somewhat higher adsorbed masses compared to PLL(20)-*g*-PEG(5) copolymers. In addition, for all three groups of copolymers the adsorbed mass is not significantly influenced by the variation in grafting ratio within the range selected in this study. The adsorbed mass is the product of the molecular weight of each copolymer molecule and the number of molecules adsorbed on the surface. Since the (average) molecular weights of the copolymers are precisely known from their structures, more insights into the adsorption behavior of the copolymers can be obtained by decomposing their adsorbed mass into various coverage parameters, as shown in Fig. 4.3.

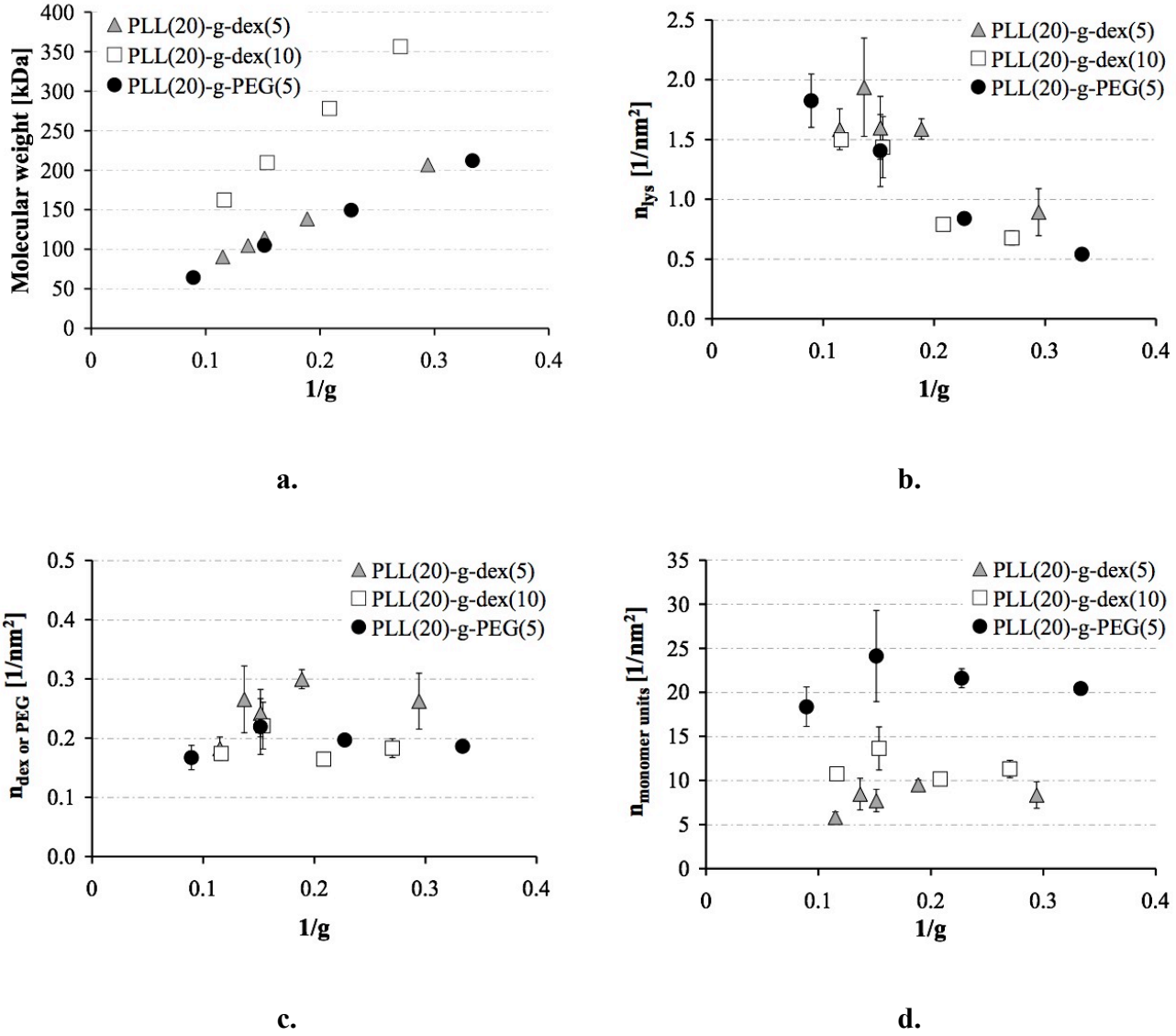

Fig. 4.3 Molecular weight (**a.**), lysine monomer density (n_{lys}) (**b.**), dextran (n_{dex}) or PEG (n_{PEG}) chain density (**c.**), and density of the monomer units of dextran or PEG ($n_{monomer\ units}$) (**d.**) of the synthesized PLL-*g*-dex copolymers and the counterpart PLL-*g*-PEG copolymers on the silica-titania surface. For some data points, error bars are smaller than the symbols.

Firstly, the molecular weights of the copolymers are shown as a function of the inverse of grafting ratio, 1/*g*, in Fig. 4.3(a); in this plot, increasing the value of 1/*g* represents the increase in the number of grafted side chains along the PLL backbone. Generally, the molecular weight of the copolymer increases linearly with increasing 1/*g* values, due to increasing number of grafted side chains. The variation of molecular weight as a function of grafting ratio is nearly identical for PLL-*g*-PEG(5) and PLL-*g*-dex(5), while the molecular weights of PLL-*g*-dex(10) copolymers are much higher. In turn, from the adsorbed mass and the compositional features of the copolymers, it is possible to calculate the surface

concentration of lysine monomers, n_{lys}, and dextran or PEG chains, $n_{dex\ or\ PEG}$. The surface concentration of lysine monomers, n_{lys}, reflects the number of copolymer molecules on the surface, whereas the surface density of dextran or PEG chains reflects the efficacy of the copolymer in grafting the hydrophilic polymer chains (either dextran or PEG) onto the surface. For the case of dextrans, since two different molecular weights (dextran chain lengths) were employed to generate PLL-*g*-dex copolymers in this study, the efficacy of grafting hydrophilic moieties can be expressed by the surface concentration of dextran monomer units (sugar rings) or EG units, $n_{\text{monomer units}}$ [43]. The surface concentration of lysine monomers, n_{lys}, dextran or PEG chains, n_{dex} or n_{PEG}, and monomer units of them, $n_{\text{monomer units}}$, are plotted as a function of the inverse of grafting ratio, 1/*g*, in Fig. 4.3(b), (c), and (d), respectively. Finally, the mean spacing between the dextran chains, *L*, as well as the ratio between the spacing and the radius of gyration of dextran chains, $L/2R_g$, can be obtained to estimate the conformation of the surface-grafted dextran or PEG chains [43]. The results of these calculations are summarized in Table 4.2.

As shown in Fig. 4.3(b), the surface concentrations of lysine monomers, n_{lys}, for PLL(20)-*g*-dex(5) copolymers show roughly constant values until 1/*g* reaches ca. 0.2, and yet rapidly decrease at higher 1/*g* values. Degraded adsorption with increasing number of side chains (increasing 1/*g*) may be due either to the decreasing number of anchoring units (free NH_3^+) and/or increasing steric hindrance between grafted side chains. A previous study [43] involving PLL(20)-*g*-PEG and varying the molecular weight of PEG side chains, including PEG(1), PEG(2), and PEG(5), has, however, confirmed that this trend is mainly driven by the steric hindrance between side chains; a decrease in n_{lys} with increasing 1/*g* was observed in the cases of PLL(20)-*g*-PEG(2) and PLL(20)-*g*-PEG(5), but not in the case of PLL-*g*-PEG(1), which has smaller steric hindrance between side chains as a consequence of the PEG(1)'s smaller radius of gyration. For PLL(20)-*g*-dex(10) and PLL(20)-*g*-PEG(5), a linear decrease of n_{lys} is observed from $1/g \approx 0.1$ to the highest value of ≈ 0.33, which implies that the steric hindrance between dex(10) or PEG(5) is more serious than in the case of dex(5). The radii of gyration for the three hydrophilic polymers are in the order dex(5) (2.35 nm [79]) < PEG(5) (2.82 nm [80]) < dex(10) (3.49 nm [79]).

The surface density of dextran or PEG chains, Fig. 4.3(c), is thus proportional to the product of the n_{lys} and the number of side chains per molecule, which also linearly increases with increasing 1/*g* values (see the Table 4.1). For PLL(20)-*g*-dex(5) copolymers, the increase in number of grafted side chains *on the backbone* leads to a proportional increase in the grafted side chains *on the surface* in the initial 1/*g* range of 0.1 ~ 0.2, and yet n_{dex} reaches a

plateau at higher 1/*g* values. Apparently, this plateau is a result of opposing effects with increasing 1/*g*—the decreasing number of copolymers on the surface, as shown by the decrease of n_{lys}, and increasing number of grafted side chain on the backbone. The radii of gyration for dex(10) and PEG(5) are larger than that of dex(5) and the plateau for the corresponding copolymers is already reached at $1/g = 0.1$. Finally, the monomer densities, as shown in Fig. 4.3(d), reveal nearly the same trends with those of n_{dex} or n_{PEG}, the relative magnitude between dex(5) and dex(10) being reversed.

4.2.3 Lubrication Properties of the Copolymers

In order to evaluate the lubricating properties of PLL-*g*-dex copolymer solutions and compare them with other standard aqueous solutions, including HEPES buffer solution, dextran solution (dex(5)), as well as PLL(20)-*g*-PEG(5) solutions, coefficient of friction (μ) vs. speed plots were acquired under both sliding and mixed sliding/rolling conditions using a pin-on-disk tribometer and MTM, respectively.

The lubricating capabilities of the copolymers in this work are considered to be directly associated with their adsorption properties onto the tribopair surfaces. Although the adsorption properties of the copolymers onto the pins (stainless steel) remain uncharacterized, the OWLS measurements shown in the previous section can represent the adsorption properties of the copolymers on the disk (glass) since silicon oxides prevail on both the waveguide and the glass disk surfaces. Given that not only adsorbed masses but also lysine monomer densities, n_{lys}, hydrophilic polymer chain densities, n_{dex} or n_{PEG}, as well as the hydrophilic monomer unit densities, $n_{monomer\ units}$, can be deduced from OWLS measurements (Table 4.2 and Fig. 4.3), it is of interest to see with which structural parameter the lubricating properties are best correlated.

In macroscopic sliding contacts between two rigid surfaces, as in this work, the lubricating capabilities of the copolymers are expected to be further influenced by their adsorption kinetics. As was previously addressed in a study employing fluorescently labeled PLL-*g*-PEG copolymers [38], the electrostatically adsorbed polymer layers are easily scraped away from the surfaces during sliding contacts in pin-on-disk tribometry, particularly due to asperity contacts arising from surface roughness and consequently high local contact pressures. Nevertheless, the excess polymers in bulk solution, if present, re-adsorb onto the area where the initially adsorbed copolymers have been desorbed, and the tribostressed area ‘self-heals’. In other words, effective lubrication of electrostatically adsorbed copolymers over a long period in the presence of excess polymer in bulk solution is rather due to their fast adsorption

kinetics than their adsorption strength. An important prerequisite to test the efficacy of the copolymers as lubricant additives and to take into account their surface adsorption kinetics behavior is to keep constant the *number* of excess polymer molecules, i.e. their molar concentration available to 'heal' the tribostressed area. For this reason, we have doubled the mass concentration of PLL(20)-*g*-dex(10) copolymers, 0.5 mg ml^{-1}, with respect to those of PLL(20)-*g*-dex(5) and PLL(20)-*g*-PEG(5) copolymers, 0.25 mg ml^{-1}, for the tribological tests. If the mass concentrations were kept constant for all the copolymers, the molar concentrations of PLL-*g*-dex(10) copolymers would be significantly lower than those of the other two types of copolymers, as shown in Fig. 4.4.

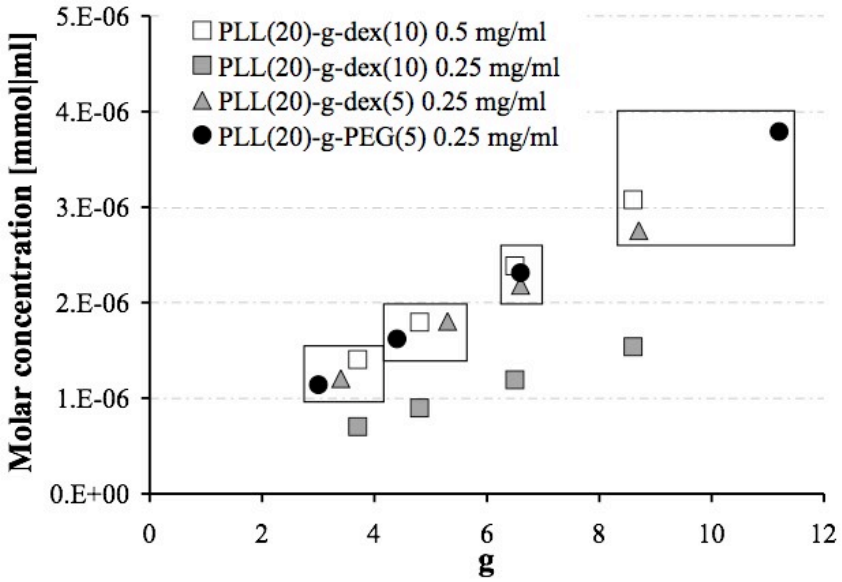

Fig. 4.4 Molar concentration [mmol/ml] of the copolymer solutions employed in this work (highlighted in the squares the concentrations chosen for the characterization of the lubricating properties of PLL-*g*-dex and the counterpart PLL-*g*-PEG).

Lubrication at Sliding Contacts: Pin-on-Disk Tribometry

Sliding-contact experiments, carried out by pin-on-disk tribometry, were intended to assess the lubricating capabilities of the polymer solutions in the boundary-lubrication regime. To compare the relative lubricating properties of three kinds of copolymers, PLL(20)-*g*-dex(5), PLL(20)-*g*-PEG(5), and PLL(20)-*g*-dex(10), they were grouped mainly according to grafting ratio (*x*-axis) as shown in Fig. 4.4. As mentioned above, this was to keep the molar concentration (*y*-axis) nearly constant for the copolymers employed for the comparison. As shown in Fig. 4.5, all copolymer solutions employed in this work led to apparent reduction in μ values compared to HEPES buffer solution (as much as 50% for most copolymers at speeds

above 10 mm s^{-1}, generally ca. 30% reduction at lower speeds). In contrast, the dex(5) solution revealed negligible improvement in the lubricating properties. This behavior is consistent with the very low adsorption of dex(5) onto the oxide surfaces, as determined by OWLS measurements.

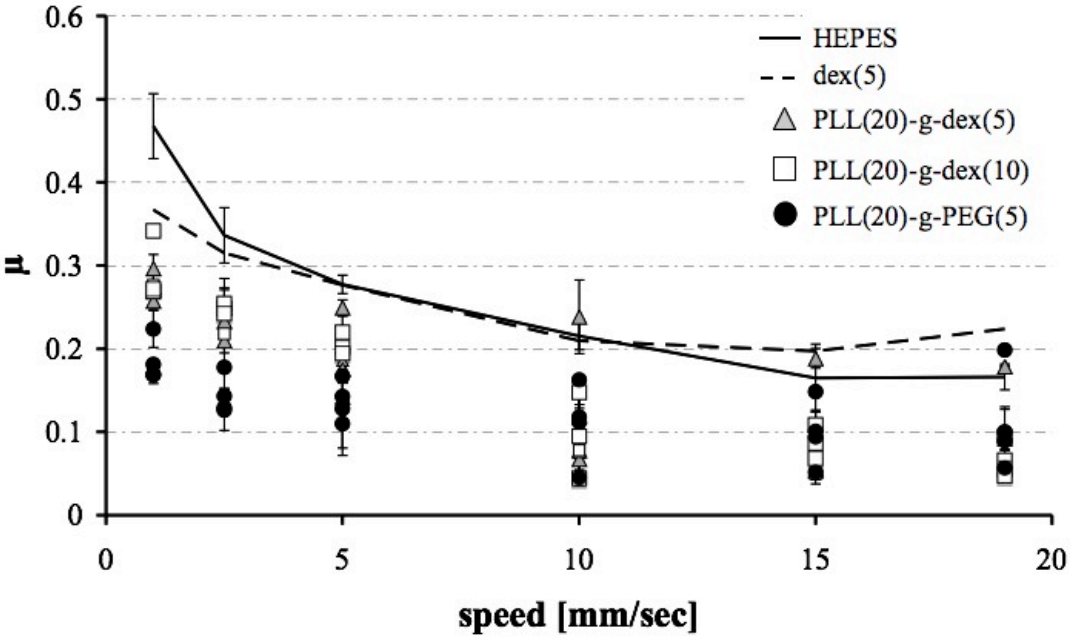

Fig. 4.5 Sliding pin-on-disk results of all PLL-*g*-dex and PLL-*g*-PEG copolymers (with grafting ratio varying from *g*[3] to *g*[11]) investigated in this work (tribopair: steel balls vs glass disks, load: 2 N, room temperature): coefficients of friction (μ) as a function of the sliding speed.

To highlight the comparison of the lubricating properties of PLL-*g*-PEG and PLL-*g*-dex, however, the data for the HEPES buffer solution and dex(5) are omitted in subsequent figures.

The μ vs. speed plots for the copolymers with ~ *g*[3.5], *g*[4.8], *g*[6.5], and high *g*[y], between ca. *g*[8] and *g*[11] (average values) are plotted in Fig. 4.6(a), (b), (c) and (d) respectively.

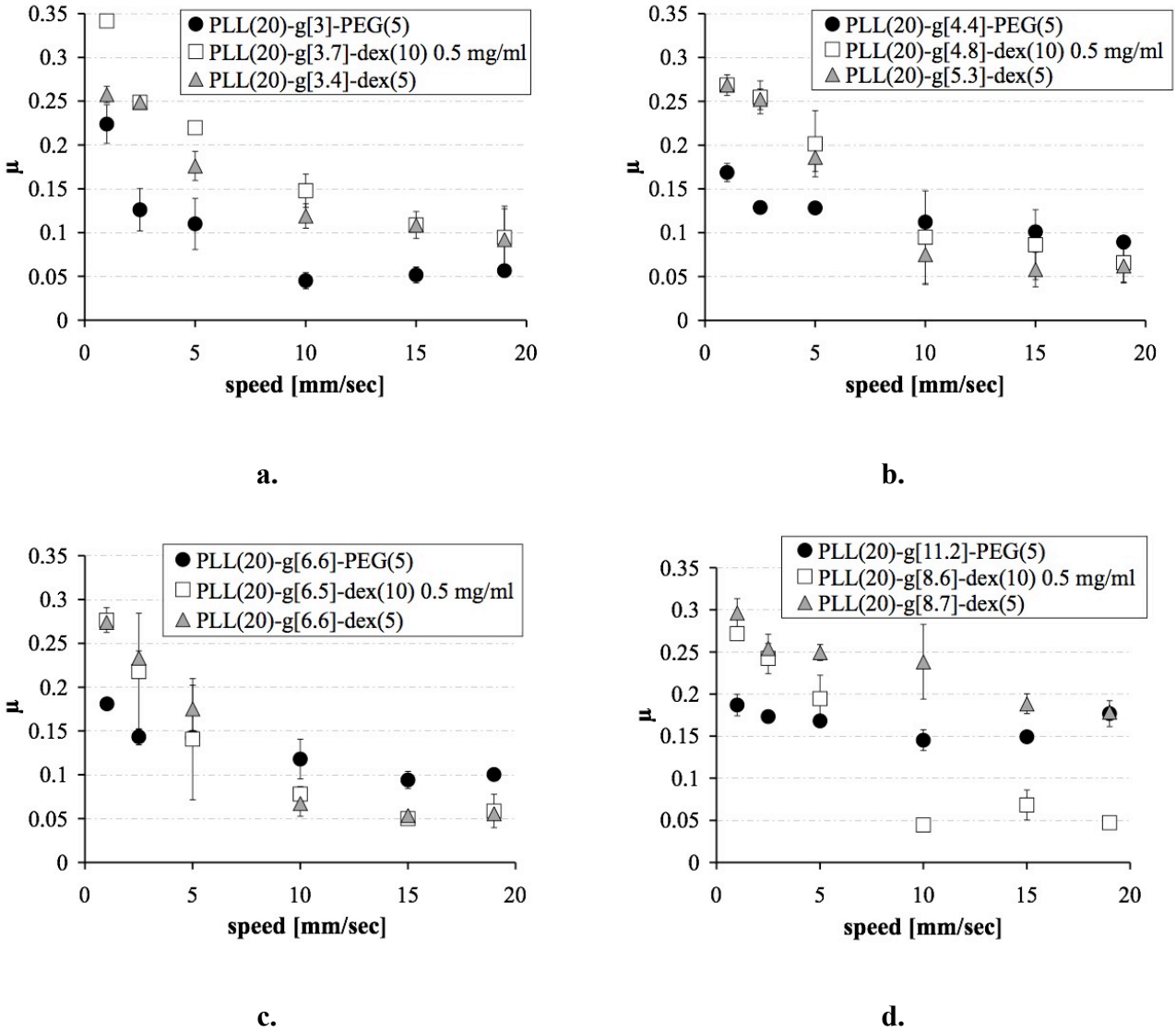

Fig. 4.6 Sliding pin-on-disk results of the PLL-*g*-dex copolymers and PLL-*g*-PEG counterparts with ca. *g*[3.5], (**a.**), ca. *g*[4.8], (**b.**), ca. *g*[6.5], (**c.**) and high grafting ratio, between ca. *g*[8] and *g*[11], (**d.**): coefficients of friction as a function of the sliding speed. For some data points, error bars are smaller than the symbols.

Generally, μ values (load = 2 N) of the copolymer solutions revealed an initial reduction with increasing sliding speed (corresponding to increasing frequency of tribocontact), but they started to level off from roughly 10 mm s^{-1} to the highest speed investigated, reaching approximately μ = 0.05 for the best-behaving copolymer in each comparison set. As shown in Fig. 4.6(a), for the copolymers possessing the grafting ratio of ~ *g*[3.5], the μ values of the two PLL-*g*-dex solutions were observed to be generally very similar, whereas those of PLL(20)-*g*-PEG(5) are slightly, yet noticeably, lower than the two PLL-*g*-dex solutions over the entire speed regime. For all other cases, as shown in Fig. 4.6(b), (c) and (d), the relative

lubricating efficacy of PLL-*g*-dex copolymers compared to PLL(20)-*g*-PEG(5) was highly dependent upon the sliding speed; in the low-speed regime (≤ 10 mm s^{-1}), the lubricating performance of PLL(20)-*g*-PEG(5) was consistently superior to those of PLL-*g*-dex copolymers. In the high-speed regime (≥ 10 mm s^{-1}), however, PLL-*g*-dex copolymers reveal lower friction forces than PLL(20)-*g*-PEG(5) in most cases. Exceptions are the case of ~*g*[3.5] (Fig. 4.6(a)) and PLL(20)-*g*[8.6]-dex(5) (Fig. 4.6(d)), which has too high a grafting ratio to be in a brush conformation.

To more clearly visualize the relative magnitude of lubricating efficacy of the copolymers employed, and also to visualize the variation of the lubricating properties as a function of architectural features of the copolymers, the μ values representing the characteristics in the low-speed regime (1 mm s^{-1}) and the high-speed regime (19 mm s^{-1}) are plotted against the inverse of grafting ratio, 1/*g*, in Fig. 4.7(a) and Fig. 4.7(b), respectively. It should be borne in mind that all speeds investigated in the pin-on-disk studies correspond to the boundary lubrication regime, and that the frequency of tribocontact is the parameter that is being investigated via speed changes.

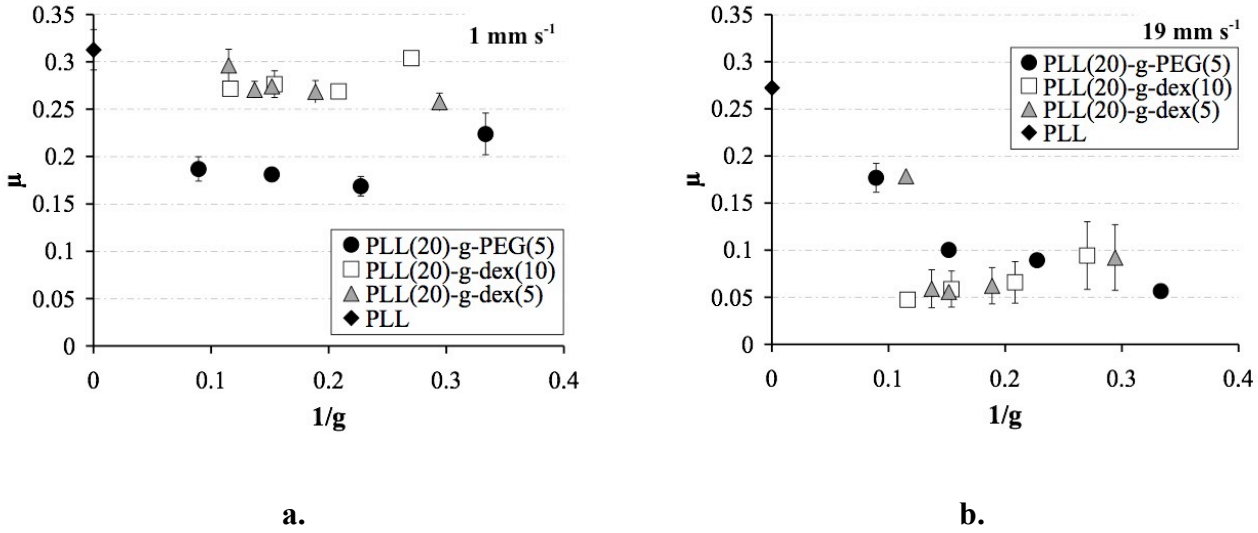

Fig. 4.7 Sliding pin-on-disk results of all PLL-*g*-dex and PLL-*g*-PEG copolymers investigated in this work at the lowest (1 mm s^{-1}), (**a.**), and highest (19 mm s^{-1}), (**b.**), speed investigated: coefficients of friction as a function of the degree of grafting of the side chains, 1/g. For some data points, error bars are smaller than the symbols.

In the low-speed regime, Fig. 4.7(a), the μ values of PLL(20)-*g*-PEG(5) compared to PLL-*g*-dex copolymers are, again, consistently lower over the entire range of grafting ratio. Since the magnitudes of extension of the PEG and dextran chains, as quantified by $L/2R_g$, are comparable for the PLL(20)-*g*-PEG(5) and PLL(20)-*g*-dex(5) copolymers (see the Table 4.2),

and in fact, those of PLL(20)-*g*-dex(10) are even greater (lower values of $L/2R_g$) than PLL(20)-*g*-PEG(5), it is unlikely that the difference in the conformation of the two different hydrophilic polymer chains on the surface is the principal cause of the superior lubricating properties of PLL(20)-*g*-PEG(5) under these conditions. Furthermore, based upon $L/2R_g$ values and the fully extended lengths of PEG(5) and dex(10), the film thicknesses are also estimated to be comparable for the two hydrophilic polymer chains. We thus speculate that dextran and PEG chains may display different innate water-based lubricating capabilities, mainly arising from different degrees and mechanisms of hydration and/or differences in the stiffness and/or dynamical behavior of the chains [81]. Quantitative measurements of the hydration for PLL-*g*-PEG and PLL-*g*-dex copolymers are presented in detail in Chapter 8.

From Fig. 4.7(a), it is also noticeable that the μ values of all the copolymers remain nearly constant over the entire range of grafting ratio, except for the onset of an increase in μ for PLL-*g*-PEG(5) and PLL-*g*-dex(10) at the highest $1/g$ value, i.e. the highest number of grafted side chains along the PLL backbone. It is important to note that although the molar concentrations of the copolymers were controlled to be constant for each set of three copolymers with similar grafting ratio, the molar concentrations of the copolymer do, of course, increase with increasing grafting ratio, (i.e. decrease with increasing $1/g$) as shown in Fig. 4.4. Thus, the molar concentrations of the copolymers shown in Fig. 4.7(a) are different as much as a factor of three. In turn, generally constant μ values observed over the entire $1/g$ range in Fig. 4.7(a) suggest that the lubricating properties in the low-speed regime are not sensitively influenced by the variation of the molar concentration. As will be discussed in more detail below, this feature is in stark contrast to the lubricating behavior in the high-speed regime, and indicates that the lubricating properties of the copolymers in the low-speed regime are mainly governed by the adsorption properties in equilibrium, since the solution concentration is considerably in excess of that necessary to achieve monolayer coverage on the sliding surfaces.

Comparing the various parameters representing adsorption properties of the copolymers, including adsorbed mass, the surface densities of lysine units, n_{lys}, surface densities of dextran or PEG chains, n_{dex} or n_{PEG}, surface densities of monomer units of dextran or PEG, $n_{monomer\ units}$, and the magnitude of brush extension, $L/2R_g$ (Table 4.2 and Fig. 4.3), the lubricating properties appear to be most highly correlated with the surface densities of dextran or PEG chains, albeit not in a simple, linear fashion; both lubricating properties and surface densities were generally insensitive to the variation of grafting ratio within the selected range. The onset of the increase in μ values observed from PLL-*g*-PEG(5) and PLL-*g*-dex(10), but not

from PLL-*g*-dex(5), is associated with the radius of gyration for the side chains changing in the order of dex(5) < PEG(5) < dex(10). As was previously addressed, too high a number of the grafted side chains along the PLL backbone tends to degrade the adsorption properties of comb-like graft copolymers, and consequently their lubricating properties. Since the steric hindrance between neighboring side chains plays a major role in this trend, larger radii of gyration of the side chains are expected to exacerbate such behavior.

In the high-speed regime, Fig. 4.7(b), μ values of all copolymers employed in this work fall in the same range, between 0.05 and 0.1, with the exception of the two values for PLL(20)-*g*[11.2]-PEG(5) and PLL(20)-*g*[8.7]-dex(5), which show significantly higher μ values (close to that of the PLL backbone alone ($1/g = 0$)) and are presumably not in a brush conformation.

PLL(20)-*g*-dex(5) and PLL(20)-*g*-dex(10) copolymers behave similarly in the regime where $1/g \geq$ ca. 0.15, their coefficient of friction slightly increasing in a fairly linear fashion. In the same regime ($1/g \geq$ ca. 0.15) PLL(20)-*g*-PEG(5) copolymers instead show a small decrease in the μ values. A general increase in μ values for PLL-*g*-dex copolymers with high $1/g$ values (high number of grafted side chains) can be readily understood in terms of smaller molar concentrations. The fact that the variation of molar concentration (from ca. 1×10^{-6} mmol/ml to ca. 4×10^{-6} mmol/ml) influences the lubricating properties of the PLL-*g*-dex copolymers exclusively in high-speed regime is closely related to the time intervals between the cycles of tribostress. Under the experimental conditions (pin-on-disk tribometry), the tribostress is applied in a cyclic fashion, the sliding speed (or rpm, to be more precise) setting the time scale during which excess polymers can replenish the area where initially adsorbed polymers may have been detached by tribostress.

With increasing $1/g$, PLL-*g*-dex copolymers become heavier (higher molecular weight) and therefore slower in returning to the surface after being scraped away from it during sliding contact; furthermore, as mentioned above, the molar concentration decreases as the degree of grafted side chains increases, meaning that the excess polymer in bulk solution available to re-adsorb, i.e. "self-heal" the tribostressed area, decreases as well.

The slight decrease of μ values for PLL(20)-*g*-PEG(5) with increasing $1/g$ suggests that the adsorption kinetics of PLL(20)-*g*-PEG(5) copolymers, unlike that of PLL-*g*-dex copolymers, are sufficiently fast that the variation of the molar concentration within the range of 1×10^{-6} mmol/ml to 4×10^{-6} mmol/ml does not lead to any substantial disadvantages in the lubricating performance. Furthermore the higher flexibility of PEG chains compared to dextran's stiffer

sugar units might facilitate the rearrangement of the polymer molecules on the surface after desorption.

Lubrication at Mixed Sliding/Rolling Contacts: MTM

The lubricating properties of PLL-*g*-dex copolymer solutions under mixed sliding/rolling contact conditions have been characterized by means of MTM. The MTM experiments serve primarily to assess the lubricating properties of the copolymers under milder contact conditions than the pure sliding contacts characteristic of pin-on-disk tribometry. Additionally, due to the much higher speed range available from MTM (up to 2500 mm s^{-1}), the formation of a full fluid-film lubricant layer by the polymer solutions can be investigated. Based on the pin-on-disk tribometry results above, two PLL-*g*-dex(5) copolymers, PLL(20)-*g*[3.4]-dex(5) and PLL(20)-*g*[5.3]-dex(5), which showed slightly different lubricating behavior in sliding contact, have been employed, together with other lubricant solutions. The results are shown in Fig. 4.8.

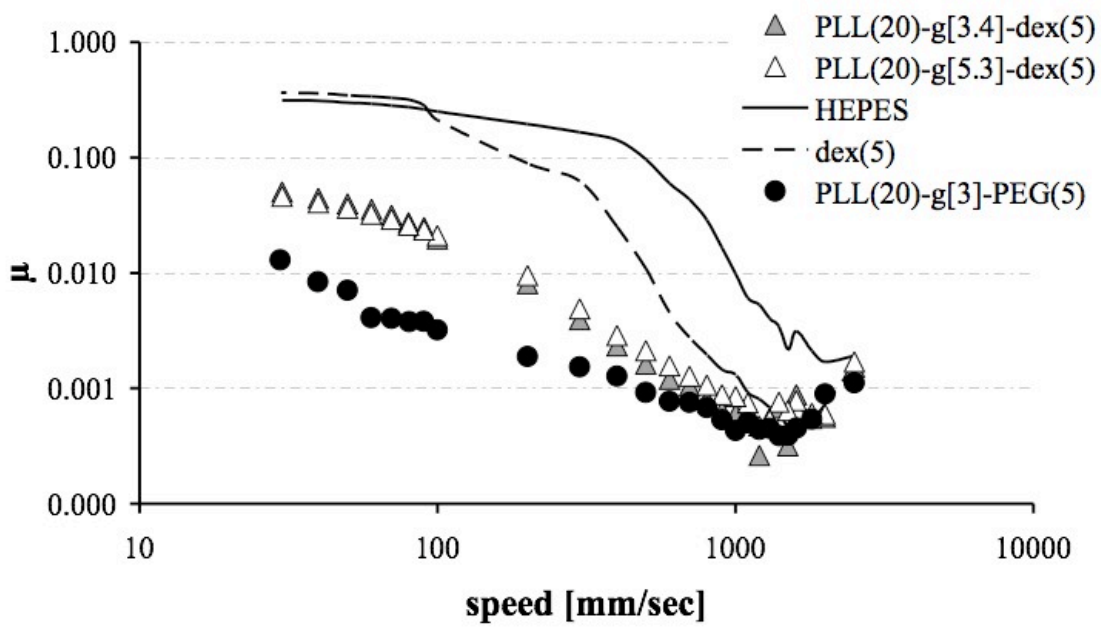

Fig. 4.8 Mixed sliding/rolling MTM results of two selected PLL(20)-*g*-dex(5) copolymers (steel balls vs glass disks, load: 10 N, room temperature): coefficients of friction as a function of the sliding speed.

The μ vs. speed plots shown in Fig. 4.8 revealed significant reduction of μ values in the high-speed regime (starting from ca. 200 mm s^{-1}) for all aqueous lubricants employed, including polymer solutions and polymer-free HEPES buffer solution. The lowest μ value for

HEPES buffer solution, 0.0019, which was achieved at the highest speed (2500 mm s^{-1}), for instance, represents roughly two orders of magnitude reduction compared with the highest μ value, 0.3, observed at the lowest speed (10 mm s^{-1}). This observation suggests that the entrainment of the base lubricant, water, is starting to contribute to the lubrication of this mixed sliding/rolling contact (SRR = 10%) in the high-speed regime. Nevertheless, all the polymer solutions investigated have been observed to further improve the lubricating properties, either in the high-speed regime alone or in both low- and high-speed regimes, depending on the type of polymers. For instance, the dextran solution revealed virtually identical μ vs. speed behavior to that of HEPES buffer in the low-speed regime (≤ 100 mm s^{-1}), whereas a significant reduction in μ was observed in the high-speed regime, as mentioned above. It should be noted that at the dex(5) concentrations employed, no detectable increase in viscosity over that of pure HEPES solution could be detected in shear rheometry measurements (data not shown). Although dex(5) chains do not display noticeable surface-adsorption properties, and thus are poor boundary-lubricating additives, they appear to facilitate the entrainment of aqueous lubricant due to their hydrophilic characteristics [82].

The two PLL-*g*-dex copolymer solutions showed a distinct reduction in μ values, both in low- and high-speed regimes, reflecting their adsorption onto the tribopair surfaces; compared to the dextran solution, the μ values are observed to be consistently lower over nearly the entire speed range investigated. This observation implies that the reduction in μ values in the high-speed regime is not entirely due to the formation of fluid-film, but also partially due to the improvement in the boundary lubrication properties. In fact, previous combined studies of the film thickness and frictional properties by means of ultra-thin film interferometry and MTM, respectively, have shown that the mixed lubrication mechanism is dominant for tribological contacts lubricated by PLL-*g*-PEG aqueous solutions [49]. In contrast to the results for sliding contacts, however, the two PLL-*g*-dex copolymers showed no noticeable difference in their lubricating properties, presumably because of the characteristics of the tribological contacts provided by MTM; firstly, the contact is much milder due to the dominance of rolling contact (SRR = 10%) under these conditions, and thus the readsorption properties of the molecules are less critical. Secondly, the entrainment of the base lubricant, water, becomes more likely with increasing speed, even in the absence of additives.

Lastly, the lubricating performance of the PLL-*g*-dex copolymers under mixed sliding/rolling contact conditions was observed to be inferior to that of PLL(20)-*g*[3.0]-PEG(5). This difference is more noticeable under low-speed conditions, and starts to diminish with increasing speed. PLL(20)-*g*[6.5]-dex(10) and its PLL-*g*-PEG counterpart were also

investigated by MTM, but they showed no difference in terms of the μ-value trend, when compared to the PLL-*g*-dex(5) copolymers employed. These results have therefore been omitted in Fig. 4.8 for clarity purposes, to highlight the results discussed above.

4.3 Conclusions

The macroscopic lubricating properties of PLL-*g*-dex copolymers have been investigated in this study.

Two series of PLL-*g*-dex copolymers, with varying grafting ratios and molecular weights of the dextran side chains (dex(5) and dex(10)), were employed and their lubricating capabilities compared to the PLL-*g*-PEG counterpart copolymers. The investigated copolymers have been shown to adsorb spontaneously onto negatively charged surfaces, similarly to PLL-*g*-PEG, and to behave as boundary lubricants, both in the pure sliding and in mixed sliding/rolling contact regimes. The selection of the two dextrans was motivated by the desire to perform a fair comparison with the PLL-*g*-PEG copolymers: dex(5) is nearly identical with PEG(5) in terms of molecular weight (diffusion properties) and dex(10) and PEG(5) are comparable for the fully extended chain length (generable film thickness). The lubricating properties of the involved copolymers, in the low-speed regime (≤ ca. 10 mm s^{-1}) appeared to be related to the adsorption properties in equilibrium and not to be significantly influenced by the variation of molar concentration. Lubricating performances of PLL-*g*-PEG compared to PLL-*g*-dex copolymers are, in this regime, better over the entire range of grafting ratio: this might be attributed to the higher degree of hydration and flexibility of PEG chains compared to the sugar units in dextran.

In the high-speed regime (≥ ca. 10 mm s^{-1}), all PLL-*g*-dex copolymers, except for the case of *g*[3.5], showed better lubricating performance than the PLL-*g*-PEG counterpart copolymers, but with a slightly different trend in the μ values with increasing 1/*g*; the self-healing behavior of PLL-*g*-dex copolymers seems to be deleteriously affected, in fact, by decreasing molar concentration and increasing of molecular weight. Nevertheless, such changes do not influence the performance of the PLL-*g*-PEG copolymers, presumably due to the greater flexibility of the PEG chains.

5 RESISTANCE TO NON-SPECIFIC PROTEIN ADSORPTION OF PLL-*G*-DEX

In this chapter the protein-resistance properties of PLL-*g*-dex copolymers with two PLL chain lengths and varying grafting ratios are investigated and compared to those of PLL(20)-*g*-PEG(5). OWLS was used to quantitatively determine the polymer and serum adsorption onto silica-titania substrates, and nanotribological analysis by atomic force microscopy (AFM) allowed for distinction between the PLL-*g*-dex copolymers that revealed only slightly different surface adsorption and antifouling properties.

5.1 Experimental

5.1.1 Materials

Poly(L-lysine)-*graft*-dextran (PLL-*g*-dex) copolymers with dex(5.9) side chains on a PLL(13) or PLL(6) backbone and varying grafting ratio between ca. *g*[3] and ca. *g*[10] were provided by Prof. Maruyama (Institute for Materials Chemistry and Engineering, Kyushu University, Japan). Details on the polymer synthesis are reported elsewhere [60, 61].

For comparison purposes, a PLL-*g*-PEG copolymer with the PEG(5) side chains (molecular weight, 5 kDa) onto PLL(20) backbone at the grafting ratio of *g*[3.0], i.e. PLL(20)-*g*[3.0]-PEG(5) provided by Susos AG (Dübendorf, Switzerland), has also been employed [42].

The detailed structural features of the copolymers employed in this study are presented in Table 5.1.

Table 5.1 Matrix of the copolymers employed in this study, with the names of the copolymers, the number of grafted side chains and of free lysines per PLL, the percentage of side-chain grafting and the molecular weights of the copolymers. (The number of lysine units for the PLL-HBr (13 kDa), PLL-HBr (6 kDa), and PLL-HBr (20 kDa), before grafting with dextran or PEG, is 62.2, 28.7 and 122 respectively. The number of monomer units for PEG(5) and dex(5.9) is 109.9 and 36.4 respectively).

Polymer	No. of grafted side chains per PLL	No. of free lysines per PLL	Percentage of side-chain grafting (%)	MW [kDa]
PLL(13)-*g*[3.9]-dex(5.9)	16.0	46.3	25.6	88
PLL(6)-*g*[5.0]-dex(5.9)	5.7	23.0	20.0	28
PLL(13)-*g*[7.1]-dex(5.9)	8.8	53.4	14.1	78
PLL(6)-*g*[10.2]-dex(5.9)	2.8	25.9	9.8	17
PLL(20)-*g*[3.0]-PEG(5)	40.7	81.3	33.3	212

The molecular weight of dextran chains (5.9 kDa) employed in this work was chosen to be comparable to that of PEG (5 kDa) in the PLL-*g*-PEG copolymer selected for comparison. The number of monomer units of dex(5.9), 36.4 sugar rings, is, however, significantly lower than that of corresponding EG units of PEG(5), 109.9, resulting in different chain lengths for the different side chains: the fully extended chain length of dextran(5.9), 25.5 nm, is significantly shorter than that of PEG(5), 39.3 nm (based on the molecular length of monomers: 0.7 nm for dextran [78] and 0.358 nm for ethylene glycol (EG) [77]).

5.1.2 Optical Waveguide Lightmode Spectroscopy

Optical waveguide lightmode spectroscopy (OWLS) was employed to characterize the adsorption properties of the copolymers and to evaluate their ability to prevent non-specific adsorption of proteins. The sensing principle of OWLS is described in detail in Section 2.2.1. Experiments were performed using an OWLS 110 instrument (Microvacuum, Budapest, Hungary).

The optical waveguides chips, the cleaning procedure of the waveguides and the values of refractive index increment (dn/dc) of dextran and PEG used in this study are the same as those reported in Chapter 4.

Compared to the Chapter 4 additional measurement step was carried out for the evaluation of the protein-resistance capabilities of the copolymers investigated. The measurement protocol for the polymer-adsorption step is same with Fig. 4.1, but shown here in Fig. 5.1 is an example of adsorption profile for PLL-*g*-dex (the case of PLL(6)-*g*[5.0]-dex(5.9)) including both the polymer-adsorption and the serum-adsorption step.

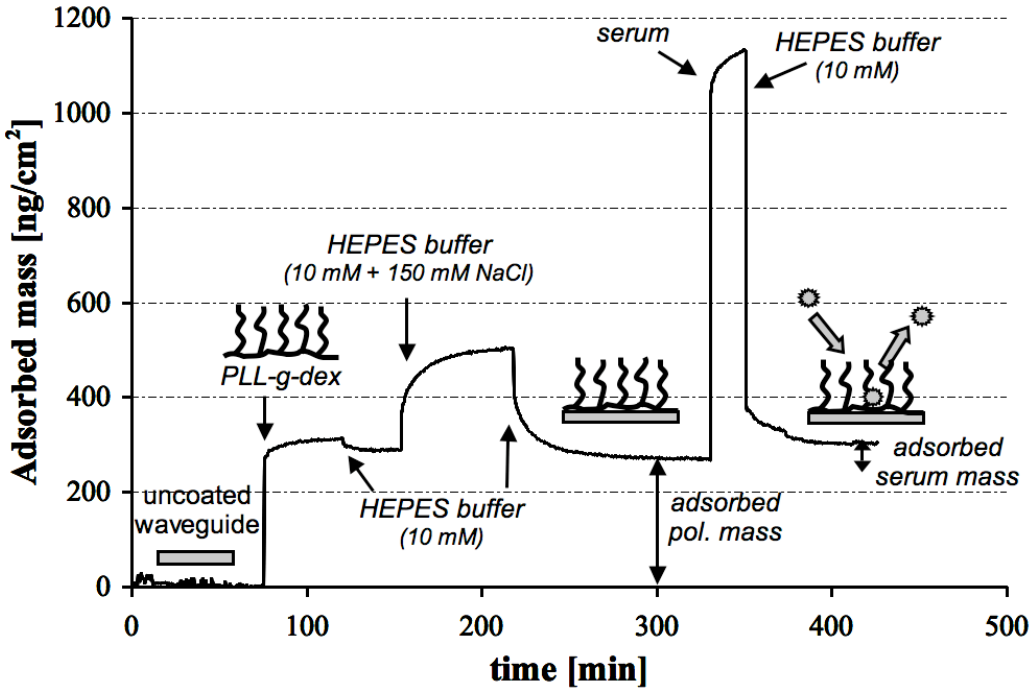

Fig. 5.1 Representative adsorption profile for PLL-*g*-dex copolymer onto a silica-titania waveguide: adsorption of the copolymer (PLL(6)-*g*[5.0]-dex(5.9)) and subsequent exposure to serum.

While low-ionic-strength HEPES was used during the polymer-adsorption step, in order to maximize the adsorbed mass, to condition the polymer layer to the ionic strength used in the subsequent serum-adsorption step for the evaluation of the protein resistance properties, the optical chips were exposed to a higher-ionic-strength HEPES solution (10 mM HEPES with 150 mM NaCl) before exchanging the buffer back to lower-ionic-strength HEPES. The waveguides were finally exposed to a solution of human serum (Control serum, Precinorm® U, Roche, Basel, Switzerland) for 30 min and then rinsed with 10 mM HEPES solution every 15 min for 2 h to check the protein-desorption process.

5.1.3 Atomic Force Microscope

A conventional beam-deflection-based atomic force microscope was employed to characterize the frictional properties of the PLL-*g*-dex copolymers adsorbed on SiO_2 surfaces on the nanometer scale in an aqueous environment. Details about the AFM technique and the apparatus used in this study are provided in Section 2.3.3.

A commercial silicon nitride AFM tip-cantilever assembly (Veeco Inc., Santa Barbara, CA, USA) was used as the counterface to the polymer-modified SiO_2 surfaces. AFM tip-cantilever assembly was air-plasma cleaned (Plasma Cleaner/Sterilizer, PDC-32G instrument,

Harrick, Ossining, NY, USA) for 10 sec immediately before the measurements and kept in distilled water prior to use. Silicon wafers (1.2 cm × 1.2 cm) were ultrasonicated in ethanol for 10 min, rinsed with Millipore water, dried under a nitrogen stream and then oxygen-plasma cleaned for 2 min (Plasma Cleaner/Sterilizer, PDC-32G instrument, Harrick, Ossining, NY, USA). After the cleaning procedure, the substrates were incubated in the polymer solution (0.1 mg ml^{-1}) for 30 min, rinsed with 10 mM HEPES buffer solution and then dried under a nitrogen stream. All measurements were performed in 10 mM HEPES buffer solution.

The nanotribological properties of PLL-*g*-dex copolymers were characterized by the acquisition of "friction-vs-load" plots in a number of areas on each sample [50]. Briefly, the sample was laterally scanned relative to a fixed tip-cantilever assembly position in a line-scan mode while the sample was simultaneously ramped up and then ramped down in vertical direction to provide a variation in normal load. Both normal and lateral deflection of the tip-cantilever assembly generated from the interaction between the probe tip and the sample surface were detected by a 4-quadrant photodiode, and interpreted as the normal load (converted based on the manufacturers' normal spring constant value, k_N = 0.58 N m^{-1}) and the frictional forces (raw photodiode signals), respectively. By plotting the friction forces as a function of normal load, "friction-vs-load" plots were obtained. To ensure a valid comparison of the frictional properties of various samples, the same tip-cantilever assembly was used for all the measurements. Calibration of the cantilever was not performed in this thesis since the main purpose was to distinguish the relative frictional properties of PLL-*g*-dex copolymers on the nanoscale.

5.2 Results and Discussion

5.2.1 Adsorption Properties: OWLS

Quantitative Analysis of Polymer Adsorption

The results of the OWLS experiments (the adsorption profile for PLL(6)-*g*[5.0]-dex(5.9) is shown in Fig. 5.1 as example) indicate that the PLL-*g*-dex copolymers spontaneously adsorb from aqueous solution (10 mM HEPES buffer, pH 7.4) onto metal oxide surfaces. Upon exposure of a waveguide surface to the polymer solution (after 70 min exposure to HEPES buffer to achieve the baseline), the adsorption process occurred rapidly, such that more than 90% of the final mass of adsorbed polymer was reached within the first 5 minutes, and resulted in the formation of a polymer adlayer on the waveguide surface, without significant polymer desorption upon rinsing with buffer solution.

The adsorbed mass of PLL-*g*-dex copolymers reported in Table 5.2 was measured, as well as that of dextran itself and PLL(20)-*g*[3.0]-PEG(5), for comparison purposes: the results are presented in Fig. 5.2. From the adsorbed polymer mass and the compositional features of the copolymers, it is possible to calculate the surface density of dextran chains, n_{dex}, and lysine monomer, n_{lys}, expressed as molecules nm^{-2}, the spacing between side chains, L, and finally to estimate the conformation of the surface-grafted dextran chains by comparing the spacing and the radius of gyration of dextran chains, $L/2R_g$. The results of these calculations are summarized in Table 5.2.

Table 5.2 Summary of the adsorption data determined by OWLS for the PLL-*g*-dex polymers. Data relative to PLL(20)-*g*[3.0]-PEG(5) and dex(5) shown for comparison purposes. (m_{pol} = adsorbed polymer mass, m_{serum} = mass of serum adsorbed, n_{lys} = surface density of lysine monomers, $n_{dex\ or\ PEG}$ = surface density of dextran or PEG, L = spacing between grafted dextran or PEG chains, $L/2R_g$ = degree of overlap of dextran or PEG chains).

Surface-bound copolymer	m_{pol} [ng/cm^2]	m_{serum} [ng/cm^2]	n_{lys} [1/nm^2]	$n_{dex\ or\ PEG}$ [1/nm^2]	L [nm]	L/2Rg
PLL(13)-*g*[3.9]-dex(5.9)	281 ± 12	12 ± 7	1.03 ± 0.05	0.26 ± 0.01	2.09 ± 0.05	0.39 ± 0.01
PLL(6)-*g*[5.0]-dex(5.9)	281 ± 11	35 ± 4	1.29 ± 0.05	0.26 ± 0.01	2.11 ± 0.04	0.39 ± 0.01
PLL(13)-*g*[7.1]-dex(5.9)	307 ± 58	16 ± 11	1.90 ± 0.39	0.27 ± 0.06	2.10 ± 0.22	0.39 ± 0.04
PLL(6)-*g*[10.2]-dex(5.9)	217 ± 2	97 ± 19	1.85 ± 0.02	0.18 ± 0.00	2.52 ± 0.01	0.47 ± 0.00
PLL(20)-*g*(3.0)-PEG(5)	160 ± 3	13 ± 8	0.54 ± 0.00	0.19 ± 0.00	2.49 ± 0.00	0.44 ± 0.00
Dex(5)	6 ± 4	713 ± 32	-	-	-	-

All the PLL-*g*-dex copolymers investigated showed significant adsorption on the OWLS waveguides, ranging from ca. 200 to ca. 300 ng cm^{-2} on average, whereas dextran alone revealed negligible adsorption onto the surfaces (5.6 ± 3.7 ng cm^{-2}). As with PLL-*g*-PEG copolymers, the adsorption of PLL-*g*-dex in an aqueous environment is thought to proceed through the electrostatic interactions between the polycationic PLL backbone and the surface: the dextran side chains stretch out towards the solution and the backbone lies flat on the substrate. In the case of dextran alone, no amino-groups are available for electrostatic interactions, resulting in almost zero adsorption.

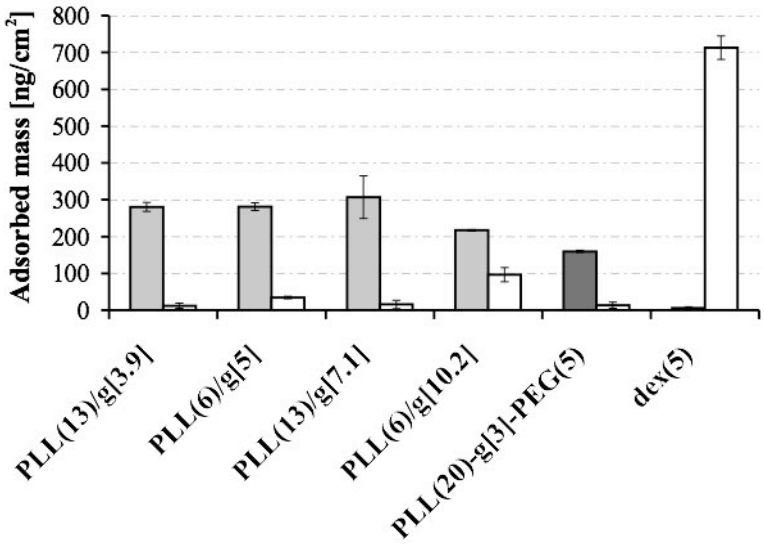

Fig. 5.2 OWLS results for the polymer (filled bars) and serum adsorption (empty bars) onto bare silica-titania waveguides, including all the investigated PLL-*g*-dex copolymers (indicated with the length of the backbone and their grafting ratio), PLL(20)-*g*[3.0]-PEG(5) and dex(5).

The molecular weight (and therefore the length) of the PLL backbone and the density of the grafted dextran side chains along the backbone were the two architectural parameters changed for the synthesis of the PLL-*g*-dex copolymers employed in this work: 6 kDa and 13 kDa PLL backbones were used and the grafting ratio was systematically varied from *g*[3.9] to *g*[10.2]. Despite the variation in these two architectural parameters, the adsorbed masses obtained from the PLL-*g*-dex copolymers employed are nearly constant within the error bars, except for PLL(6)-*g*[10.2]-dex(5.9), which possesses too few dextran side chains, and they showed no clear trend as the molecular weight of the PLL backbone or grafting ratio were changed. The negligible influence of the PLL molecular weight on the adsorption properties is thought to be due to the fact that the length of PLL backbones selected in this work, 6 kDa or 13 kDa, is sufficiently short that a 'flat-lying' conformation of PLL is readily achieved in both

cases. Secondly, the negligible influence of the grafting ratio can be attributed to the opposing effects of the molecular weight of a single PLL-*g*-dex copolymer and the probability of adsorption onto surfaces as a function of the grafting ratio. For instance, the grafting ratios *g*[3.9] and *g*[5.0] for the PLL(13)-*g*[3.9]-dex(5.9) and PLL(6)-*g*[5.0]-dex(5.9) represent very different total numbers of grafted dextran chains on a single copolymer molecule, 16 and 5.7 respectively, and different total molecular weights, 88 kDa and 28 kDa, respectively (structural details are summarized in Table 5.1). In terms of molecular weight, the copolymer with the lowest grafting ratio, *g*[3.9], might show higher mass of surface adsorption due to the higher number of dextran chains per single molecule. The number of anchoring groups (free lysine groups) is, however, higher for higher grafting ratios while at the same time, the steric hindrance between neighboring dextran side chains is smaller, both of which are advantageous for polymer adsorption. The control of the amount of polymer adsorption by the balance between the attractive electrostatic backbone-surface interactions and a steric repulsion between dextran side chains is more directly manifested in the plot of the lysine monomer density (n_{lys}) and the dextran chain density (n_{dex}) of the copolymers as a function of the grafting ratio (Fig. 5.3).

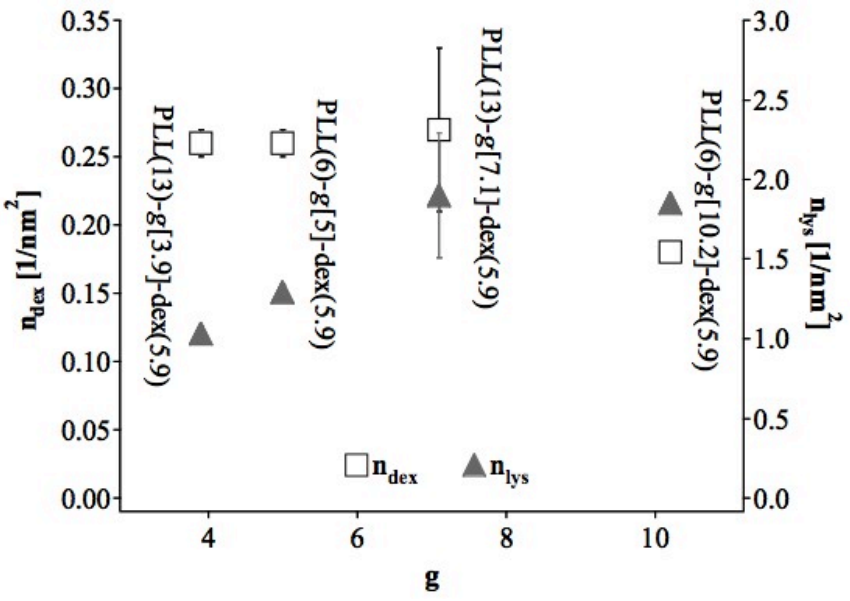

Fig. 5.3 Lysine monomer density (n_{lys}) and dextran chain density (n_{dex}) as a function of grafting ratio (g) for the PLL(13)-*g*-dex(5.9) and PLL(6)-*g*-dex(5.9) copolymers.

If the PLL(6)-*g*[10.2]-dex(5.9) is still considered as an outlying exception, the lysine (or the polymer) molar surface density increases almost linearly with increasing grafting ratio,

whereas n_{dex}, which represents the efficiency of the copolymers in grafting dextran chains onto the surface is nearly constant. Among the four copolymers investigated, PLL(6)-*g*[10.2]-dex(5.9) is the one with the highest grafting ratio i.e. the lowest molecular weight: in this case the effect of the molecular weight overwhelms that of the available anchoring points and/or steric hindrance in determining the amount of polymer adsorbed at the equilibrium that a very small adsorbed mass was observed. Compared to PLL(20)-*g*[3.0]-PEG(5), all PLL-*g*-dex copolymers examined showed higher adsorbed masses (ca. 200 to 300 ng cm^{-2} vs ca. 160 ng cm^{-2}), although the molecular weight is definitely higher for PLL(20)-*g*[3.0]-PEG(5) than for all the PLL-*g*-dex copolymers. The difference in the radius of gyration (R_g) of the side chains, 2.68 nm for dex(5.9) [79] vs 2.82 nm for PEG(5) [80], might explain the different amounts of polymer adsorbed: a smaller R_g of the side chains of the copolymer is, in fact, expected to enhance the surface adsorption due to the weaker shielding of the free lysine monomers (anchoring groups) by the side chains. In addition, the smaller the R_g, the weaker the steric interactions between neighboring side chains.

Quantitative Analysis of Protein Adsorption

OWLS measurements revealed that the amount of protein adsorbed can be greatly reduced by the presence of a PLL-*g*-dex adlayer on the surface. As summarized in Table 5.2 and shown in Fig. 5.2 silica-titania surfaces exposed to a dextran solution, which showed negligible adsorption of dextran (5.6 ± 3.7 ng cm^{-2}) and can be therefore considered as bare substrates, adsorbed a significant amount of serum (713 ± 32 ng cm^{-2}), whereas all PLL-*g*-dex coated waveguides revealed significant reduction in protein adsorption.

Similarly to PLL-*g*-PEG, as shown in a previous study employing a broad range of polymer architectures (from ca. *g*[2] to *g*[20], PEG molecular weight = 1, 2 and 5 kDa) [43], the capabilities to resist non-specific protein adsorption of the PLL-*g*-dex copolymers examined in this work were observed to be dependent on the surface density of the dextran chains (Fig. 5.4): the amount of serum adsorbed decreases as the dextran density at the surface, n_{dex}, increases. As long as the grafting density is sufficiently large and thus a sufficiently high value for n_{dex} is obtained, PLL-*g*-dex copolymers greatly reduce the non-specific adsorption of proteins, reaching a level comparable to that observed for PLL-*g*-PEG coatings.

The protein-resistance capabilities of PLL-*g*-PEG copolymers have previously proven to be dependent also on another factor: the degree of overlap between the PEG chains. This can be viewed as the product of the PEG chain length and density, and it is still related to the surface density of the surface-grafted chains [43]. It can be quantitatively estimated by using a characteristic parameter, $L/2R_g$, which compares the average spacing between neighboring polymer chains, L, to their radius of gyration, R_g. When $L/2R_g$ is smaller than one, the grafted polymer chains would overlap, were they to be in a mushroom configuration, and therefore they stretch out to form a brush structure. As shown in Fig. 5.5, the dependence of the antifouling properties on $L/2R_g$ was also observed for the PLL-*g*-dex copolymers investigated.

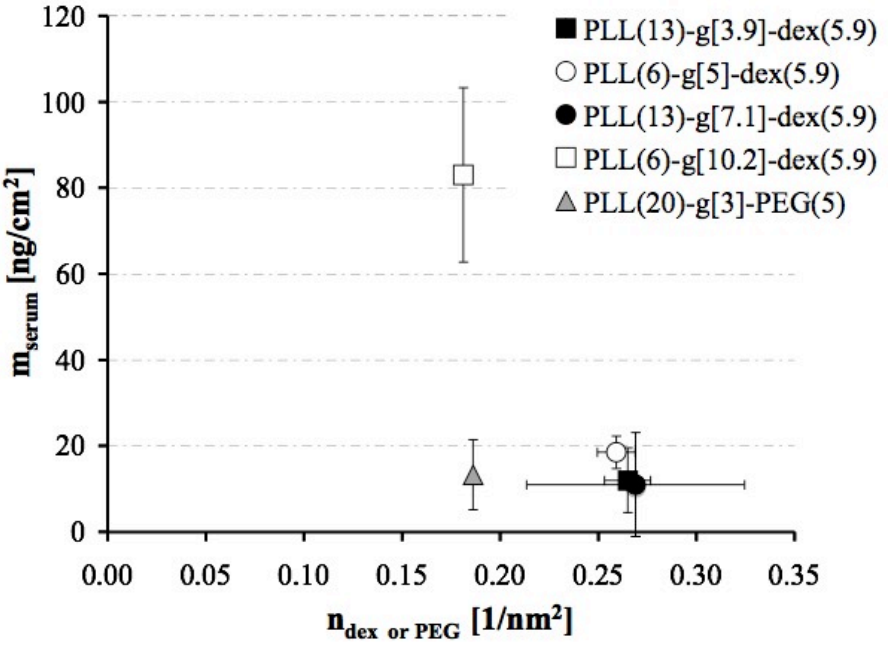

Fig. 5.4 Adsorbed mass of serum, m_{serum}, as a function of the surface concentration of grafted dextran or PEG chains, $n_{dex\ or\ PEG}$.

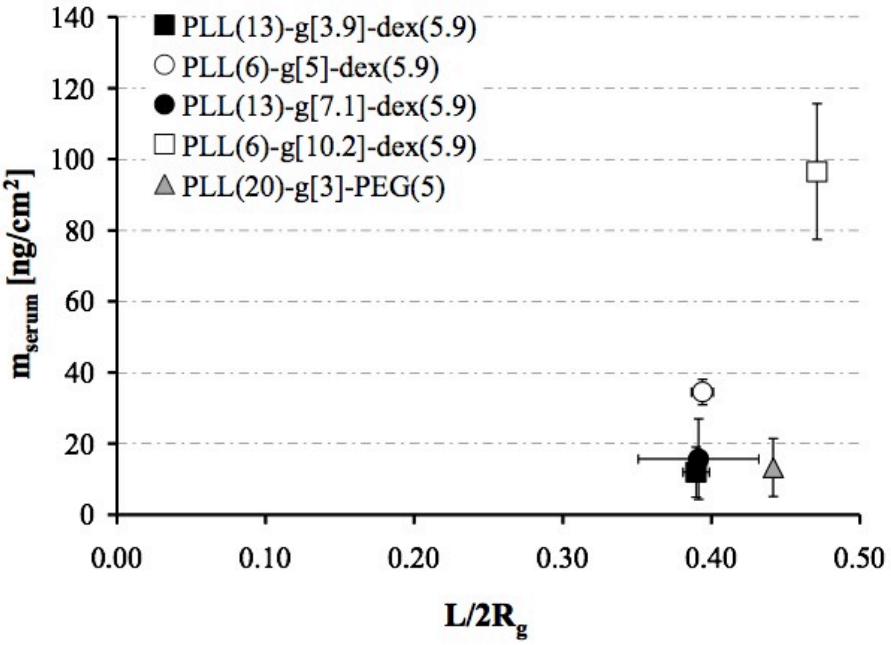

Fig. 5.5 Adsorbed mass of serum, m_{serum}, as a function of the degree of overlap of dextran or PEG chains, $L/2R_g$. L denotes the average mean distance between dextran or PEG chains of the PLL-*g*-dex/PLL-*g*-PEG coated surfaces, calculated from the mass of polymer adsorbed and from the grafting ratios.

According to what was observed in this work, however, dextran chains need to overlap more ($L/2R_g \leq 0.4$) than PEG chains ($L/2R_g$= 0.4-0.7 [43]) to render the surface protein resistant.

Compared to the PLL-*g*-PEG copolymer involved in this work, much higher values of surface density in the grafted chains and lower values of $L/2R_g$ are needed for PLL-*g*-dex copolymers to achieve comparable antifouling capabilities, as judged from the adsorbed amount of proteins from serum (Fig. 5.2 and Table 5.2). For example, PLL(6)-*g*[10.2]-dex(5.9), which shows almost the same surface chain density and a similar value of $L/2R_g$ to those of PLL(20)-*g*[3.0]-PEG(5), shows markedly inferior protein-repelling properties. This might be attributed to the higher flexibility and degree of hydration of PEG chains compared to dextran's bulkier sugar units, and consequently to the larger excluded volume of PEG in water, which allows PEG chains to form a more significant barrier against protein adsorption, even at smaller degree of side-chain overlap.

5.2.2 Nanotribological Analysis

Nanotribological measurements of the PLL-*g*-dex copolymers by means of AFM served as a further probe of the difference in the architectural features of the copolymer. Previous studies have shown that the tribological properties of comb-like graft copolymers, such as PLL-*g*-PEG, are significantly influenced by the architectural features, including side chain length [49, 83], grafting ratio [83], and the backbone length [49].

The nanotribological properties characterized by AFM (Fig. 5.6) are indeed able to clearly distinguish between copolymers with different architectural features (grafting ratio and length of backbone), most of which were indistinguishable in their adsorption behavior and the protein-resistance properties. For instance, the two copolymers with 13 kDa PLL backbone and PLL(6)-*g*[5.0]-dex(5.9), which were only marginally different in their surface adsorption and antifouling properties, were observed to reveal distinctively different frictional behavior; the frictional forces being in the order of PLL(6)-*g*[10.2]-dex(5.9) >> PLL(13)-*g*[3.9]-dex(5.9) > PLL(6)-*g*[5.0]-dex(5.9) > PLL(13)-*g*[7.1]-dex(5.9).

Significantly higher frictional forces observed from the PLL(6)-*g*[10.2]-dex(5.9) can be attributed to the distinctly smaller surface-grafted dextran chain density, n_{dex} (Table 5.2), which, in turn, leads to its inferior capabilities to generate an aqueous lubricating film at the interface. On the other hand, since the n_{dex} and $L/2R_g$ values for the other copolymers are fairly similar, the improved lubricating behavior with increasing grafting ratio, within *g*[3.9] to *g*[7.1], might be associated with the stability of the polymer adlayer. For instance, the copolymer with higher grafting ratio, such as PLL(13)-*g*[7.1]-dex(5.9), may have stronger binding to the surface due to the higher number of available anchoring points, as well as lower steric hindrance between side chains, allowing easier access to the surface by the positively charged amine groups on the backbone. Finally, as with the surface adsorption and antifouling properties, the effect of the molecular weight of the PLL backbone between 6 kDa and 13 kDa was observed to be inconsequential for the nanotribological properties.

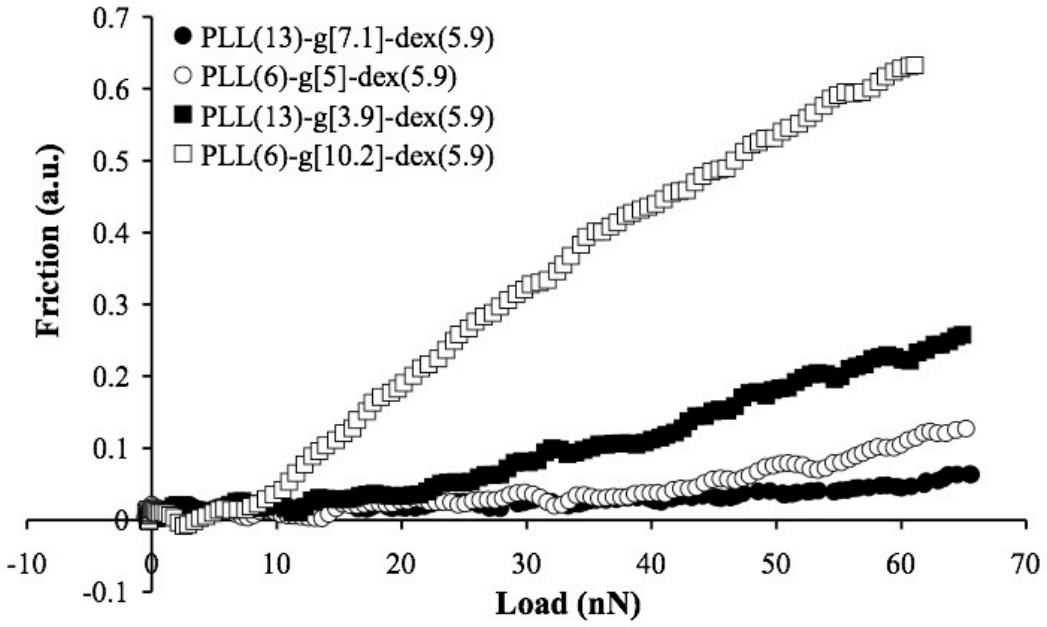

Fig. 5.6 AFM results: friction force measured as a function of increasing load for the contact of a bare silicon nitride tip and silicon wafers coated with PLL-*g*-dex copolymers.

5.3 Conclusions

The protein-repelling capabilities of PLL-*g*-dex copolymers with different grafting ratios and lengths of the PLL backbone, were investigated by means of OWLS and compared to PLL(20)-*g*[3.0]-PEG(5).

Similarly to PLL-*g*-PEG, the amount of proteins adsorbed onto PLL-*g*-dex-coated silica-titania waveguides was observed to be dependent on the surface concentration (n_{dex}) and degree of overlap ($L/2R_g$) of the surface-grafted polymer chains: PLL-*g*-dex copolymers with high values of n_{dex} (≥ 0.26 nm^{-2}) greatly reduce the non-specific adsorption of proteins to a level comparable to those observed from PLL-*g*-PEG coatings. Nanotribological measurements by AFM were performed in order to further distinguish between the investigated copolymers: those PLL-*g*-dex copolymers that showed the optimum, and yet indistinguishable, surface adsorption and antifouling properties, resulted in notably different lubricating properties. For the PLL-*g*-dex copolymers employed in this work, the grafting ratio was observed to be the most important architectural parameter in determining the nanotribological properties. While the tribological studies in this work were motivated primarily by an attempt to better probe the architectural features of the PLL-*g*-dex

copolymers, the combination of good lubricating and antifouling properties is highly desirable for some biomedical applications involving moving parts, e.g. coatings for stents, contact lenses, catheters, and endoscopes. The comparison of OWLS and AFM data can in this case be very helpful for the selection of the "ideal" polymer architecture for such applications.

6 INFLUENCE OF THE POLYMER ARCHITECTURE OF PLL-*G*-DEX ON ITS PROTEIN-RESISTANCE PROPERTIES AND COMPARISON TO PLL-*G*-PEG

The protein-resistance capabilities of PLL-*g*-dex copolymers have already been shown in Chapter 5 to be dependent on both the dextran surface coverage and the degree of overlap of the surface-grafted polymer chains. Compared to Chapter 5, this chapter provides a quantitative evaluation of the protein-resistance properties of a larger matrix of PLL-*g*-dex copolymers with varying grafting ratios as well as dextran molecular weights, but with constant molecular weight of the PLL backbone, and a comparison with a series of PLL(20)-*g*-PEG(5) copolymers covering a similar range of brush densities.

6.1 Experimental

6.1.1 Materials

All PLL-*g*-dex copolymers synthesized for this thesis (see Section 3.3, Table 3.1) were employed in this study. Details on the polymer synthesis are provided in Section 3.1. The molecular weight of the PLL backbone was kept constant at 20 kDa, whereas different grafting ratios (from ca g[2] to ca g[9]) and molecular weights of dextran (dex(5), dex(10) and dex(20)) were investigated.

For comparison purposes, the same series of PLL(20)-*g*-PEG(5) copolymers employed for the study of the macroscopic lubricating properties reported in Chapter 4 has been used.

6.1.2 Optical Waveguide Lightmode Spectroscopy

The optical waveguide chips, the cleaning procedure of the waveguides and the values of refractive index increment (dn/dc) of dextran and PEG, as well as the measurement protocol (for both the polymer-adsorption and the serum-adsorption step) used in this study are the same as those reported in Chapters 4 and 5.

6.2 Results and Discussion

6.2.1 Synthesis and Structural Features of PLL-g-dex copolymers

The structural features of the copolymers employed in this study are presented in detail in Table 6.1.

The selection of dex(5) and dex(10) in this work was motivated by the same reasons reported in Section 4.2.1. Copolymers with dex(20) as side chains were also included, dex(20) having similar number of monomer units (126.5 sugar rings) with the PEG(5) (109.9 EG units) of the PLL-*g*-PEG copolymers used for comparison purpose.

Table 6.1 Matrix of all copolymers (synthesized PLL-*g*-dex copolymers and PLL-*g*-PEG copolymers used for comparison purposes) employed in this study, with the names of the copolymers, the number of grafted side chains and of free lysines per PLL, the percentage of side-chain grafting and the molecular weights of the copolymers.

Polymer	No. of grafted side chains per PLL	No. of free lysines per PLL	Percentage of side-chain grafting (%)	MW [kDa]
PLL(20)-*g*[3.4]-dex(5)	37.0	88.8	29.4	207
PLL(20)-*g*[5.3]-dex(5)	23.7	102.1	18.9	139
PLL(20)-*g*[6.6]-dex(5)	19.1	106.8	15.2	114
PLL(20)-*g*[7.3]-dex(5)	17.2	108.6	13.7	105
PLL(20)-*g*[8.7]-dex(5)	14.5	111.4	11.5	91
PLL(20)-*g*[3.7]-dex(10)	34.0	91.8	27.0	356
PLL(20)-*g*[4.8]-dex(10)	26.2	99.6	20.8	278
PLL(20)-*g*[6.5]-dex(10)	19.4	106.5	15.4	210
PLL(20)-*g*[8.6]-dex(10)	14.6	111.2	11.6	162
PLL(20)-*g*[1.7]-dex(20)	31.9	49.6	60.6	1580
PLL(20)-*g*[3.6]-dex(20)	76.3	82.9	27.8	669
PLL(20)-*g*[5.1]-dex(20)	24.6	101.3	19.5	520
PLL(20)-*g*[8.8]-dex(20)	14.4	111.5	11.4	311
PLL(20)-*g*[3.0]-PEG(5)	40.7	81.3	33.3	212
PLL(20)-*g*[4.4]-PEG(5)	27.7	94.3	22.7	150
PLL(20)-*g*[6.6]-PEG(5)	18.5	103.5	15.2	105
PLL(20)-*g*[11.2]-PEG(5)	10.3	104.6	8.9	64

6.2.2 Adsorption Properties: OWLS

The adsorption data for all copolymers investigated in this study (Table 6.2) are the same as those reported in Table 4.2, with the addition here of the results relative to PLL(20)-*g*-dex(20) copolymers and of all serum-adsorption data. The adsorbed mass of dextran itself (dex(5)) and the relative mass of adsorbed serum were also measured for comparison purposes.

Table 6.2 Summary of the adsorption data determined by OWLS for the synthesized PLL-*g*-dex copolymers. (m_{pol} = adsorbed polymer mass, m_{serum} = mass of serum adsorbed, n_{lys} = surface density of lysine monomers, $n_{dex\ or\ PEG}$ = surface density of dextran or PEG, $n_{monomer\ units}$ = surface density of the monomer units of dextran or PEG, L/2Rg = degree of overlap of dextran/PEG chains).

Surface-bound copolymer	m_{pol} [ng/cm^2]	m_{serum} [ng/cm^2]	n_{lys} [1/nm^2]	$n_{dex\ or\ PEG}$ [1/nm^2]	$n_{monomer\ units}$ [1/nm^2]	L/2Rg
PLL(20)-g[3.4]-dex(5)	244 ± 44	28 ± 8	0.89 ± 0.20	0.26 ± 0.05	8.36 ± 1.51	0.45 ± 0.04
PLL(20)-g[5.3]-dex(5)	290 ± 16	28 ± 2	1.59 ± 0.09	0.30 ± 0.02	9.53 ± 0.52	0.42 ± 0.01
PLL(20)-g[6.6]-dex(5)	241 ± 40	42 ± 17	1.60 ± 0.26	0.24 ± 0.04	7.71 ± 1.27	0.47 ± 0.04
PLL(20)-g[7.3]-dex(5)	269 ± 57	33 ± 21	1.94 ± 0.41	0.27 ± 0.06	8.45 ± 1.80	0.45 ± 0.05
PLL(20)-g[8.7]-dex(5)	190 ± 21	110	1.59 ± 0.17	0.18 ± 0.02	5.80 ± 0.62	0.54 ± 0.03
PLL(20)-g[3.7]-dex(10)	319 ± 28	18	0.68 ± 0.06	0.18 ± 0.02	11.31 ± 0.99	0.36 ± 0.02
PLL(20)-g[4.8]-dex(10)	290 ± 17	7 ± 4	0.79 ± 0.05	0.16 ± 0.01	10.16 ± 0.58	0.38 ± 0.01
PLL(20)-g[6.5]-dex(10)	397 ± 71	17 ± 2	1.44 ± 0.26	0.22 ± 0.04	13.63 ± 2.43	0.33 ± 0.03
PLL(20)-g[8.6]-dex(10)	321 ± 2	26	1.50 ± 0.01	0.17 ± 0.00	10.75 ± 0.07	0.37 ± 0.00
PLL(20)-g[1.7]-dex(20)	347 ± 83	32 ± 11	0.17 ± 0.04	0.10 ± 0.02	12.77 ± 3.03	0.35 ± 0.04
PLL(20)-g[3.6]-dex(20)	313	54	0.33	0.09	11.38	0.51
PLL(20)-g[5.1]-dex(20)	345 ± 29	10 ± 11	0.52 ± 0.04	0.10 ± 0.01	12.44 ± 1.06	0.45 ± 0.1
PLL(20)-g[8.8]-dex(20)	397	23	0.99	0.11	13.99	0.33
PLL(20)-g(3)-PEG(5)	160 ± 3	13 ± 8	0.54 ± 0.00	0.19 ± 0.00	20.44 ± 0.07	0.44 ± 0.00
PLL(20)-g[4.4]-PEG(5)	176 ± 9	32	0.84 ± 0.04	0.20 ± 0.01	21.62 ± 1.07	0.43 ± 0.01
PLL(20)-g[6.6]-PEG(5)	207 ± 45	13	1.41 ± 0.30	0.22 ± 0.05	24.12 ± 5.17	0.41 ± 0.04
PLL(20)-g[11.2]-PEG(5)	174 ± 22	43	1.82 ± 0.22	0.17 ± 0.02	18.37 ± 2.25	0.47 ± 0.03
Dex(5)	6 ± 4	713 ± 32	-	-	-	-

Quantitative Analysis of Polymer Adsorption

A detailed discussion of the polymer-adsorption data for PLL-*g*-dex(5) and PLL-*g*-dex(10) copolymers, included a comparison with the counterpart PLL-*g*-PEG(5) copolymers and dextran (dex(5)) is provided in Section 4.2.2. PLL-*g*-dex(20) copolymers revealed similar amounts of adsorption as PLL-*g*-dex(10) copolymers, ranging from ca. 300 to 400 ng cm^{-2} (see Table 6.2 and Fig. 6.1) and, similarly with all other three groups of copolymers investigated (PLL-*g*-dex(5), PLL-*g*-dex(10) and PLL-*g*-PEG(5)), they did not reveal significant influence of the variation in grafting ratio (between ca. *g*[2] and ca. *g*[9]) on the adsorbed mass, due to the balance between steric repulsion between side chains and number of anchoring groups available for the polymer adsorption.

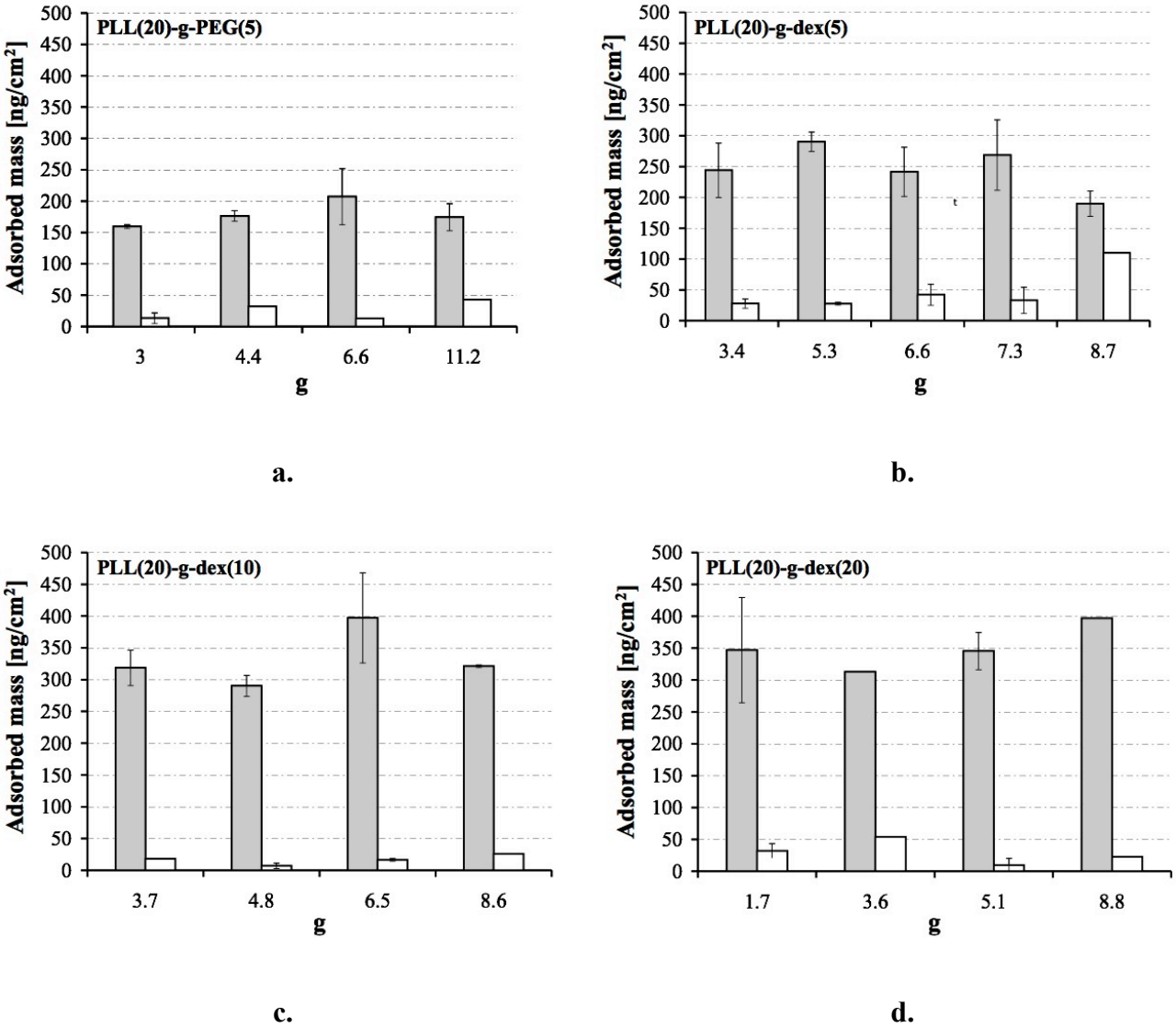

Fig. 6.1 OWLS results (mass of polymer adsorbed (filled bars) and mass of serum adsorbed (empty bars) onto bare silica-titania waveguides) for all PLL-*g*-dex copolymers (PLL(20)-*g*-dex(5), **b.**, PLL(20)-*g*-dex(10), **c.**, PLL(20)-*g*-dex(20), **d.**) and the counterpart PLL-*g*-PEG copolymers (PLL(20)-*g*-PEG(5), **a.**) employed in this study. For some data points, error bars are smaller than the symbols. PLL(20)-*g*[3.6]-dex(20) and PLL(20)-*g*[8.8]-dex(20) were measured only once. The measurement of the serum adsorption was not repeated for PLL(20)-*g*[8.7]-dex(5), PLL(20)-*g*[3.7]-dex(10), PLL(20)-*g*[8.6]-dex(10), PLL(20)-*g*[4.4]-PEG(5), PLL(20)-*g*[6.6]-PEG(5) and PLL(20)-*g*[11.2]-PEG(5) either.

Similarly with Chapter 4, the adsorbed masses were decomposed into various coverage parameters, the surface density of dextran, n_{dex}, or PEG chains, n_{PEG}, of monomer units of dextran or PEG, $n_{monomer\ units}$, and of lysine monomers, n_{lys}, presented in Fig. 6.2 as a function of the inverse of the grafting ratio, 1/*g* (an increase in 1/*g* represents the increase in the number of grafted side chains along the PLL backbone). As shown in Fig. 6.2(b), the surface density of lysine monomers, n_{Lys}, for PLL(20)-*g*-dex(20) copolymers shows a similar trend to PLL(20)-*g*-dex(10) and PLL(20)-*g*-PEG(5) copolymers, but noticeably lower absolute values,

probably due to the significantly higher steric hindrance between dex(20) than between PEG(5) or dex(10), the radii of gyration for the three hydrophilic polymers being in the order PEG(5) (2.82 nm [80]) < dex(10) (3.49 nm [79]) < dex(20) (5.0 nm [79]). The steric hindrance between dextran chains is not that serious for the case of PLL(20)-*g*-dex(5) copolymers that show degraded adsorption (a decrease in n_{lys}) only for *1/g* > ca. 0.2.

The surface density of dextran chains, Fig. 6.2(c), as well as that one of monomer units, Fig. 6.2(d), for PLL(20)-*g*-dex(20) copolymers show nearly constant values over the range of grafting ratios investigated, again similarly with PLL(20)-*g*-dex(10) and PLL(20)-*g*-PEG(5). A more detailed discussion of the trends of the coverage parameters is provided in Section 4.2.2.

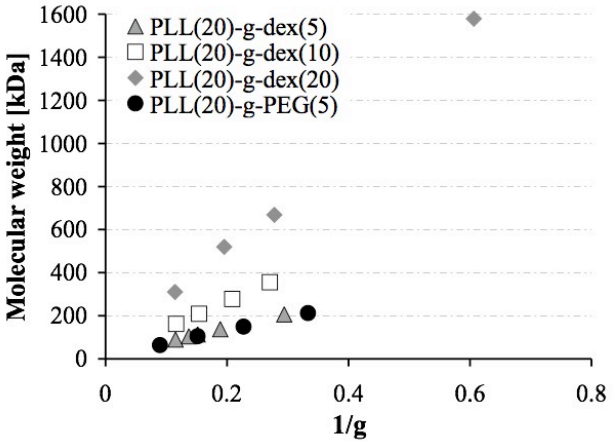

a.

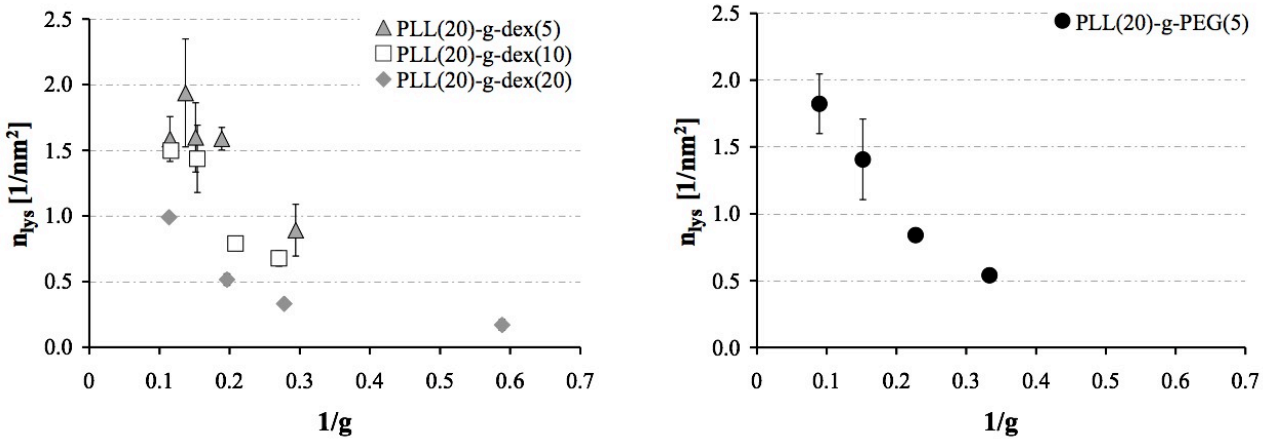

b.

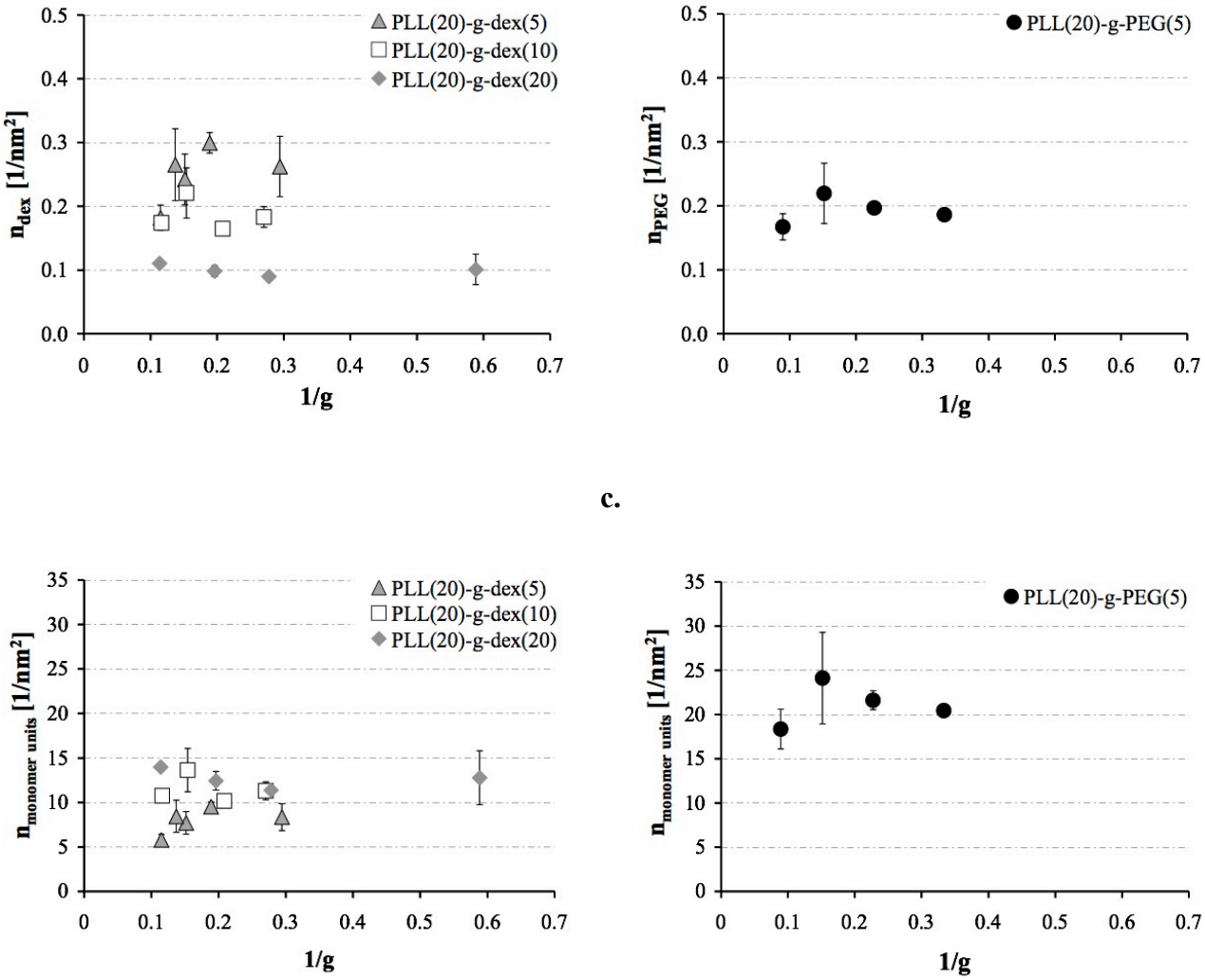

Fig. 6.2 Molecular weight (**a.**), lysine monomer density of PLL-*g*-dex (left) or PLL-*g*-PEG (right) copolymers (n_{lys}) (**b.**), dextran, n_{dex} (left) or PEG, n_{PEG} (right) chain density (**c.**), and density of the monomer units ($n_{monomer\ units}$) of dextran (left) or PEG (right) (**d.**) of the synthesized PLL-*g*-dex copolymers and the counterpart PLL-*g*-PEG copolymers on the silica-titania surface. For some data points, error bars are smaller than the symbols. PLL(20)-*g*[3.6]-dex(20) ($1/g \approx 0.3$) and PLL(20)-*g*[8.8]-dex(20) ($1/g \approx 0.1$) were measured only once.

Quantitative Analysis of Protein Adsorption

As shown in Table 6.2, all copolymers investigated in this work, when adsorbed on the surface of a waveguide, led to an apparent reduction in the mass of serum adsorbed, m_{serum}, compared to the surface exposed to a dextran solution which, consistent with the negligible adsorption of dextran (5.6 ± 3.7 ng cm^{-2}), adsorbed a significant amount of serum (713 ± 32 ng cm^{-2}).

As already discussed in Section 5.2.1 and shown here in Fig. 6.3, for PLL-*g*-dex(5) and PLL-*g*-PEG(5) copolymers the amount of serum adsorbed decreases as the surface density of hydrophilic chains, $n_{dex\ or\ PEG}$, Fig. 6.3(a), and the degree of overlap between dextran or PEG chains, estimated by using the parameter $L/2R_g$, Fig. 6.3(c), increase. However, as already shown in Chapter 5 for PLL-*g*-dex(5.9) copolymers, higher values of surface density in the grafted chains and lower values of $L/2R_g$ are needed for PLL-*g*-dex(5) copolymers to achieve comparable antifouling capabilities with PLL-*g*-PEG(5), this being probably due to the higher flexibility and degree of hydration of PEG chains compared to dextran's bulkier sugar units. For the case of PLL-*g*-dex(10) and PLL-*g*-dex(20), since dex(10) and dex(20) have different molecular weights from dex(5) and PEG(5), the amount of serum adsorbed is presented here as a function of the surface density of dextran monomer units, $n_{monomer\ units}$, as shown in Fig. 6.3(b). Neither PLL-*g*-dex(10) nor PLL-*g*-dex(20) copolymers revealed clear dependence of m_{serum} on $n_{monomer\ units}$ and both groups of copolymers showed comparable antifouling capabilities with PLL-*g*-PEG(5), m_{serum} ranging from ca. 10 to 25 for PLL-*g*-dex(10) and from ca. 10 to ca. 40 ng cm^{-2} for PLL-*g*-dex(20), if the outlier relative to PLL-*g*[3.6]-dex(20) (m_{serum} = 54 ng cm^{-2}) in Fig. 6.3(b) is not considered. The high molecular weight of dextran as well as the relatively low grafting ratio must make PLL-*g*[3.6]-dex(20) rather bulky and stiff, not only in comparison with PLL-*g*-PEG(5) but also with the other PLL-*g*-dex copolymers employed in this work. It might therefore be more difficult for this copolymer to achieve a conformation on the surface that allows for an effective prevention of protein adsorption. This speculation is supported by the relatively high value of $L/2R_g$ (i.e. low degree of overlap between dextran chains) and relatively low surface density of lysine monomers, n_{lys} (i.e. sparsely distributed copolymer molecules on the surface) shown by PLL-*g*[3.6]-dex(20).

Finally, for both groups of PLL-*g*-dex(10) and PLL-*g*-dex(20) copolymers, probably due, as just mentioned, to the higher stiffness of the longer dextran chains, even lower $L/2R_g$ values than for PLL-*g*-dex(5) are needed to reduce the amount of serum adsorbed to a level comparable with PLL-*g*-PEG(5) copolymers.

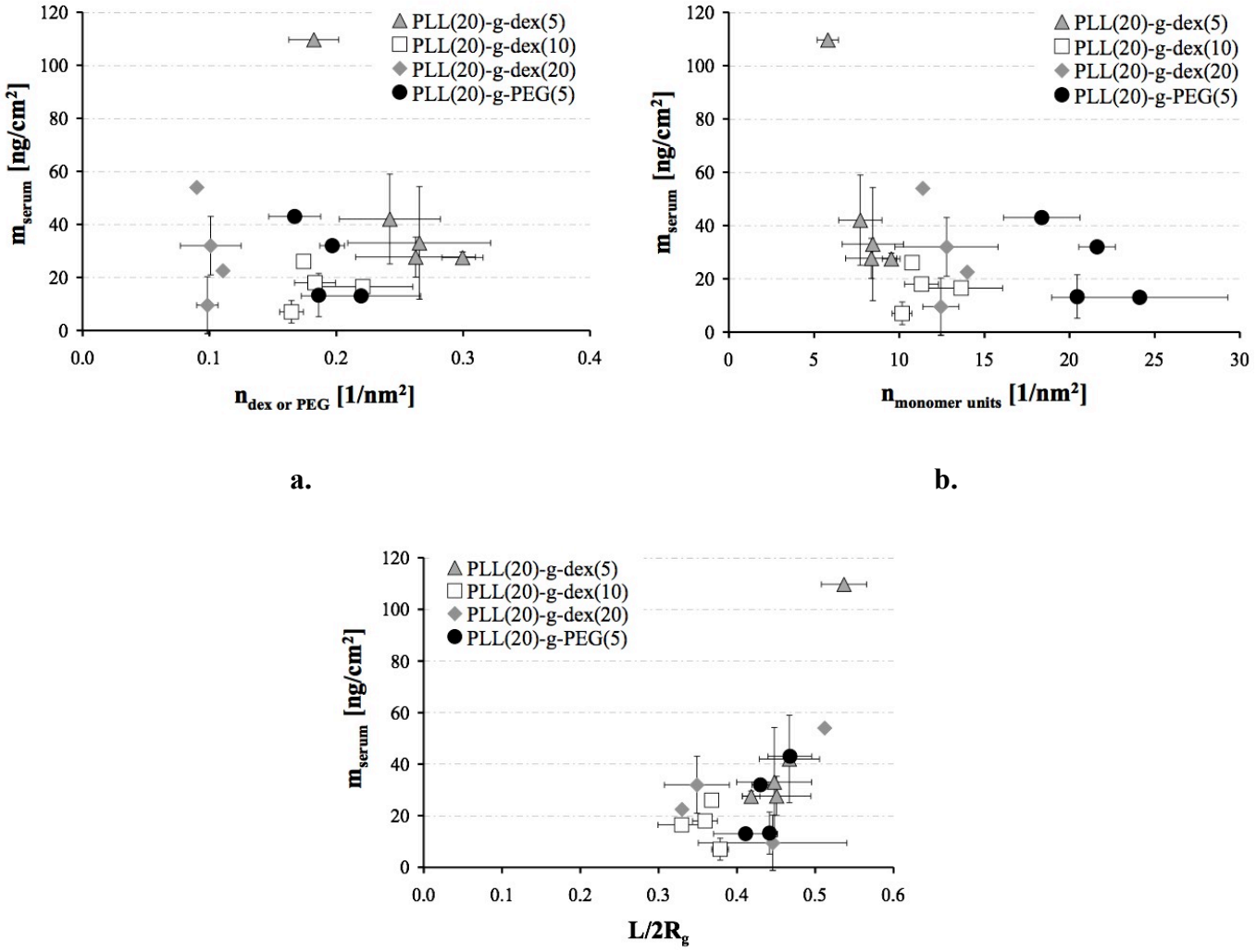

Fig. 6.3 Adsorbed mass of serum, m_{serum}, as a function of the surface density of grafted dextran or PEG chains, $n_{dex\ or\ PEG}$ (**a.**), the surface density of monomer units of dextran or PEG, $n_{monomer\ units}$ (**b.**), and the degree of overlap of dextran or PEG chains, $L/2R_g$ (**c.**). L denotes the average mean distance between dextran or PEG chains of the PLL-*g*-dex/PLL-*g*-PEG coated surfaces, calculated from the mass of polymer adsorbed and from the grafting ratios.

6.3 Conclusions

The protein-repelling capabilities of PLL-*g*-dex copolymers with varying grafting ratios and dextran molecular weights, at constant molecular weight of the PLL backbone, were investigated by means of OWLS and compared to a group of PLL(20)-*g*-PEG(5) copolymers covering a similar range of grafting ratios.

The results shown here confirm those presented in Chapter 5, PLL-*g*-dex copolymers being able to greatly reduce the non-specific adsorption of proteins onto silica-titania waveguides to a level comparable to those observed from PLL-*g*-PEG coatings.

Generally higher degrees of overlap between hydrophilic chains (i.e. lower values of $L/2R_g$) are needed for PLL-*g*-dex copolymers to achieve comparable antifouling capabilities with PLL-*g*-PEG copolymers with similar architecture: this is especially valid for PLL-*g*-dex(10) and PLL-*g*-dex(20) copolymers, dextran chains with high molecular weight being presumably stiffer than dex(5) and therefore making it more difficult for the copolymer to assume the ideal conformation on the surface for an effective reduction of protein adsorption.

However, it should be borne in mind that, to more fairly compare the antifouling properties of PLL-*g*-dex(10) and PLL-*g*-dex(20) with those of PLL-*g*-PEG copolymers, PLL-*g*-PEG copolymers with PEG(10) and PEG(20) chains should be also included in this study

7 BACTERIALLY INDUCED DEGRADATION OF AQUEOUS SOLUTIONS OF PLL-*g*-DEX AND PLL-*g*-PEG AND CONSEQUENCES FOR THEIR LUBRICATION PROPERTIES

The control of chemical stability and an understanding of the factors determining the degradation of lubricants are important for the development of effective, long-lasting, and economical lubricating systems.

Potential sources of lubricant degradation are temperature, light, exposure to irradiation, as well as atmospheric, particulate, or bacterial contamination. In particular, bacterial contamination can be due to a lack of cleanliness in production operations, improper handling during usage or poor storage conditions. Contamination by bacteria can lead to changes in the physicochemical properties of lubricants and impair their performance, with consequent risk of equipment failure, with associated economic and environmental consequences [84]. Microbial contamination of circulating oil systems in steam turbines causes, for instance, degradation of oil quality and oil performance. It also produces corrosive byproducts, and in polymer-containing, oil-based coolants in metal-cutting applications bacterial contamination has been shown to result in severe corrosion of the steel holding tanks [84, 85]. Prevention and control of bacterial contamination are therefore needed to avoid costly repairs, extended downtime and a significant expenditure of resources.

While in Chapter 4 only the lubricating properties of freshly prepared and tested PLL-*g*-PEG and PLL-*g*-dex solutions have been thoroughly investigated, this chapter is focussed on the "shelf life" of polymer solutions and on the evaluation of the effects of aging on their lubricating performance. Both prolonged exposure to ambient light and bacterial contamination of the samples at room temperature were considered as possible factors

influencing the estimated "shelf life" and physicochemical and lubricating properties of the PLL-*g*-PEG or PLL-*g*-dex.

7.1 Experimental

7.1.1 Copolymer Selection

PLL(20)-*g*[3.6]-PEG(5) was selected for this study for its optimal grafting ratio and molecular weight for lubricating performance, as described previously by Müller, et al. [38]. Two PLL-*g*-dex molecular structures, both effective at lubrication [62], PLL(20)-*g*[5.3]-dex(5) and PLL(20)-*g*[4.8]-dex(10), were also selected: the 5 kDa dextran side chains are equivalent in molecular weight to the PEG side chains, whereas the 10 kDa dextran side chains are approximately equal in fully extended chain length to that of 5 kDa PEG chains.

7.1.2 Solution Preparation and Description of Aging Process

Copolymer solutions were prepared in 10 mM 4-(2-hydroxyethyl)piperazine-1-ethanesulfonic acid (HEPES) aqueous buffer (pH 7.4) at a constant molar concentration of copolymer of 1.7 μM (corresponding to 0.25 mg ml^{-1} for PLL(20)-*g*[3.6]-PEG(5), 0.18 mg ml^{-1} for PLL(20)-*g*[5.3]-dex(5) and 0.36 mg ml^{-1} for PLL(20)-*g*[4.8]-dex(10)). Solution preparation was performed by adding the required amount of solid polymer to 20 ml of 10 mM HEPES buffered water in a translucent polypropylene test tube and vigorously hand mixing for approximately 1 minute. Aging consisted of placing these tubes on a laboratory shelf indirectly exposed to ambient daylight at room temperature (these will be referred to as "light-exposed" solutions). Another set of solutions was aged by storing in polypropylene tubes in a dark environment at room temperature but exposed to stagnant laboratory air by leaving the caps off the tubes (these will be referred to as "air-exposed" solutions); the tubes were wrapped in aluminium foil to protect from light during solution preparation and promptly stored in a lab cabinet for the duration of aging.

Optical microscopy of the aged solutions to detect the presence of bacteria was carried out by extracting the solution from the tribometer testing cup immediately after tribotesting (~ 15 ml out of initially prepared 20 ml) and centrifuging to concentrate bacteria at the bottom of the sample tube. Immediately after centrifuging a syringe was used to remove all but the bottom 1 ml of solution with the goal of removing mostly HEPES buffered water and

retaining solid matter in high concentration. A 10 µl sample of the high concentration solution was placed on a microscope slide for observation using a Zeiss Axiovert 200M microscope.

Sodium azide was used as an antibacterial agent in further aging experiments once bacteria colonization was identified as a possible source of degradation. A concentration of sodium azide of 1.5 mM was added to the polymer solutions immediately after preparation.

7.1.3 Bacterial Inoculation Procedure

In order to test whether bacteria are a possible source for the alteration of the polymer lubrication properties polymer solutions were inoculated with DH5α (*E. Coli*, Invitrogen). First one loop of DH5α bacteria from a glycerol stock was inoculated into 5 ml of LB Broth nutrition media (Sigma, Cat. No.: L7275). Then the bacteria were incubated overnight at 37 °C with shaking at 250 rpm. The following day 20 ml of polymer solution of the appropriate concentration in 10 mM HEPES buffer (pH 7.4) was inoculated with 50 µl of the overnight bacterial culture and 48 h after incubation at room temperature the lubrication properties were analyzed.

7.1.4 Pin-on-Disk Tribometry

A pin-on-disk tribometer (CSM Instruments, Switzerland) was implemented for all friction measurements. The tribopair (steel ball against flat glass square), the speed range, the applied load, the cleaning procedure for balls, disks and instrumental parts and the measurement protocol are the same as those reported in Chapter 4. Ambient temperature of ~ 25 °C was maintained at all times.

7.1.5 Optical Waveguide Lightmode Spectroscopy

The optical waveguide chips, the cleaning procedure of the waveguides and the values of refractive index increment (dn/dc) of dextran and PEG, as well as the measurement protocol used in this study are the same as those reported in Chapter 4.

7.2 Results and Discussion

7.2.1 Degradation of Aqueous Solutions of Copolymer Brushes

Fig. 7.1 shows steady-state friction coefficient values as a function of sliding speed for PLL(20)-*g*[3.6]-PEG(5) and PLL(20)-*g*[5.3]-dex(5) in 10 mM HEPES buffer tested at various aging intervals.

The data labelled *fresh* corresponds to a solution tested immediately after preparation (no degradation). The data labelled *HEPES* shows a data set where the buffer was used as lubricant without any polymer additive. After aging, PLL-*g*-PEG showed slight degradation at relatively low sliding speeds, whereas a slight improvement in lubrication at relatively higher sliding speeds could be observed. Nevertheless, the magnitude of change in friction coefficients for PLL-*g*-PEG is insignificant over most of the investigated speed range. On the other hand, PLL-*g*-dex showed dramatic degradation after as little aging time as 2 weeks. The degradation seems to take place mostly within 2 weeks of sample preparation, after which the values only slightly degrade after as much as 8 weeks. Friction data for

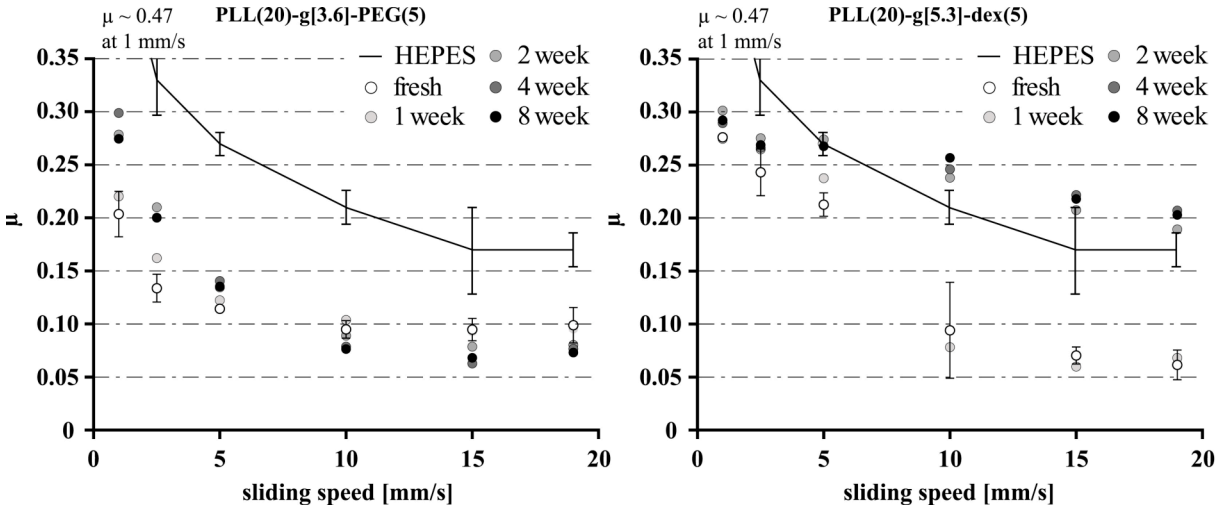

Fig. 7.1 Friction coefficient versus sliding speed as a function of aging time for 10 mM HEPES buffer solution (pH 7.4) of PLL(20)-*g*[3.6]-PEG(5) and PLL(20)-*g*[5.3]-dex(5) showing degradation behavior; this data set also includes control data sets using only HEPES as a lubricant and using a freshly prepared and tested solution of each copolymer; tests were performed on a pin-on-disk tribometer with a 6 mm diameter steel pin on a glass counterface under a 2 N normal load; error bars correspond to standard deviation calculated from repeat experiments (three times), some error bars are smaller than the symbol used (e.g. fresh PLL-*g*-PEG at 5 mm/s sliding speed); aged solution tribotests were not repeated.

PLL-*g*-dex(10) are not reported in the results section as there was no difference in friction or degradation behavior between the 5 kDa and 10 kDa dextran copolymers.

The "light-exposed" and "air-exposed" sets of experiments described in section 7.1.2 revealed no apparent difference in the friction coefficient degradation over the two-week period for either copolymer in either aging environment, suggesting that ambient daylight or exposure to air have little effect on polymer degradation. Data relating to the "air-exposed" set of experiments are therefore omitted.

7.2.2 OWLS Adsorption Behavior

Apparent Significant Increase in Copolymer Mass Adsorption Suggests Bacteria Growth

Copolymer mass adsorption measurements on silica-titania substrates using the OWLS technique revealed an increase in the adsorbed mass of copolymer after 2 weeks following sample preparation (see Table 7.1).

Table 7.1 Adsorbed mass per unit area onto silica-titania substrates; copolymer solutions in 10 mM HEPES buffer are aged in the same conditions as the solutions used for friction measurements; copolymer is injected into OWLS cell and allowed to reach steady state (~ 45 min), then flushed with 10 mM HEPES buffer to remove un-adsorbed polymer; data shows increasing adsorbed mass with respect to aging time occurring after 2 weeks following sample preparation, reflecting the observed transition in friction coefficient with aging (see Fig. 7.1 values for PLL(20)-g[5.3]-dex(5)).

Polymer	**Adsorbed polymer mass [ng/cm^2]**	
	fresh	*2 weeks*
PLL(20)-*g*[5.3]-dex(5)	290 ± 16	361
PLL(20)-*g*[4.8]-dex(10)	290 ± 17	375

An increase in the adsorbed mass occurred after 2 weeks following sample preparation, similarly with the transition observed in friction coefficient for these copolymers. Solutions were prepared and aged under the same conditions as those used for friction measurements. Both architectures of PLL-*g*-dex copolymers show increasing mass adsorption, while friction coefficient data show degradation in lubricating ability (Fig. 7.1). The discrepancy between increasing adsorption mass and degraded lubricating properties with aging time suggests that the increased mass with aging may not represent adsorbed copolymers but some other contaminants. The fact that the degradation in lubricating capabilities was observed from sugar-based copolymer (PLL-*g*-dex), but not from the PEG-based copolymer (PLL-*g*-PEG),

further suggests that these contaminants may be bacteria. This prompted a further investigation to confirm this hypothesis using optical microscopy.

7.2.3 Evidence of Bacteria in Aged Solutions of PLL-g-PEG and PLL-g-dex

The three copolymer solutions (PLL-*g*-PEG, PLL-*g*-dex(10), and PLL-*g*-dex(5)), aged in polypropylene tubes for 8 weeks and exposed to ambient daylight were scrutinized for the presence of bacteria.

Fig. 7.2 shows optical micrographs of each concentrated copolymer solution revealing live (visibly mobile) bacteria present in all solutions. Bacteria found in the PLL-*g*-PEG solution were noticeably longer and less mobile, whereas bacteria on both samples of PLL-*g*-dex solutions were shorter and highly mobile. Although bacteria were present in both copolymer solutions, it is to be borne in mind that only PLL-*g*-dex showed a dramatic reduction in lubrication behaviour. Thus, the presence of bacteria itself does not directly result in the degradation of lubricating capabilities of the copolymers. While further systematic studies on the relationship between the shape/activity of bacteria on the two surfaces to correlate with their influences on the lubricating properties are required in the future, we suggest that the bacteria on the PLL-*g*-dex surface decomposed the polymer by enzymatic digestion, whereas those on PLL-*g*-PEG surface are simply present, while showing little apparent interaction with the polymer (the source of nourishment for bacteria growing in PLL-*g*-PEG solutions remains to be determined as degradation in the copolymer's lubricious properties was

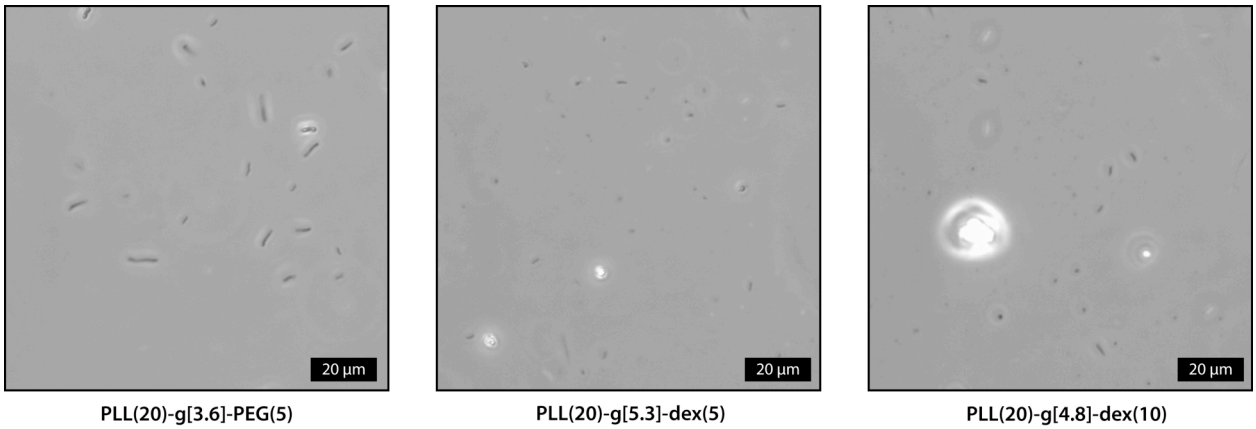

Fig. 7.2 Optical microscopy images of concentrated solutions of each copolymer in 10 mM HEPES buffer (pH 7.4) after concentration via centrifugation; bacteria were present in all three copolymer solutions (dark elongated regions in the images); in the dextran-containing polymer solutions single bacteria could be observed, which were very mobile, whereas in the PLL-*g*-PEG solution the bacteria tended to form elongated structures of multiple bacteria.

negligible). This hypothesis is based on previous literature where dextran was found to be susceptible to degradation by intestinal bacteria [86].

7.2.4 Degradation Comparison of Aged Polymer Solutions, both Sterile and with Deliberate Bacterial Contamination

Fig. 7.3 shows a comparison of friction data for three copolymer solution sets, one freshly prepared and tested control set, one set of bacteria-inoculated samples analyzed 48 hours after inoculation and one set of solutions aged for 4 weeks after being prepared under sterile conditions (further studies have shown no change in friction behavior for PLL-g-dex(5) solutions prepared in a sterile environment and aged up to 8 weeks). The observed trends support the hypothesis that bacteria were responsible for the degradation observed in the data shown in Fig. 7.1. The PLL-*g*-PEG solutions again do not show a significant increase in friction coefficient over the speed range investigated after 4 weeks of aging, compared to the control experiments (labelled *fresh* in the figures), where solutions were tested immediately after preparation. The PLL-*g*-dex shows dramatic degradation in the bacteria-inoculated solution at relatively high speeds, though apparently no degradation in the sterile prepared and aged solution.

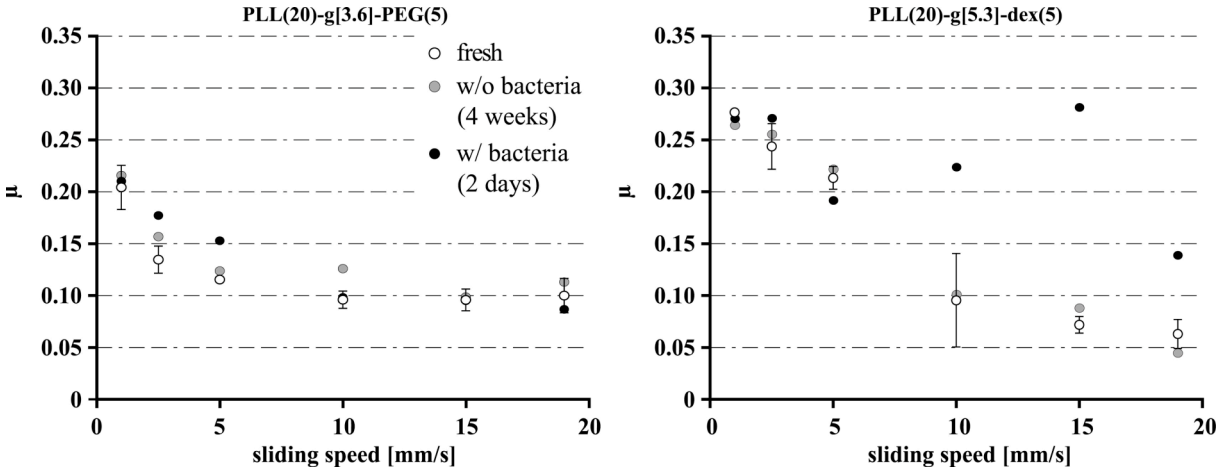

Fig. 7.3 Friction-coefficient-vs-sliding-speed data for PLL(20)-*g*[3.6]-PEG(5) and PLL(20)-*g*[5.3]-dex(5) copolymer solutions in 10 mM HEPES buffer (pH 7.4). The *fresh* data set is a reference set of experiments where solutions were prepared and tested immediately, a second set was prepared under sterile conditions and aged 4 weeks and the third was deliberately inoculated with 50 µL of DH5α (*E. Coli*) in 20 mL of polymer solution right after preparation and aged 48 hours; error bars on fresh data represent the standard deviation of repeat tests.

As a control experiment, the effect of bacteria in HEPES-buffered water (pH 7.4) was investigated and the results are shown in Fig. 7.4. Friction data for 10 mM HEPES buffered

water with and without the inclusion of DH5α (E. Coli) show that the bacteria appear to lubricate the sliding interface at relatively low speeds. Friction coefficient values for PLL-g-dex at low speed (Fig. 7.1) are similar to values achieved using only bacteria in HEPES buffer (Fig. 7.4), suggesting that bacteria are responsible for residual lubrication at low speed after polymer degradation.

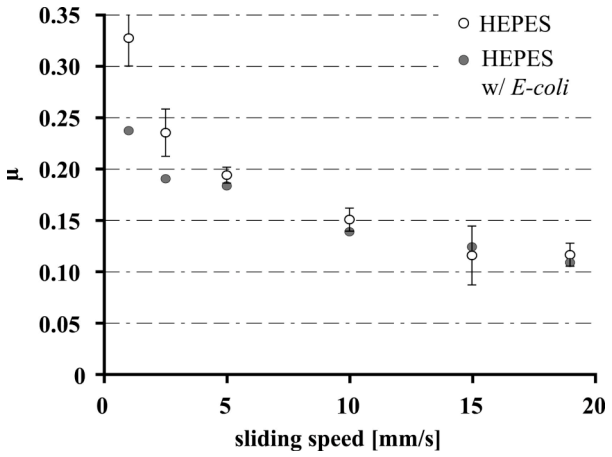

Fig. 7.4 Friction coefficient versus sliding speed for 10 mM HEPES buffered water solutions (pH 7.4) with and without the inclusion of DH5α (*E. Coli*) bacteria; error bars correspond to standard deviation of repeat experiments (repeat experiments were performed for the HEPES only but not for the HEPES w/ E-coli data).

7.2.5 Addition of Anti-bacterial Additive (Sodium Azide) and the Importance of Bacteria at the Sliding Interface

Fig. 7.5 shows friction-coefficient values versus sliding speed for solutions of PLL-*g*-PEG and PLL-*g*-dex with the addition, at the time of solution preparation, of sodium azide as an antibacterial agent after 4 weeks of aging as well as *fresh* (prepared and immediately tested) results. Friction coefficient values for pin-on-disk tests using the solutions prepared with the inclusion of sodium azide were comparable to the freshly prepared and tested solutions. The data set labelled *w/ filtering* corresponds to solutions prepared in non-sterile conditions, aged 4 weeks, and filtered using a 0.20 μm particle filter prior to testing. Apparently, filtering of the aged PLL-*g*-dex solution, which is presumably contaminated by bacteria, does not prevent the increase in friction coefficient, indicating that while the bacteria themselves are not responsible for the change in lubrication properties, such changes have occurred by bacterial action (i.e. enzymatic digestion).

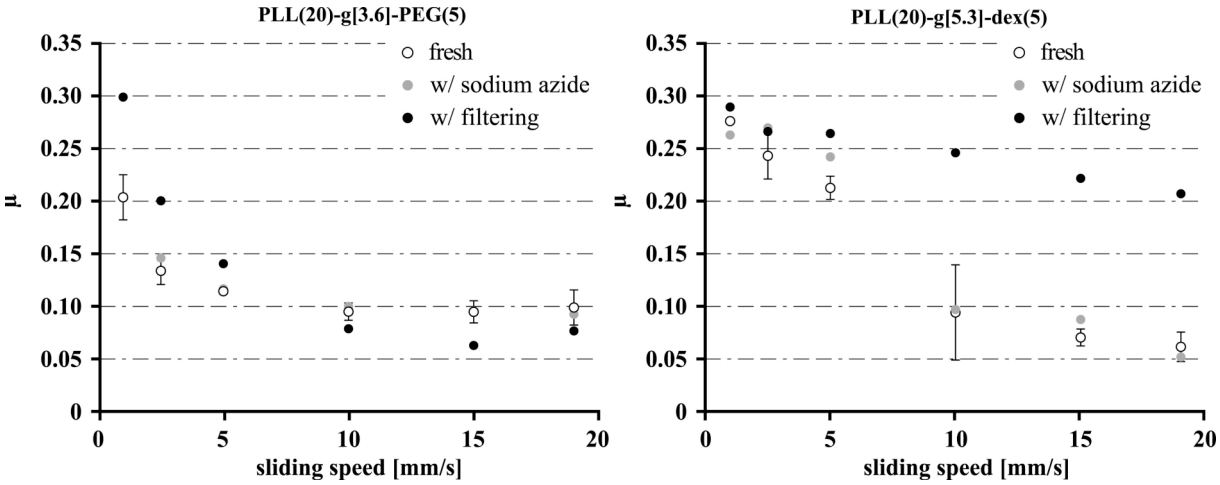

Fig. 7.5 Friction coefficient versus sliding speed for 10 mM HEPES buffered (pH 7.4) solutions of PLL(20)-*g*[3.6]-PEG(5) and PLL(20)-*g*[5.3]-dex(5), one set prepared with the addition of sodium azide (1.5 mM) and aged 4 weeks, and one set aged 4 weeks and filtered through a 0.20 μm filter immediately prior to tribotesting, as well as a set of data from freshly prepared and tested solutions of both copolymers in HEPES; error bars correspond to standard deviation of repeat experiments (only fresh solutions were tested multiple times).

7.3 Conclusions

PLL-*g*-dex copolymer solutions showed constant and comparable friction-coefficient-versus-sliding-speed behavior to PLL-*g*-PEG, when prepared and stored in a sterile environment, after as much as 8 weeks of aging. Friction-coefficient values for PLL-*g*-dex also remained unchanged after as much as 4 weeks when bacteria colonization was prevented by addition of the antibacterial agent sodium azide. PLL-*g*-dex solutions deliberately exposed to bacteria (*E. Coli*) upon preparation and tested 48 h after bacteria inoculation showed as much as a two-fold increase in friction coefficient. The PLL-g-PEG solutions appeared relatively insensitive to the presence of bacteria after aging in the presence of bacterial contamination for as much as 8 weeks. The degradation of the bacteria-containing PLL-*g*-dex copolymer solution after 2 weeks is comparable to that observed after 8 weeks, suggesting that bacterial degradation takes place in the first two weeks when stored under ambient conditions. Independent experiments studying the effect of exposure to ambient daylight on friction behavior showed comparable results to experiments in which solutions were aged in a dark environment after as much as 4 weeks, suggesting that the polymers are unaffected by storage and aging in daylight. Filtering prior to friction testing showed that the actual presence of bacteria at the sliding interface did not have a significant effect on measured

friction coefficients at the sliding speeds (corresponding to the boundary lubrication regime) and interfacial pressure (0.5 GPa max Hertzian contact pressure) investigated, but that it was the action of the bacteria that was significant. Lubricant applications of PLL-*g*-dex in an aqueous medium should therefore remain under sterile conditions or, if appropriate, make use of an antibacterial additive (such as sodium azide) during storage prior to use.

8 QUANTITATIVE COMPARISON OF THE HYDRATION CAPACITY OF SURFACE-BOUND DEXTRAN AND POLYETHYLENE GLYCOL

In the previous chapters the effectiveness of PLL-*g*-dex as an antifouling agent as well as an aqueous lubricant additive has been demonstrated and the comparison with the antifouling and lubricating performances of PLL-*g*-PEG copolymers suggested that dextran can be considered as an alternative to PEG. In comparison with PEG, however, dextran has consistently shown slightly less favorable behavior both in antifouling [87-89] and aqueous lubrication properties [62].

Discussion of the possible reasons for the differences between the surface-tethered polymer chains composed of dextran and PEG has been largely speculative. Factors suggested have included the higher flexibility of PEG chains compared to dextran's bulkier sugar units [87], the chemical structure of dextran, which contains both hydrogen bond acceptors and donors [90], the different conformation of the chains [88, 89], and the different degree of hydration [61, 87]. However, experimental verification of these speculations has been extremely rare to date. This chapter provides a quantitative investigation of the hydration capacity (i.e. capability to incorporate water molecules) of PLL-*g*-dex and PLL-*g*-PEG copolymers, which might play an important role in determining their performance as lubricant additives and protein-resistant coatings. The amount of solvent absorbed within PLL-*g*-PEG copolymers, and brush-like copolymers in general, has in fact been shown to be an important parameter affecting both their lubricating [50, 91] and protein-resistance behavior [44, 92].

PEG has been shown to form a unique structure with water: the water-binding properties of aqueous PEG solutions have been investigated by many experimental techniques, such as light scattering, NMR, infrared spectroscopy, calorimetry, viscosity measurements [93-98],

and by molecular dynamics simulations as well [99]. According to the most widely accepted models, hydrated PEG chains preferentially maintain a trans-gauche-trans (tgt) conformation, adopting a "cage-like" helical structure, whereby the hydrophobic ethylene units (CH_2CH_2) are shielded from contacting water molecules, while the ether oxygen atoms undergo hydrogen bonding to the water molecules, with 2-3 bound water molecules per ethylene oxide [53, 96, 100], as schematically shown in Fig. 8.1.

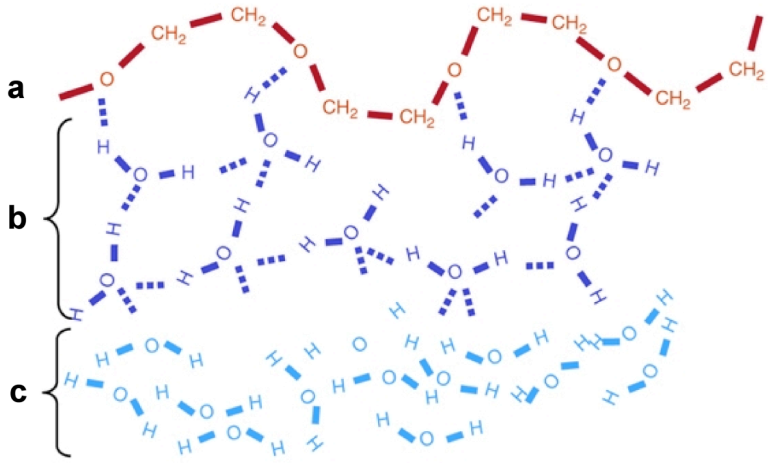

Fig. 8.1 Schematic illustration of the hydration structure of water around PEG: a) a PEG molecule backbone, b) cluster of structured water molecules bonded to the PEG molecule with hydrogen bonds, c) layer of loosely bound water. [101]

The solution properties of dextran and its interactions with water have also been investigated by many experimental techniques, such as light scattering, sedimentation velocity, viscosity measurements, and ultrasonic velocity measurements [102-106]. Gekko et al. determined, for instance, the amount of bound water of dextran fractions with molecular weights below 50 kDa by means of sound-velocity measurements; the bound water expressed as mol/OH group showed a decreasing trend (from 0.9 to 0.49) with increasing molecular weight from 0.4 kDa to 2 kDa, and then stayed constant at 0.5 for higher molecular weights. The decrease of bound water with increase of molecular weight of dextran was attributed to the decrease of the number of free OH groups available for the interaction with water molecules owing to the formation of intramolecular hydrogen bonding between OH groups or to steric hindrance between glucose units [104].

On the basis of this general knowledge on the solvation properties of PEG and dextran, and with the particular purpose of comparing PLL-*g*-dex and PLL-*g*-PEG, the quantification of the hydration capacity of the two copolymers was achieved through the combined

experimental approach of optical waveguide lightmode spectroscopy (OWLS) and quartz crystal microbalance with dissipation monitoring (QCM-D) to yield a value for areal solvation (Ψ), i.e. mass of absorbed solvent molecules per unit substrate area [50].

8.1 Experimental

8.1.1 Materials

PLL-*g*-dex copolymers with varying dextran chain length (dex(5), dex(10) and dex(20)) and grafting ratio (from ca. *g*[2] to ca. *g*[9]), but with constant molecular weight of the PLL backbone (20 kDa) were employed in this study. Details on the polymer synthesis are provided in Section 3.1.

For comparison purposes, the same series of PLL(20)-*g*-PEG(5) copolymers employed for the study of the macroscopic lubricating properties reported in Chapter 4 has been used.

8.1.2 Optical Waveguide Lightmode Spectroscopy

Optical waveguide lightmode spectroscopy (OWLS) was employed to determine the "dry mass" of polymer adsorbed onto the surface of a silica-titania waveguide. Experiments were performed using an OWLS 110 instrument (Microvacuum, Budapest, Hungary).

The operational principle of OWLS is described in detail in Section 2.2.1: briefly, the adsorbed mass is calculated from the change in the refractive index in the vicinity of the waveguide surface upon adsorption of molecules. Since the solvent molecules coupled to the adsorbed polymer do not contribute to a *change* in the refractive index before and after the polymer adsorption, they also do not contribute to the adsorbed mass detected by OWLS ("dry mass", i.e. dry areal mass density, m_{dry} [ng cm^{-2}]).

The optical waveguide chips, the cleaning procedure of the waveguides and the values of refractive index increment (dn/dc) of dextran and PEG, as well as the measurement protocol used in this study are the same as those reported in Chapter 4.

8.1.3 Quartz Crystal Microbalance with Dissipation Monitoring (QCM-D)

All QCM-D measurements were performed with a commercial quartz crystal microbalance with dissipation monitoring (Q-Sense E4, Gothenburg, Sweden). The operational principle of QCM-D is described in detail in Section 2.2.2.

The total mass sensed by QCM-D is the mass of the polymer plus that of the absorbed solvent molecules, m_{wet}, in contrast to the "dry mass", m_{dry}, that is measured by OWLS.

The sensor crystals used in the measurements were 5-MHz AT-cut crystals, sputter-coated with SiO_2 (Q-Sense E4, Gothenburg, Sweden). The changes of resonance frequency (Δf) and energy dissipation (ΔD) were measured simultaneously at 6 different overtones of the fundamental frequency (third overtone at 15 MHz, fifth overtone at 25 MHz, seventh overtone at 35 MHz, ninth overtone at 45 MHz, eleventh overtone at 55 MHz, and thirteenth overtone at 65 MHz). Measurements at the fundamental frequency (5 MHz) were not considered due to this resonance being very sensitive to bulk solution changes and generating unreliable data. The QCM liquid chambers were temperature-stabilized to 25 ± 0.02 °C.

All measurements were performed under flow conditions. The resonance frequency, f_0, and the dissipation factor, D, of the quartz crystals were measured first in aqueous HEPES buffer solution, in order to set the baseline. The polymer-free aqueous HEPES buffer solution was then replaced by PLL-*g*-dex- or PLL-*g*-PEG-containing aqueous HEPES buffer solution (0.25 mg ml^{-1}). After adsorption for 30 min (at a flow rate of 20 µl min^{-1}), the liquid cell was rinsed with polymer-free aqueous HEPES buffer solution to confirm that no noticeable polymer desorption had occurred.

The areal solvation of the brush copolymers, Ψ, defined as the mass of solvent molecules per unit area, absorbed within the structure of the surface-bound copolymers, can be derived by subtracting the "dry mass", m_{dry}, calculated from OWLS measurements, from the "wet mass", m_{wet}, calculated from QCM-D measurements. In the present work, m_{wet} was calculated using the Sauerbrey equation:

$$\Delta m = -\frac{C \cdot \Delta f}{n} \qquad \text{Eq. 8.1}$$

where Δm is the change in the total mass of the crystal induced upon adsorption, Δf is the change in frequency, n is the overtone number and C is a constant characteristic of the crystal (C = 17.7 ng/Hz for a 5 MHz quartz crystal).

8.2 Results and Discussion

8.2.1 Structural Features of the PLL-g-dex and PLL-g-PEG copolymers

The structural features of the PLL-*g*-dex and PLL-*g*-PEG copolymers employed in this study are presented in detail in Table 8.1. The selection of dex(5), dex(10) and dex(20) was motivated by the same reasons reported in Section 4.2.1 and Section 6.2.1.

Table 8.1 Matrix of all copolymers (synthesized PLL-*g*-dex copolymers and PLL-*g*-PEG copolymers used for comparison purposes) employed in this study, with the names of the copolymers, the number of grafted side chains and of free lysines per PLL, the percentage of side-chain grafting and the molecular weights of the copolymers.

Polymer	No. of grafted side chains per PLL	No. of free lysines per PLL	Percentage of side-chain grafting (%)	MW [kDa]
PLL(20)-*g*[3.4]-dex(5)	37.0	88.8	29.4	207
PLL(20)-*g*[5.3]-dex(5)	23.7	102.1	18.9	139
PLL(20)-*g*[7.3]-dex(5)	17.2	108.6	13.7	105
PLL(20)-*g*[8.7]-dex(5)	14.5	111.4	11.5	91
PLL(20)-*g*[3.7]-dex(10)	34.0	91.8	27.0	356
PLL(20)-*g*[4.8]-dex(10)	26.2	99.6	20.8	278
PLL(20)-*g*[6.5]-dex(10)	19.4	106.5	15.4	210
PLL(20)-*g*[8.6]-dex(10)	14.6	111.2	11.6	162
PLL(20)-*g*[1.7]-dex(20)	31.9	49.6	60.6	1580
PLL(20)-*g*[3.6]-dex(20)	76.3	82.9	27.8	669
PLL(20)-*g*[5.1]-dex(20)	24.6	101.3	19.5	520
PLL(20)-*g*[8.8]-dex(20)	14.4	111.5	11.4	311
PLL(20)-*g*[3.0]-PEG(5)	40.7	81.3	33.3	212
PLL(20)-*g*[4.4]-PEG(5)	27.7	94.3	22.7	150
PLL(20)-*g*[6.6]-PEG(5)	18.5	103.5	15.2	105
PLL(20)-*g*[11.2]-PEG(5)	10.3	104.6	8.9	64

8.2.2 Comparative Adsorption Measurements Using OWLS and QCM-D

The areal solvation, Ψ, of the surface-bound, brush-like copolymers employed in this work was determined by applying the combined experimental approach of OWLS and QCM-D.

In situ OWLS measurements were performed to obtain the average "dry mass" (m_{dry}) of the surface-adsorbed copolymers. From the adsorbed masses and the compositional features of the copolymers it was possible to calculate the surface density of lysine monomer, n_{lys}, and dextran or PEG chains, $n_{dex\ or\ PEG}$, the former reflecting the number of copolymer units on the surface, the latter reflecting the efficacy of the copolymer in grafting the hydrophilic polymer

chains (dextran or PEG) onto the surface. QCM-D was used to quantify the "wet mass" (m_{wet}) consisting of the mass of polymer along with solvent molecules absorbed within the brush structure.

Ψ values were calculated by subtracting the "dry mass", m_{dry}, obtained by OWLS, from the "wet mass", m_{wet}, obtained by QCM-D. The adsorption data determined by OWLS and QCM-D are reported in Table 8.2 and Table 8.3, respectively.

Both OWLS and QCM-D revealed a rapid adsorption of all copolymers investigated onto the substrates. Upon exposure of the surface to the polymer solution, more than 90% of the final adsorbed mass was reached within the first 5 min and no apparent polymer desorption could be observed upon rinsing with buffer solution.

Table 8.2 Summary of the adsorption data determined by OWLS for the PLL-*g*-dex and PLL-*g*-PEG copolymers investigated (m_{dry} = adsorbed mass determined by OWLS, n_{lys} = surface density of lysine monomers, $n_{dex\ or\ PEG}$ = surface density of dextran or PEG, $n_{monomer\ units}$ = surface density of the monomer units of dextran or PEG).

Surface-bound copolymer	m_{dry} [ng/cm^2]	n_{lys} [1/nm^2]	$n_{dex\ or\ PEG}$ [1/nm^2]	$n_{monomer\ units}$ [1/nm^2]
PLL(20)-*g*[3.4]-dex(5)	244 ± 44	0.89 ± 0.20	0.26 ± 0.05	8.36 ± 1.51
PLL(20)-*g*[5.3]-dex(5)	290 ± 16	1.59 ± 0.09	0.30 ± 0.02	9.53 ± 0.52
PLL(20)-*g*[7.3]-dex(5)	269 ± 57	1.94 ± 0.41	0.27 ± 0.06	8.45 ± 1.80
PLL(20)-*g*[8.7]-dex(5)	190 ± 21	1.59 ± 0.17	0.18 ± 0.02	5.80 ± 0.62
PLL(20)-*g*[3.7]-dex(10)	319 ± 28	0.68 ± 0.06	0.18 ± 0.02	11.31 ± 0.99
PLL(20)-*g*[4.8]-dex(10)	290 ± 17	0.79 ± 0.05	0.16 ± 0.01	10.16 ± 0.58
PLL(20)-*g*[6.5]-dex(10)	397 ± 71	1.44 ± 0.26	0.22 ± 0.04	13.63 ± 2.43
PLL(20)-*g*[8.6]-dex(10)	321 ± 2	1.50 ± 0.01	0.17 ± 0.00	10.75 ± 0.07
PLL(20)-*g*[1.7]-dex(20)	347 ± 83	0.17 ± 0.04	0.10 ± 0.02	12.77 ± 3.03
PLL(20)-*g*[3.6]-dex(20)	313	0.33	0.09	11.38
PLL(20)-*g*[5.1]-dex(20)	345 ± 29	0.52 ± 0.04	0.10 ± 0.01	12.44 ± 1.06
PLL(20)-*g*[8.8]-dex(20)	397	0.99	0.11	13.99
PLL(20)-*g*(3.0)-PEG(5)	160 ± 3	0.54 ± 0.00	0.19 ± 0.00	20.44 ± 0.07
PLL(20)-*g*[4.4]-PEG(5)	176 ± 9	0.84 ± 0.04	0.20 ± 0.01	21.62 ± 1.07
PLL(20)-*g*[6.6]-PEG(5)	207 ± 45	1.41 ± 0.30	0.22 ± 0.05	24.12 ± 5.17
PLL(20)-*g*[11.2]-PEG(5)	174 ± 22	1.82 ± 0.22	0.17 ± 0.02	18.37 ± 2.25

Table 8.3 Summary of the adsorption data determined by QCM-D for the PLL-*g*-dex and PLL-*g*-PEG copolymers investigated (m_{wet} = adsorbed mass determined by QCM-D, Ψ = areal solvation, m_{wet} - m_{dry}, $N_{H2O/HG}$ = number of water molecules per hydrophilic group).

Surface-bound copolymer	m_{wet} [ng/cm^2]	Ψ [ng/cm^2]	$N_{H2O/HG}$
PLL(20)-*g*[3.4]-dex(5)	929	686	5
PLL(20)-*g*[5.3]-dex(5)	749	459	3
PLL(20)-*g*[7.3]-dex(5)	710	442	4
PLL(20)-*g*[8.7]-dex(5)	611	421	5
PLL(20)-*g*[3.7]-dex(10)	1085 ± 66	766 ± 94	5
PLL(20)-*g*[4.8]-dex(10)	961	671	4
PLL(20)-*g*[6.5]-dex(10)	1002 ± 36	605 ± 107	3
PLL(20)-*g*[8.6]-dex(10)	920	599	4
PLL(20)-*g*[1.7]-dex(20)	1331	985	5
PLL(20)-*g*[3.6]-dex(20)	1411 ± 13	1098	5
PLL(20)-*g*[5.1]-dex(20)	1214	869	4
PLL(20)-*g*[8.8]-dex(20)	1271	874	6
PLL(20)-*g*(3.0)-PEG(5)	1115	992	16
PLL(20)-*g*[4.4]-PEG(5)	1039	863	13
PLL(20)-*g*[6.6]-PEG(5)	821 ± 54	614 ± 99	9
PLL(20)-*g*[11.2]-PEG(5)	674 ± 25	500 ± 47	8

Comparison between the solvation capabilities of PLL(20)-g-PEG(5) and PLL(20)-g-dex(10) copolymers

While the hydration capabilities of all three series of PLL-*g*-dex copolymers, PLL(20)-*g*-dex(5), PLL(20)-*g*-dex(10), and PLL(20)-*g*-dex(20), have been characterized, the comparison with PLL(20)-*g*-PEG(5) was made with the series of PLL(20)-*g*-dex(10) copolymers, since they showed comparable values of surface density of hydrophilic chains ($n_{dex\ or\ PEG}$): ca. 0.17 to 0.22 chains nm^{-2} for the series of PLL(20)-*g*-PEG(5) copolymers and ca. 0.16 to 0.22 chains nm^{-2} for the series of PLL(20)-*g*-dex(10).

The values of areal solvation relative to PLL-*g*-PEG and PLL-*g*-dex(10) copolymers are presented as a function of $n_{dex\ or\ PEG}$, as shown in Fig. 8.2. The Ψ values for PLL-*g*[3.7]-dex(10) (766 ± 94 ng cm^{-2}) and PLL-*g*[4.8]-dex(10) (671 ng cm^{-2}) are significantly lower than those of their counterparts, PLL-*g*[3.0]-PEG(5) (992 ng cm^{-2}) and PLL-*g*[4.4]-PEG(5) (863 ng cm^{-2}), suggesting higher hydration capacity of PLL-*g*-PEG copolymers. However, the difference between PLL-*g*-dex(10) and PLL-*g*-PEG copolymers becomes smaller with increasing grafting ratio: in the case of a dense polymer brush, tightly bound water (structural water) is likely to mostly contribute to the areal solvation and it is in this regime that the

difference between PEG- and dextran-based brushes is more evident. PEG chains are, in fact, reported to be more prone than dextran to form ordered complexes with water by hydrogen bonding [53, 104]; when the grafting ratio increases, the distance between hydrophilic side chains increases as well and more space is left for "free" water to be accommodated between the polymer chains, it is therefore likely that the contribution of loosely bound water becomes predominant, and the differences between PLL-*g*-dex and PLL-*g*-PEG copolymers are consequently smaller.

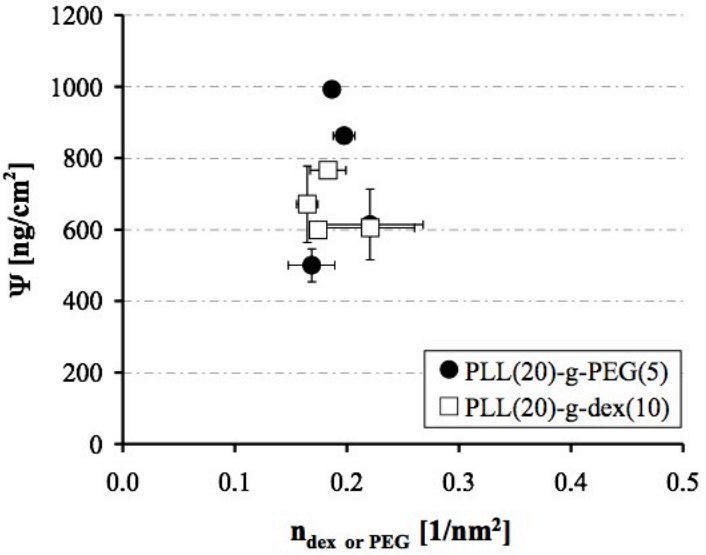

Fig. 8.2 Areal solvation, Ψ, as a function of the surface density of hydrophilic chains ($n_{dex\ or\ PEG}$) for PLL(20)-*g*-PEG(5) and PLL(20)-*g*-dex(10) copolymers with similar range of grafting ratios.

The differences in the hydration power of the PLL-*g*-PEG and PLL-*g*-dex copolymers might be related to their different lubricating performances. A previous study comparing the boundary lubricating properties of the PLL(20)-*g*-PEG(5) and PLL(20)-*g*-dex(10) copolymers employed in the present study [62], revealed slightly, yet noticeably higher lubricating efficacy of PLL-*g*-PEG copolymers compared to PLL-*g*-dex(10) in the low-speed regime (≤ 5 mm sec^{-1}), regardless of the grafting ratio. Although, as shown in Fig. 8.2, it was only at relatively low grafting ratios (≤ *g*[4.8]) that PLL-*g*-PEG copolymers revealed significantly higher Ψ values than their PLL-*g*-dex counterparts, for lower brush densities the areal solvation was comparable or even slightly higher for PLL-*g*-dex. The lubricating performance of PLL-*g*-PEG, however, was shown to be better for all the grafting ratios investigated. As hypothesized above, the relatively high Ψ values shown by PLL-*g*-dex copolymers with high grafting ratio most likely reflect the loosely (hydrodynamically) bound water and it is

therefore presumable that this water, assumed to have a higher degree of freedom than the structural water (covalently bound water), is more easily squeezed out from the tribocontact, and does not really contribute to the lubricating capabilities of the copolymers.

The lower hydration capabilities of PLL-*g*-dex copolymers might also explain the need of both higher surface densities in the grafted hydrophilic chains and higher degree of overlap between them to achieve comparable antifouling capabilities with PLL-*g*-PEG copolymers, as shown in a previous study comparing the resistance to non-specific protein adsorption of PLL-*g*-dex and PLL-*g*-PEG copolymers [61].

In order to more clearly visualize the different capabilities of PLL-*g*-PEG and PLL-*g*-dex(10) copolymers to incorporate water, the number of water molecules per monomer unit (EG monomer or sugar ring), $N_{H2O/mon\ unit}$, was determined for each copolymer by applying the following equations:

$$\Sigma_{solv} = \frac{N_A \cdot (m_{wet} - m_{dry})}{MW_{solv}} \qquad \text{Eq. 8.2}$$

$$\Sigma_{mon\ units} = \frac{MW_{PLL} \cdot MW_{PEG\ or\ dex} \cdot m_{dry} \cdot N_A}{MW_{mon\ unit} \cdot MW_{Lys} \cdot g \cdot \left(MW_{PLL} + \frac{MW_{PLL} \cdot MW_{PEG\ or\ dex}}{g \cdot MW_{Lys}} \right)} \qquad \text{Eq. 8.3}$$

$$N_{H2O\ /\ mon\ unit} = \frac{\Sigma_{solv}}{\Sigma_{mon\ unit}} \qquad \text{Eq. 8.4}$$

where Σ_{solv} and $\Sigma_{mon\ units}$ are the areal density of the solvent molecules and monomer units respectively, N_A is the Avogadro constant, MW_{solv} is the molecular weight of the solvent, MW_{PLL} is the molecular weight of the PLL backbone, MW_{Lys} is the molecular weight of a lysine monomer, $MW_{PEG\ or\ dex}$ and $MW_{mon\ unit}$ are the molecular weights of the hydrophilic side chains, PEG or dextran, and of the monomer unit (EG monomer or dextran ring) respectively and *g* is the grafting ratio. From $N_{H2O/mon\ unit}$, from the surface density of dextran or PEG chains determined by OWLS ($n_{dex\ or\ PEG}$) and from the compositional features of the copolymers, it is then possible to calculate the number of water molecules per hydrophilic group (HG), $N_{H2O/HG}$, having considered in this work one hydrophilic group (the ether oxygen, -O-) per EG monomer and 5 hydrophilic groups (3 -OH and 2 -O-) per sugar unit.

The resulting values are presented in Fig. 8.3 as a function of the surface density of hydrophilic groups, n_{HG}.

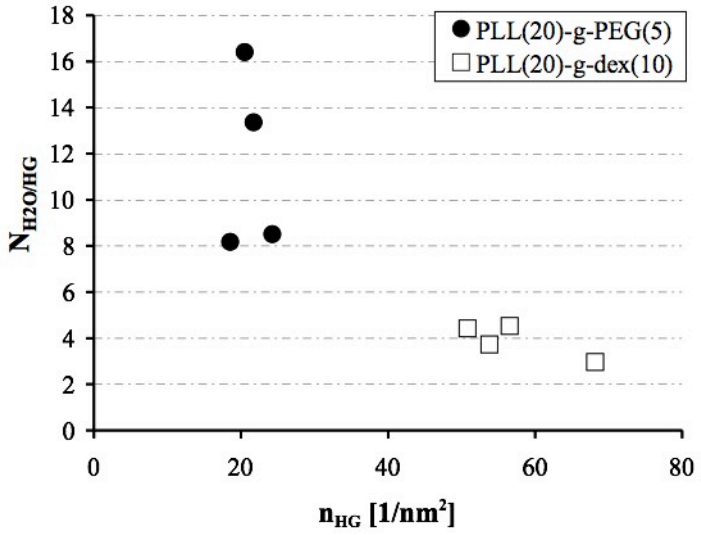

Fig. 8.3 Number of water molecules per hydrophilic group, $N_{H2O/HG}$, as a function of the surface density of hydrophilic groups (n_{HG}) for PLL(20)-*g*-PEG(5) and PLL(20)-*g*-dex(10) copolymers with similar ranges of grafting ratios.

Although n_{HG} values are always higher for PLL-*g*-dex(10) copolymers, the highest $N_{H2O/HG}$ value revealed by PLL-*g*-dex(10) (5 water molecules per hydrophilic group for the case of PLL-*g*[3.7]-dex(10)) is less than one third of the highest $N_{H2O/HG}$ value shown by PLL-*g*-PEG copolymers (16 water molecules per hydrophilic group for the case of PLL-*g*[3.0]-PEG) and even lower than the lowest value relative to the PLL-*g*[11.2]-PEG (8 water molecules per hydrophilic group). Even when for the PLL-*g*-dex copolymers only the OH groups are taken into account as hydrophilic groups (data not shown) the values of $N_{H2O/HG}$ for all copolymers employed remain significantly lower than those of the PLL-*g*-PEG copolymers. In contrast to PEG, it is therefore less likely that dextran forms ordered complexes with water, being instead "randomly" hydrated by water molecules.

The values of $N_{H2O/HG}$ further confirm that both tightly and loosely bound water molecules are absorbed within the PLL-*g*-dex and PLL-*g*-PEG brush: in fact, while a minimum of 2-3 water molecules forming hydrogen bonds with one EG monomer is needed to satisfy basic hydration of PEG [77, 107], in the case of PLL-*g*-PEG copolymers, depending on the grafting ratio, 6-14 additional water molecules per ethylene oxide unit are detected in the brush and represent the "free", non-structural, water. In the case of dextran, according to Gekko et al. [104], the amount of bound water molecules per OH group stays constant at about 0.5 for

molecular weights of dextran between 2 kDa and 50 kDa, implying that for the PLL-*g*-dex copolymers investigated in this work 2.5 to 4.5 loosely bound water molecules per hydrophilic group are absorbed within the brush.

8.2.3 Comparison between the Solvation Capabilities of PLL(20)-g-dex Copolymers with Different Molecular Weight of Dextran

The values of areal solvation for all PLL-*g*-dex copolymers investigated are plotted in Fig. 8.4 against the surface density of monomer units, whereas in Fig. 8.5, $N_{H2O/HG}$ is plotted against the surface density of hydrophilic groups, n_{HG}. As shown in Fig. 8.4, the Ψ values for the three series of copolymers is in the order PLL-*g*-dex(5) < PLL-*g*-dex(10) < PLL-*g*-dex(20): the number of absorbed water molecules per hydrophilic group stays, in fact, nearly constant for all dextran lengths investigated, consistent with the findings of Gekko et al. [104], this resulting in an increased overall areal solvation with increasing molecular weight of dextran.

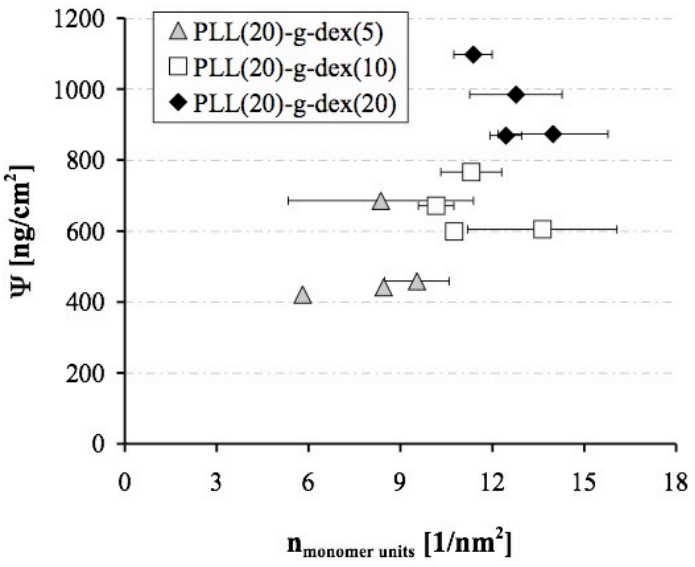

Fig. 8.4 Areal solvation, Ψ, as a function of the surface density of sugar units ($n_{monomer\ units}$) for PLL(20)-*g*-dex copolymers differing in the molecular weight of the dextran side chains and in the grafting ratio.

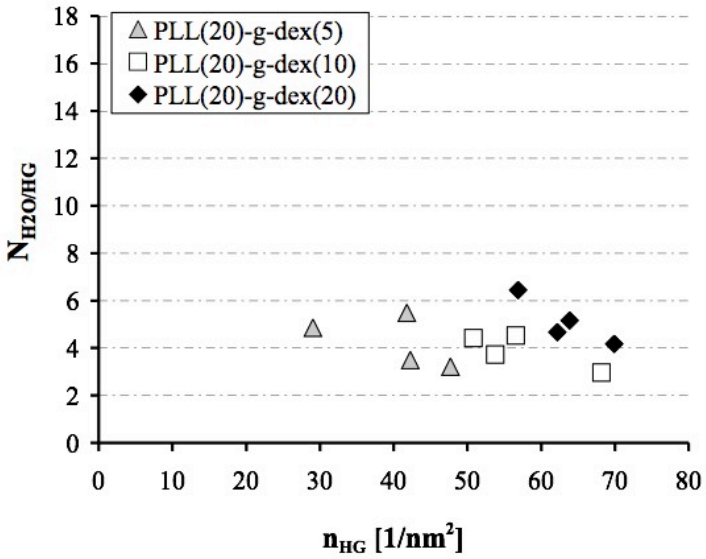

Fig. 8.5 Number of water molecules per hydrophilic group, $N_{H2O/HG}$, as a function of the surface density of hydrophilic groups (n_{HG}) for PLL(20)-*g*-dex copolymers differing in the molecular weight of the dextran side chains and in the grafting ratio.

8.3 Conclusions

The hydration capabilities of surface-bound PLL-*g*-PEG and PLL-*g*-dex copolymers have been quantitatively investigated. The areal solvation, Ψ, and the number of water molecules per hydrophilic group, $N_{H2O/HG}$, absorbed within the polymer layer were determined by combining QCM-D and OWLS data. The experimental results of this study revealed higher hydration capacity of PLL-*g*-PEG copolymers compared to their PLL-*g*-dex counterparts showing comparable values of surface density of hydrophilic chains, suggesting a rather random hydration of dextran, in contrast with the known ability of hydrated PEG to form a unique ordered "cage-like" structure. Copolymers with high grafting ratio revealed more similar values of areal solvation, this being presumably due to the fact that the contribution of loosely bound water becomes predominant for low brush densities.

The quantification of the amount of water absorbed in the brush-like structure of PLL-*g*-PEG and PLL-*g*-dex copolymers is important for the understanding of the differences in their lubricating and antifouling behavior. However, further investigations are required to directly and quantitatively relate these sets of properties.

References

1. Havet, L., et al., *Tribological characteristics of some environmentally friendly lubricants*. Wear, 2001. **248**: p. 140-146.
2. Willing, A., *Lubricants based on renewable resources - an environmentally compatible alternative to mineral oil products*. Chemosphere 2001. **43**: p. 89-98.
3. Ratoi, M. and H.A. Spikes, *Lubricating properties of aqueous surfactant solutions*. Tribology Transactions, 1999. **42**(3): p. 479-486.
4. McArthur, S.L., et al., *Effect of polysaccharide structure on protein adsorption*. Colloids and Surfaces B: Biointerfaces, 2000. **17**(1): p. 37-48.
5. Sen Gupta, A., et al., *Glycocalyx-mimetic dextran-modified poly(vinyl amine) surfactant coating reduces platelet adhesion on medical-grade polycarbonate surface*. Biomaterials, 2006. **27**(16): p. 3084-3095.
6. Griesser, H.J., et al., *Interfacial properties and protein resistance of nano-scale polysaccharide coatings*. Smart Materials and Structures, 2002. **11**: p. 652-661.
7. Brady, R.F., *No more tin: what now for fouling control?* Journal of Protective Coatings & Linings, 2000. **17**(6): p. 42-46.
8. Flemming, H.-C., T. Griebe, and G. Schaule, *Antifouling strategies in technical systems - a short review*. Water Science and Technology, 1996. **34**(5): p. 517-524.
9. Melo, L.F. and T.R. Bott, *Biofouling in water systems*. Experimental Thermal and Fluid Science, 1997. **14**(4): p. 375-381.
10. Rajagopal, S., et al., *Some observations on biofouling in the cooling water conduits of a coastal power plant*. Biofouling, 1991. **3**(4): p. 311-324.
11. Townsin, R.L., *The Ship Hull Fouling Penalty*. Biofouling, 2003. **19**: p. 9-15.
12. Dalsin, J.L., *Mussel Adhesive-Inspired Surface Modification for the Preparation of Nonfouling Biomaterials*. PhD Diss., Northwestern University, 2004.
13. Jeon, S.I., et al., *Protein-Surface Interactions in the Presence of Polyethylene Oxide*. Journal of Colloid and Interface Science, 1990. **142**(1): p. 149-158.
14. Metzke, M., J.Z. Bai, and Z. Guan, *A Novel Carbohydrate-Derived Side-Chain Polyether with Excellent Protein Resistance*. Journal of American Chemical Society, 2003. **125**: p. 7760-7761.
15. Stanczak, M., *Biofouling: It's Not Just Barnacles Anymore*. ProQuest-CSA, 2004.
16. Lee, S. and N.D. Spencer, *Sweet, Hairy, Soft and Slippery*. Science, 2008. **139**: p. 575-576.
17. Bansil, R., E. Stanley, and J.T. Lamont, *Mucin Biophysics*. Annual Review of Physiology, 1995. **57**: p. 635-657.
18. Lee, S., et al., *Porcine Gastric Mucin (PGM) at the Water/ Poly(Dimethylsiloxane) (PDMS) Interface: Influence of pH and Ionic Strength on Its Conformation, Adsorption, and Aqueous Lubrication Properties*. Langmuir, 2005. **21**: p. 8344-8353.
19. Naka, M., Y. Morita, and K. Ikeuchi, *Influence of proteoglycan contents and of tissue hydration on the frictional characteristics of articular cartilage*. Proceedings of the Institution of Mechanical Engineers, Part H: Journal of Engineering in Medicine, 2005. **219**(3): p. 175-182.
20. Pickard, J., et al., *Investigation into the effect of proteoglycan molecules on the tribological properties of cartilage joint tissues*. Proc Instn Mech Engrs 1998. **212**(3): p. 177-182
21. Reitsma, S., et al., *The endothelial glycocalyx: composition, functions, and visualization*. European Journal of Physiology, 2007. **454**: p. 345-359.

22. Qiu, Y., et al., *Novel Nonionic Oligosaccharide Surfactant Polymers Derived from Poly(vinylamine) with Pendant Dextran and Hexanoyl Groups*. Macromolecules, 1998. **31**(1): p. 165-171.
23. Holland, N.B., et al., *Biomimetic engineering of non-adhesive glycocalyx-like surfaces using oligosaccharide surfactant polymers*. Nature, 1998. **392**: p. 799-801.
24. Milner, S.T., *Polymer Brushes*. Science, 1991. **251**: p. 905-914.
25. Zhao, B. and W.J. Brittain, *Polymer brushes: surface-immobilized macromolecules*. Progress in Polymer Science, 2000. **25**: p. 677-710.
26. Goedel, W.A. and R. Heger, *Monolayers of a solvent-free polymer brush: Part 1. Thermodynamics at the air/water interface*. Supramolecular Science, 1997. **4**: p. 293-300.
27. *Polymer Brushes: Polymerization to Control Interfacial Properties*, in *Encyclopedia of Materials: Science and Technology*. 2001, Elsevier Science Ltd. p. 7213-7218.
28. Birshtein, T.M. and Y.V. Lyatskaya, *Polymer brush in a mixed solvent*. Colloids and Surfaces A: Physicochemical and Engineering Aspects, 1994. **86**: p. 77-83.
29. Rühe, J., *Polymer Brushes: On the Way to Tailor-Made Surfaces*, in *Polymer Brushes. Synthesis, Characterization, Applications*, C. Rigoberto, et al., Editors. 2004, Wiley-VCH: Weinheim.
30. Kizhakkedathu, J.N., et al., *Synthesis and characterization of well-defined hydrophilic block copolymer brushes by aqueous ATRP*. Polymer 2004. **45**: p. 7471-7489.
31. Boyes, S.G., et al., *Polymer brushes—surface immobilized polymers*. Surface Science, 2004. **570**: p. 1-12.
32. Ji, H. and P.G. de Gennes, *Adhesion via Connector Molecules: The Many-Stitch Problem*. Macromolecules, 1993. **26**: p. 520-525.
33. Raphaèl, E. and P.G. de Gennes, *Rubber-Rubber Adhesion with Connector Molecules*. Journal of Physical Chemistry, 1992. **96**: p. 4002-4007.
34. Czeslik, C. and G. Jackler, *Protein Binding to Like-Charged Polyelectrolyte Brushes by Counterion Evaporation* Journal of Physical Chemistry, 2004. **108**(35): p. 13395-13402.
35. Ma, H., et al., *"Non-Fouling" Oligo(ethylene glycol)-Functionalized Polymer Brushes Synthesized by Surface-Initiated Atom Transfer Radical Polymerization*. Advanced Materials, 2004. **16**(4): p. 338-341.
36. Otsuka, H., et al., *Functionalized PEG-brush layer for controlling protein and cell interactions*. European Cells and Materials, 2003. **6**(1): p. 102.
37. Joanny, J.-F., *Lubrication by Molten Polymer Brushes*. Langmuir, 1992. **8**: p. 989-995.
38. Lee, S., et al., *Self-healing behavior of a polyelectrolyte-based lubricant additive for aqueous lubrication of oxide materials*. Tribology Letters, 2006. **24**(3): p. 217-223.
39. Sawhney, A.S. and J.A. Hubbell, *Poly(ethylene oxide)-graft-poly(L-lysine) copolymers to enhance the biocompatibility of poly(L-lysine)-alginate microcapsule membranes*. Biomaterials, 1992. **13**: p. 863-870.
40. Heuberger, M., T. Drobek, and N.D. Spencer, *Interaction Forces and Morphology of a Protein-Resistant Poly(ethylene glycol) Layer* Biophysical Journal, 2005. **88**: p. 495-504.
41. Huang, N., et al., *Poly(L-lysine)-g-poly(ethylene glycol) Layers on Metal Oxide Surfaces: Surface-Analytical Characterization and Resistance to Serum and Fibrinogen Adsorption*. Langmuir, 2001. **17**: p. 489-498.
42. Kenausis, G.L., et al., *Poly(L-lysine)-g-Poly(ethylene glycol) Layers on Metal Oxide Surfaces: Attachment Mechanism and Effects of Polymer Architecture on Resistance to Protein Adsorption*. J. Phys. Chem. B, 2000. **104**: p. 3298-3309.

43. Pasche, S., et al., *Poly(L-lysine)-graft-poly(ethylene glycol) Assembled Monolayers on Niobium Oxide Surfaces: A Quantitative Study of The Influence of Polymer Interfacial Architecture on Resistance to Protein Adsorption by ToF-SIMS and in Situ OWLS*. Langmuir, 2003. **19**: p. 9216-9225.
44. Pasche, S., et al., *Relationship between Interfacial Forces Measured by Colloid-Probe Atomic Force Microscopy and Protein Resistance of Poly(ethylene glycol)-Grafted Poly(L-lysine) Adlayers on Niobia Surfaces*. Langmuir, 2005. **21**: p. 6508-6520.
45. Pasche, S., et al., *Effects of ionic Strength and Surface Charge on Protein Adsorption at PEGylated Surfaces*. J. Phys. Chem. B, 2005. **109**: p. 17545-17552.
46. Blätter, T.M., et al., *High Salt Stability and Protein Resistance of Poly(L-lysine)-g-poly(ethylene glycol) Copolymers Covalently Immobilized via Aldehyde Plasma Polymer Interlayers on Inorganic and Polymeric Substrates*. Langmuir, 2006. **22**: p. 5760-5769.
47. Lee, S., et al., *Boundary Lubrication of Oxide Surfaces by Poly(L-lysine)-g-poly(ethylene glycol) (PLL-g-PEG) in Aqueous Media*. Tribology Letters, 2003. **15**(3): p. 231-239.
48. Müller, M., *Aqueous Lubrication by Means of Surface-Bound Brush-Like Copolymers*. ETH Zurich, 2005.
49. Müller, M., et al., *The Influence of Molecular Architecture on the Macroscopic Lubrication Properties of the Brush-Like Co-polyelectrolyte Poly(L-lysine)-g-poly(ethylene glycol) (PLL-g-PEG) Absorbed on Oxide Surfaces*. Tribology Letters, 2003. **15**(4): p. 395-405.
50. Müller, M., et al., *Lubrication Properties of a Brushlike Copolymer as a Function of the Amount of Solvent Absorbed within the Brush.* Macromolecules, 2005. **38**(13): p. 5706-5713.
51. Han, S., C. Kim, and D. Kwon, *Thermal/oxidative degradation and stabilization of polyethylene glycol*. Polymer, 1997. **38**(2): p. 317-323.
52. Bailey, F.E. and R.W. Callard, J. Appl. Polym. Sci. **1**(1): p. 56-62.
53. Kjellander, R. and E. Florin, *Water structure and changes in thermal stability of the system poly(ethylene oxide)–water*. J. Chem. Soc., Faraday Trans., 1981. **1**(77): p. 2053-2077.
54. Han, S., C. Kim, and D. Kwon, *Thermal degradation of poly(ethyleneglycol)*. Polymer Degradation and Stability, 1995. **47**(2): p. 203-208.
55. Drobek, T., N.D. Spencer, and M. Heuberger, *Compressing PEG Brushes*. Macromolecules, 2005. **38**: p. 5254-5259.
56. Choi, S.W., et al., *Preparation of cationic comb-type copolymer having guanidino moieties and its interaction with DNAs*. J. Biomater. Sci. Polymer Edn., 2004. **15**(9): p. 1099-1110.
57. Ferdous, A., T. Akaike, and A. Maruyama, *Inhibition of Sequence-Specific Protein-DNA Interaction and Restriction Endonuclease Cleavage via Triplex Stabilization by Poly(L-lysine)-graft-dextran Copolymer*. Biomacromolecules, 2000. **1**: p. 186-193.
58. Ferdous, A., et al., *Comb-Type Copolymer: Stabilization of Triplex DNA and Possible Application in Antigene Strategy*. Journal of Pharmaceutical Sciences, 1998. **87**(11): p. 1400-1405.
59. Ferdous, A., et al., *Poly(L-lysine)–graft–dextran copolymer: amazing effects on triplex stabilization under physiological pH and ionic conditions (in vitro)*. Nucleic Acid Research, 1998. **26**(17): p. 3949-3954.
60. Maruyama, A., et al., *Characterization of Interpolyelectrolyte Complexes between Double-Stranded DNA and Polylysine Comb-type Copolymers Having Hydrophilic Side Chains*. Bioconjugate Chem., 1998. **9**.

61. Perrino, C., S. Lee, and N.D. Spencer, *A Biomimetic Alternative to PEG as an Antifouling Coating: Resistance to Non-Specific Protein Adsorption of Poly(L-lysine)-graft-Dextran*. Langmuir, 2008. **24**: p. 8850-8856.
62. Perrino, C., S. Lee, and N.D. Spencer, *End-grafted Sugar Chains as Aqueous Lubricant Additives: Synthesis and Macrotribological Tests of Poly(L-lysine)-graft-Dextran (PLL-g-dex) Copolymers*. Tribology Letters, 2009. **33**(2): p. 83-96.
63. Hatton, M.N., et al., *Masticatory lubrication*. Journal of Biochemistry, 1985. **230**: p. 817-820.
64. Jay, G.D., K. Haberstroh, and C.-J. Cha, *Comparison of the boundary-lubricating ability of bovine synovial fluid, lubricin, and Healon*. Journal of Biomedical Material Research, 1998. **40**(3): p. 414-418.
65. Zappone, B., et al., *Adsorption, Lubrication, and Wear of Lubricin on Model Surfaces: Polymer Brush-Like Behavior of a Glycoprotein*. Biophysical Journal, 2007. **92**: p. 1693-1708.
66. Aguirre, A., et al., *Lubrication of selected salivary molecules and artificial salivas* Dysphagia, 2006. **4**(2): p. 95-100.
67. Gerken, T.A., *Biophysical Approaches to Salivary Mucin Structure, Conformation and Dynamics*. Critical Reviews in Oral Biology and Medicine, 1993. **4**: p. 261-270.
68. Edwards, J.C., *Principles of NMR*. http://www.process-nmr.com/nmr.htm.
69. House, W.V., *Introduction to the Principles of NMR* IEEE Transactions on Nuclear Science 1980. **NS-27**(3): p. 1220-1226.
70. Trummer, N., et al., *Modification of the surface of integrated optical wave-guide sensors for immunosensor applications*. Journal of Analytical Chemistry, 2001. **371**: p. 21-24.
71. Vörös, J., et al., *Optical grating coupler biosensors*. Biomaterials 2002. **23**: p. 3699-3710.
72. Kurrat, R., et al., *Instrumental improvements in optical waveguide light mode spectroscopy for the study of biomolecule adsorption*. Rev. Sci. Instrum., 1997. **68**(5): p. 2172-2176.
73. Hook, F., et al., *A comparative study of protein adsorption on titanium oxide surfaces using in situ ellipsometry, optical waveguide lightmode spectroscopy, and quartz crystal microbalance/dissipation*. Colloids and Surfaces B: Biointerfaces, 2002. **24**: p. 155-170.
74. Modin, C., et al., *QCM-D studies of attachment and differential spreading of pre-osteoblastic cells on Ta and Cr surfaces*. Biomaterials, 2006. **27**: p. 1346-1354.
75. Talib, Z.A., et al., *Frequency Behavior of a Quartz Crystal Microbalance (QCM) in Contact with Selected Solutions*. American Journal of Applied Sciences, 2006. **3**(5): p. 1853-1858.
76. Buttry, D.A. and M.D. Ward, *Measurement of Interfacial Processes at Electrode Surfaces with the Electrochemical Quartz Crystal Microbalance*. Chemical Reviews, 1992. **92**: p. 1355-1379.
77. Rixman, M.A., D. Dean, and C. Ortiz, *Nanoscale Intermolecular Interactions between Human Serum Albumin and Low Grafting Density Surfaces of Poly(ethylene oxide)*. Langmuir, 2003. **19**: p. 9357-9372.
78. Kawaguchi, T. and M. Hasegawa, *Structure of dextran-magnetite complex: relation between conformation of dextran chains covering core and its molecular weight*. Journal of Material Science: Materials in Medicine, 2000. **11**: p. 31-35.
79. Görisch, S.M., et al., *Histone acetylation increases chromatin accessibility*. Journal of Cell Science, 2005. **118**: p. 5825-5834.

80. Kawaguchi, S., et al., *Aqueous solution properties of oligo- and poly(ethylene oxide) by static light scattering and intrinsic viscosity*. Polymer, 1997. **38**(12): p. 2885-2891.
81. Tyrode, E., et al., *Hydration state of nonionic surfactant monolayers at the liquid/vapor interface: Structure determination by vibrational sum frequency spectroscopy*. Journal of American Chemical Society 2005. **127**(48): p. 16848-16859.
82. Smeeth, M., H.A. Spikes, and S. Gunsel, *The Formation of Viscous Surface Films by Polymer Solutions: Boundary or Elastohydrodynamic Lubrication?*. Tribol. Trans., 1996. **39**: p. 720-725.
83. Yan, X., et al., *Reduction of Friction at Oxide Interfaces upon Polymer Adsorption from Aqueous Solutions*. Langmuir, 2004. **20**: p. 423-428.
84. Mikitenko, V.S., et al., *Effect of Bacteria in Changing Physicochemical Properties of Lubricant/Coolant Fluids*. Chemistry and Technology of Fuels and Oils, 1976. **12**: p. 601-603.
85. Winslow, R., T. Naman, and G. Jenneman, *Effects of Bacterial Contamination on Steam Turbine Oil Systems* Tribology & Lubrication Technology, 2005. **61**(3): p. 26-35.
86. Sery, T.W. and E.J. Hehre, *Degradation of dextrans by enzymes of intestinal bacteria*. J. Bacteriol. , 1956. **71**: p. 373-380.
87. Bosker, W.T.E., et al., *Sweet brushes and dirty proteins*. Soft Matter, 2007. **3**: p. 754-762.
88. Österberg, E., et al., *Comparison of polysaccharide and poly(ethylene glycol) coatings for reduction of protein adsorption on polystyrene surfaces*. Colloids and Surfaces A: Physicochemical and Engineering Aspects, 1993. **77**: p. 159-169.
89. Österberg, E., et al., *Protein-rejecting ability of surface-bound dextran in end-on and side-on configurations: Comparison to PEG*. J. Biomed. Mat. Research 1995. **29**: p. 741-747.
90. Martwiset, S., *Nonfouling Characteristics of Dextran-Containing Surfaces*. Langmuir, 2006. **22**: p. 8192-8196.
91. Raviv, U., R. Tadmor, and J. Klein, *Shear and Frictional Interactions between Adsorbed Polymer Layers in a Good Solvent*. J. Phys. Chem. B, 2001. **105**: p. 8125-8134.
92. Koehler, J.A., M. Ulbricht, and G. Belfort, *Intermolecular Forces between Proteins and Polymer Films with Relevance to Filtration*. Langmuir, 1997. **13**: p. 4162-4171.
93. Davanand, K. and J.C. Selser, *Polyethylene oxide does not necessarily aggregate in water*. Nature, 1990. **343**: p. 739-741.
94. Begum, R. and H. Matsuura, *Conformational properties of short poly(oxyethylene) chains in water studied by IR spectroscopy*. Journal of the Chemical Society-Faraday Transactions, 1997. **93**(21): p. 3839-3848.
95. Lui, K.J. and J. Parson, *Solvent Effects on the Preferred Conformation of Poly(ethylene glycols)*. Macromolecules 1969. **2**(5): p. 529-533.
96. Lüsse, S. and K. Arnold, *The Interaction of Poly(ethylene glycol) with Water Studied by 1H and 2H NMR Relaxation Time Measurements*. Macromolecules, 1996. **29**: p. 4251-4257.
97. Graham, N.B., et al., *Interaction of poly(ethylene oxide) with solvents: 2. Water-poly(ethylene glycol)*. 1989. **30**: p. 528-533.
98. Hager, S.L. and T.B. Macrury, *Investigation of Phase Behavior and Water Binding in Poly(alkylene Oxide) Solutions*. Journal of Applied Polymer Science, 1980. **25**: p. 1559-1571.
99. Tasaky, K., *Poly(oxyethylene)-water interactions: a molecular dynamic study*. Journal of the American Chemical Society, 1996. **118**(35): p. 8459-8469.

100. Hammouda, B., L.H. Derek, and S. Kline, *Insight into Clustering in Poly(ethylene oxide) Solutions*. Macromolecules, 2004. **37**: p. 6932-6937.
101. Hauet, T. and M. Eugene, *A new approach in organ preservation: potential role of new polymers*. Kidney International, 2008. **74**: p. 998-1003.
102. Granath, K.A., *Solution properties of branched dextrans*. Journal of Colloid Science, 1958. **13**: p. 308-328.
103. Senti, F.R., et al., *Viscosity, Sedimentation, and Light-Scattering Properties of Fractions of an Acid-Hydrolyzed Dextran*. Journal of Polymer Science, 1955. **17**: p. 527-546.
104. Gekko, K. and H. Noguchi, *Physicochemical Studies of Oligodextran. I. Molecular Weight Dependence of Intrinsic Viscosity, Partial Specific Compressibility and Hydrated Water*. Biopolymers, 1971. **10**: p. 1513-1524.
105. Nomura, H., O. Makoto, and Y. Miyahara, *Preferential Solvation of Dextran in Water-Ethanol Mixtures*. Polymer Journal, 1982. **14**(4): p. 249-253.
106. Nomura, H., S. Yamaguchi, and Y. Miyahara, *Partial Specific Compressibility of Dextran*. Journal of Applied Polymer Science, 1964. **8**: p. 2731-2734.
107. Heuberger, M., T. Drobek, and J. Vörös, *About the role of water in surface-grafted poly(ethylene glycol) layers*. Langmuir, 2004. **20**(22): p. 9445-9448.

Acknowledgements

It's now time to say "thanks" to all people who helped and supported me during the last three years and contributed to the successful completion of my thesis.

First of all I would like to acknowledge Prof. Nic Spencer who gave me the unexpected opportunity to carry out my PhD thesis in his laboratory. It was not that easy in the beginning, being a "freaky hydrogel girl", to start doing research in such a different field, but fruitful discussions with Nic and his constant guidance over all my PhD helped me a lot in becoming interested in tribology and enthusiast of my project.

The same gratitude goes to my direct supervisor, Dr. Seunghwan Lee, who helped me a lot in healing from my "tribologist disease", as he was used to call my not really optimistic feeling of the project in the first few months of my PhD. Seunghwan motivated and encouraged me a lot offering his excellent supervision and always going along with my scientific interests. Many thanks to Seunghwan also for his friendly attitude and especially for having updated me with all possible versions of "Bella ciao!".

I would like to thank Dr. Rowena Crockett who made the MTM available to me and always helped me when I came across technical problems.

My acknowledgments also to Prof. Maruyama who kindly provided some PLL-g-dex copolymers that were employed in this thesis.

Thanks to the SuSoS team, especially to Samuele, the first person of the group I met, even before coming to Switzerland. He did a lot in the beginning to make me feel at home, introducing me to all his friends, organizing nice dinners everywhere and driving me all around Zurich, when I used to stay in the student house at the far east of Zurich. Probably tired of being my taxi driver, he also helped me in the difficult search of a flat and, once I finally found a place, he did most of the work in building up my Ikea flat. Grazie Sammy!

Thanks to Stefan Zürcher, for his advices for the synthesis of PLL-*g*-dex and his help in the interpretation of NMR spectra.

I am also grateful to Dr. Paola Petrini, my supervisor during my Master thesis in Milano and now one of my best friends: she always encouraged me, making me look at the best side of everything and, even if she was not directly involved in my project, she gave me a hand,

especially in the very beginning, with the preparation of my first presentations in English and, as a great organic chemist, with the synthetic part of my work.

I would also like to thank numerous more people from and outside the group who have contributed to make unforgettable the past three years in one way or the other:

Marcella who shared a tiny room with me at the student house for more than 4 months, Marta, from whom I learned that "brindare alle *ritrovaglie*" is always worth it and for the nice chats on Skype at midnight! Bara for the wonderful time we spent together during the *biking & wine tasting* in the South of Czech Republic and for having taught me some essential Czech that I will never forget, such as "ve vine je pravda", Vincent who knows Milano (and also Saronno!!) better than me and for having appreciated my grandmother's limoncello so much, Ciccio for being so good in speaking Italian and making me speak German and for his very unique attitude, Rafi, Whitney, Prathima and Jarred with whom I shared a lot of time, especially during the never-ending tribology meetings, and for their useful scientific inputs, Prathima again and Emily for having cooperated with me and kindly helped me with the experiments during the last few months, all my not yet mentioned office mates for making nice and not boring at all the working time, with jokes and funny discussions, Tobias, the "Thesis Doktor", for having offered me his Word template for the PhD dissertation and given me many tricks to use it efficiently, Marco for the originality of his English with an "e" at the end of each word and for his unique kindness, Sameer, my hoodmate, for always being patient with a biomedical engineer trying to put herself in a chemist's shoes, Geraldine for the nice cooperation we had for a small but very interesting project, Josephine Baer and Esther Stähli for all their administrative work and for their extremely efficient response to all my queries regarding bureaucratic stuff, Tomas Bartos for his IT support, Nick Argibay who carried out with uncommon enthusiasm a small but successful project within my thesis, Lucy who organized an extremely nice bachelorette party for me and managed to keep everything secret until the last minute! and all girls who joined the organization and the party.

I would also like to thank all my Italian friends in Zurich, especially Flavio, the first Italian I met at the student house, for his friendship and for one special reason, Valerio, Matteo, Marta and Walter with whom I shared a lot of time all together during lunch and practicing our table soccer skills, Stefano, not for the broken crystal glass ;-), but for his sense of humor and his optimistic attitude, and Stefania, my "Marchigian" neighbor. I can really feel the Italian atmosphere and I don't miss Italy at all when I stay with all of them!

Special thanks also to my parents and my family who mostly spurred me on to come to Zurich, a choice that I will never regret, always welcomed me back at home with their love, always supported me during the difficult times of the last three years and of all my life.

Finally, thanks to Damiano, the best gift of my PhD life: thanks for his unconditional patience and for the sacrifices he did for me before and after we got married, thanks for encouraging me, always being at my side and sharing everything with me, for making me laugh or cry, but always for joy, and for always laughing in a way that I really love!, for being an unbelievably excellent housewife, for trying to teach me how to play the guitar, for his positive attitude in learning skiing, for his true love and for being the best husband I could possibly imagine. And thanks for our coming soon Giuseppe!!

Curriculum Vitae

Personal

Chiara Perrino
Friesenbergstrasse 28
8055 Zürich

Date of birth: 30 July 1981
Nationality: Italian
Marital status: married

Mobile phone: 078 670 84 36
E-mail: chiara.perrino@mat.ethz.ch

Education

- Ph.D. Student at Laboratory for Surface Science & Technology, Department of Materials, ETH Zurich — since 2006
- Politecnico di Milano, Milano (Italy) — 2000–2005
  Master Degree in Biomedical Engineering (110/110 cum laude)
  Bachelor Degree in Biomedical Engineering (110/110 cum laude)
- Liceo Classico Giosuè Carducci, Milano (Italy) — 1995–2000
  High School Diploma (100/100)

Working Experience

- Supervision of a student for a summer project at LSST, ETH Zurich — summer 2008
  Title: Stability comparison of PLL-*g*-PEG and PLL-*g*-dex
- Supervision of a Bachelor student for the Bachelor thesis, Laboratory of Biosensors and Bioelectronics, ETH Zurich — spring 2008
  Title: Nanogel particles for biosensing applications
- Responsible for tutorials within the course of "Biomaterials Laboratory and Instrumental Analysis", Politecnico di Milano (Italy) — 2005
- Master thesis at the Biomaterials Laboratory, Politecnico di Milano (Italy) — 2005
  Title: Synthesis and characterization of polyurethane hydrogels with controlled solubility
- Bachelor thesis at the Biomaterials Laboratory, Politecnico di Milano (Italy) — summer 2003
  Title: Crosslinking methods of UHMWPE to increase the wear resistance of hip implants
- Internship at Fondazione Don Carlo Gnocchi, Milano (Italy) — September 2003
  (Laboratory of Movement Analysis)

Languages

- Italian: native speaker
- English: fluent
- German: basic knowledge

Presentations

Poly(L-lysine)-*g*-dextran (PLL-*g*-dex): Brush-forming, Biomimetic Carbohydrate Chains that Inhibit Fouling and Promote Lubricity *(oral presentation)*

C. Perrino, S. Lee, N.D. Spencer

Kolloquium D-MATL, November 5, 2008, ETH Zurich, Switzerland

Poly(L-lysine)-*g*-dextran (PLL-*g*-dex): Brush-like, Carbohydrate Chains as a Biomimetic Antifouling and Lubricating Coating *(oral presentation)*

C. Perrino, S. Lee, N.D. Spencer

30th Australian Polymer Symposium (30 APS), November 30 – December 4, 2008, Melbourne, Australia

Poly(L-lysine)-*g*-dextran (PLL-*g*-dex): Brush-like, Carbohydrate Chains as Biomimetic Lubricating Additives *(poster presentation)*

C. Perrino, S. Lee, N.D. Spencer

Tribology Gordon Research Conference: Advancing Interfacial Science and Engineering, July 6–11, 2008, Waterville, Maine

Surface Modification with Carbohydrate-based Graft Copolymers: Impact on Biomimetic Lubrication and Biofouling *(poster presentation)*

C. Perrino, S. Lee, N.D. Spencer

24st Meeting - Schweizerische Arbeitsgemeinschaft Oberflächen und Grenzflächen (SAOG), January 25, 2008, Freiburg, Switzerland

PLL-*g*-PEG/PEG-mannose functionalized nanogels for cell-receptor-targeted drug delivery application *(poster presentation)*

C. Perrino, N. Csaba, G. Coullerez, G. Gorodyska, S. Bravo, H.P. Merkle, M. Textor

Biosurf VII – Functional Interfaces for Directing Biological Response, August 28–31, 2007, Zurich, Switzerland

Surface Modification with Carbohydrate-based Copolymers: its Impact on Biofouling and Biomimetic Lubrication *(oral presentation)*

C. Perrino, S. Lee, N.D. Spencer

Development of Polyurethane Hydrogels with Controlled Solubility *(oral presentation)*

P. Petrini, C. Perrino, S. Bozzini, L. Visai, M.C. Tanzi

FBPS 07 – 7th International Symposium on Frontiers in Biomedical Polymers, June 24–27, 2007, Ghent, Belgium

Carbohydrate-based brush copolymers as biomimetic lubricant additives: synthesis and tribological characterization *(poster presentation)*

C. Perrino, S. Lee, N.D. Spencer

International Nanotribology Forum (INF): The Hoi An Discussions, March 26–30, 2007, Hoi An, Vietnam

Carbohydrate-based brush copolymers as lubricant additives: synthesis, characterization and preliminary tribological tests *(poster presentation)*

C. Perrino, S. Lee, S. Zürcher, N.D. Spencer

Physics of Friction – Short Course, November 20–24, 2006, Valprè, France

Byohybrid Hydrogels: Polyurethane Grafting onto Chitosan *(oral presentation)*

P. Petrini, G. Bianchi, C. Perrino, S. Bozzini, M.C. Tanzi

International Conference on Advances in Biomaterials for Drug Delivery and Regenerative Medicine, June 11–16, 2006, Capri, Italy

Development of Hydrogels with Controlled Solubility for Applications in Tissue Engineering *(oral presentation)*

C. Perrino, P. Petrini, G. Bianchi, M. Roba, M.C. Tanzi

Congresso Nazionale di Biomateriali, October 26–27, 2005, Milano, Italy

Publications

End-grafted Sugar Chains as Aqueous Lubricant Additives: Synthesis and Macrotribological Tests of Poly(L-lysine)-*graft*-Dextran (PLL-*g*-dex) Copolymers
C. Perrino, S. Lee, N.D. Spencer
Tribology Letters, 2009. **33**(2): p. 83-96

A Biomimetic Alternative to PEG as an Antifouling Coating: Resistance to Non-Specific Protein Adsorption of Poly(L-lysine)-*graft*-dextran
C. Perrino, S. Lee, N.D. Spencer
Langmuir, 2008. **24**: p. 8850-8856

Mucins, grafted sugars, and PEG-brushes: learning from nature in the design of new lubricant systems
S. Lee, C. Perrino, W. Hartung, N.D. Spencer
Symposium on Tribology 2006, Sep 12-15, 2006, Leeds, U.K.

Bacterially induced degradation of aqueous solutions of poly(L-lysine)-*graft*-poly(ethylene glycol) (PLL-*g*-PEG) and poly(L-lysine)-*graft*-dextran (PLL-*g*-dex) and consequences for their lubrication properties
N. Argibay, C. Perrino, M. Rimann, S. Lee, N.D. Spencer
submitted to Lubrication Science

Quantitative comparison of the hydration capacity of surface-bound dextran and poly(ethylene glycol)
C. Perrino, S. Lee, N.D. Spencer
in preparation